INSTITUT FOR BÆRENDE KONSTRUKTIONER OG MATERIALER

DTU

Strength of Cracked Concrete

Part 3
Load Carrying Capacity of Panels Subjected to In-plane Stresses

JIN-PING ZHANG

DEPARTMENT OF STRUCTURAL ENGINEERING AND MATERIALS
TECHNICAL UNIVERSITY OF DENMARK Series R No 18 1997

STRENGTH OF CRACKED CONCRETE

Part 3 --- Load Carrying Capacity of Panels Subjected to In-plane Stresses

Jin-Ping Zhang

Strength of Cracked Concrete
Part 3.. Load Carrying Capacity of Panels Subjected to In-Plane Stresses

Tryk: LTT
Danmarks Tekniske Universitet
Lyngby
ISBN 87-7740-200-6
ISSN 1396-2167
Bogbinder:
H. Meyer, Bygning 101, DTU

PREFACE

This paper has been prepared as the third part of the thesis to obtain the Ph.D. degree at the Technical University of Denmark.

The first two parts of the thesis are

Part 1 - Shear Strength of Conventional Reinforced Concrete Beams, Deep beams, Corbels, and Prestressed Reinforced Concrete Beams without Shear Reinforcement

Part 2 - Micromechanical Modeling of Shear Failure in Cement Paste and Concrete

of which Part 1 has been published at the Department of Structural Engineering, Report R-311, 1994.

The work has been carried out at the Department of Structural Engineering under the supervision of Professor, Dr.techn. M.P.Nielsen.

I wish to express my sincere appreciation to my supervisor for his inspiring advice and encouragement, and to the entire staff at the department for their help during the time I have been here.

Financial assistance from the Danish Council for Scientific and Technical Research (STVF) is gratefully acknowledged.

Lyngby, 1996

Jin-Ping Zhang

Summary

This report deals with the load carrying capacity of concrete specimens subjected to in-plane stresses by means of the theory of plasticity.

A review on the experiments of concrete specimens subjected to in-plane stresses is carried out. By applying the hypothesis that cracking of concrete introduces potential yield lines which may be more dangerous than the ones found by the usual plastic theory, the load carrying capacity of cracked specimens under different conditions is investigated. A mechanism of strength reduction is proposed based on the analysis of the damage caused by stressed transverse reinforcement. By comparing with the test results of panels subjected to in-plane stresses, an expression of the effectiveness factor as a function of the transverse tensile stresses is suggested.

By assuming sliding failure along the existing cracks, an upper bound solution and a lower bound solution for the load carrying capacity of panels subjected to in-plane shear are proposed. The calculation is compared with the test results, and a good agreement has been found.

Resumé

Denne rapport behandler, ved hjælp af plasticitetsteorien, bæreevnen af skiver af beton.

Der gives først en oversigt over de forsøg, der er udført.

Derefter foretages en beregning af bæreevnen af revnet beton i forskellige tilfælde ud fra den forudsætning, at revnerne kan være potentielle flydelinier, der er farligere end de sædvanlige flydelinier gennem urevnet beton.

Videre foreslås en model for styrkereduktionen på grund af revnerne, når disse krydses af trækpåvirket armering. En sammenligning med forsøgsresultaterne fører til et simpel udtryk for effektivitetsfaktoren som funktion af armeringsforholdet og trækpåvirkningen på tværs af revnerne.

Endelig er der udført beregninger af bæreevnen af skiver påvirket i deres egen plan unde hensyn til glidningsbrud i revnerne. Beregningerne er sammenlignet med forsøg, og der er fundet god overensstemmelse.

TABLE OF CONTENTS

NOTATIONS

c	: Cohesion of uncracked concrete, concrete cover
c'	: Cohesion of cracked concrete, cohesion in a crack or joint
d	: Diameter of reinforcing bar
E_s	: Young's modulus of reinforcement
E_c	: Young's modulus of concrete
f_c	: Uniaxial compressive cylinder strength of concrete
f_c'	: Reduced compressive strength of concrete due to cracks
$f_{c.panel}$	: Uniaxial compressive panel strength of concrete
f_t	: Tensile strength of concrete
f_t'	: Tensile strength of concrete perpendicular to a crack
f_v	: Shear strength of panels
f_Y	: Yield stress of reinforcement
G'	: Shear modulus of cracked concrete
G_{c0}	: Shear modulus of uncracked concrete
h	: Depth of punching cone
k	: Material constant, $k=(1+\sin\varphi)/(1-\sin\varphi)$
l_0	: $=2h$
l_{tr}	: Transfer length
u	: Relative displacement in yield line
W_i	: Internal work per unit volume
W_I	: Internal work per unit length
W_E	: External work
x_0	: Depth of initial punching cone
α	: Angle of relative displacement to yield line
β	: Angle of joints
θ	: Angle of uniaxial compression field in panels, angle of reinforcement direction
γ	: Angle of yield line
μ	: Coefficient of friction for uncracked concrete, $\mu=\tan\varphi$

μ' : Coefficient of friction for cracked concrete, $\mu'=\tan\varphi'$, coefficient of friction in a crack or joint

ν_0 : Effectiveness factor of uncracked concrete

ν_s : Sliding reduction factor due to cracking

σ : Normal stress

σ_s : Tensile stress in reinforcement

τ : Shear stress

φ : Friction angle of concrete

φ' : Friction angle of cracked concrete, friction angle in a crack or joint

ρ : Reinforcement ratio

ϕ : Diameter of cylinder test specimen or of reinforcement bars

Φ : Mechanical degree of reinforcement, $\Phi=\rho f_Y/f_c$

I. Introduction

In the last few decades, great effort has been placed on the study of the behavior and strength reduction mechanism of concrete under tension-compression stress states. In [82,1] F.Vecchio and M.P.Collins published their first test results concerning the load carrying capacity of concrete panels subjected to in-plane stresses. Based on the tests, they suggested that the uniaxial compressive strength of concrete is a function of the transverse tensile strains. For large transversal strains they found a substantial strength reduction. The Vecchio/Collins formulas regarding the compressive strength of concrete versus the transverse tensile strain have become very popular and a large number of research groups around the world have made similar experiments to verify the empirical formulas. However, the test results are rather confusing. The strong dependency of the compressive strength of concrete on the transverse tensile strains is not observed in all or most of the tests. From a large number of test results, it appears that the compressive strength of concrete does decrease when the tensile strains are increased, but only to a certain degree. The compressive strength of concrete seems to have a low limit around $0.6\sim0.7f_c$ regardless the transverse tensile strains, f_c being the standard compressive cylinder strength of concrete.

In this thesis an alternative explanation of the strength reduction is given.

From the observation in the experiments, we can see that cracks were created prior to the compression failure. As in Part 1 and Part 2 of the thesis, failure is assumed to take place preferably along the cracked surfaces because the strength is considerably reduced in the cracks. By means of plastic theory, the effect of the formation of the cracks may be found out.

In pull-out tests, cracks in the surrounding concrete are created when the reinforcing bars are tensioned, the higher the tensile stress, the more severe the cracking is. A similar effect is produced by the reinforcement near any primary cracks. Further internal cracking is produced by the bursting stresses around the reinforcement bars leading possibly to the spalling off of the cover. When the specimens are loaded in compression in the transverse direction, the strength is bound to be reduced due to the formation of these load induced cracks. In this way, a certain relationship between the compressive strength and the transverse tensile stress might be found.

In the tests of panels in pure shear, a shift of direction of the cracks at failure

is observed. Based on the assumption, as discussed in Part 1 and Part 2, that the sliding resistance of concrete along cracks is substantially reduced and that the yield line at failure may follow the existing cracks, an upper bound as well as a lower bound solution according to plastic theory is postulated.

The solutions are compared with the available experimental results. A fairly good agreement has been found.

II. Review of previous research and discussions

In plane problems, concrete under tension-compression states is of great interest to the engineering profession and to researches at the moment. The reasons for such an interest are partly due to the practical significance of the problem, and partly due to the controversy of the test results obtained by different research groups.

A comprehensive review of the previous experiments on slabs and panels may be found in [89,1][90,3][92,1]. In this section, we will only concentrate on the experiments of panels or disks subjected to in-plane stresses, and experiments of joints.

The basic compressive strength of concrete is normally obtained on a standard cylinder of size ϕ150×300mm or a cube. When larger specimens, especially panels where the dimension in one direction is much smaller than the other dimensions, are subjected to uniaxial compression, the ultimate stress obtained is bound to be smaller than the corresponding standard compressive strength. This tendency can also be observed in some test results listed below. To distinguish the uniaxial compressive strength obtained on a panel from the standard cylinder compressive strength of concrete, we term the ultimate compressive stress of panels subjected to uniaxial compression the uniaxial compressive panel strength, denoted by $f_{c.panel}$.

A large deviation from panel strength to cylinder strength is particularly observed when the panel is cast in a vertical position. Then, due to the upstreaming of water when compacting the concrete, the water/cement ratio is bound to be larger in the top than in the bottom. The strength will increase from the top to the lower part of the panel. Usually a region of a depth around 300~400mm measured from the top will suffer a lower strength. A strength reduction of the order 10~20% is found quite often. This fact is demonstrated by several of the test series treated below. Of course, size effects may also play a role, since the panels are often rather slender compared with the test cylinders.

2.1 Tension-compression panel tests

Tests by J.M.Demorieux [69,1]

The test series by Demorieux [69,1]was composed of 12 specimens which were divided into 3 groups: uniaxial compression of plain concrete plates, uniaxial compression of laterally reinforced concrete plates and tension-compression of laterally reinforced concrete plates. The size of the specimen was 42×45× 10cm. The set up of the tests is illustrated in Fig.2.1.1. The reinforcing bars were placed in two layers, and the arrangement is schematically shown in Fig.2.1.2. The cylinder used to obtain the standard compressive strength of concrete was ϕ16×32cm. In tension-compression tests, the forces were proportionally applied keeping $P_1/b=P_2/a$.

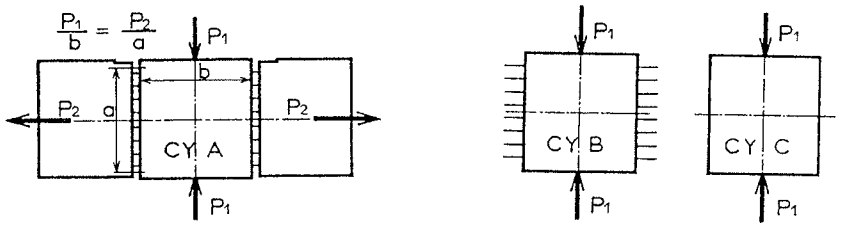

Fig.2.1.1 Principle and group division of the tests by Demorieux[69,1]

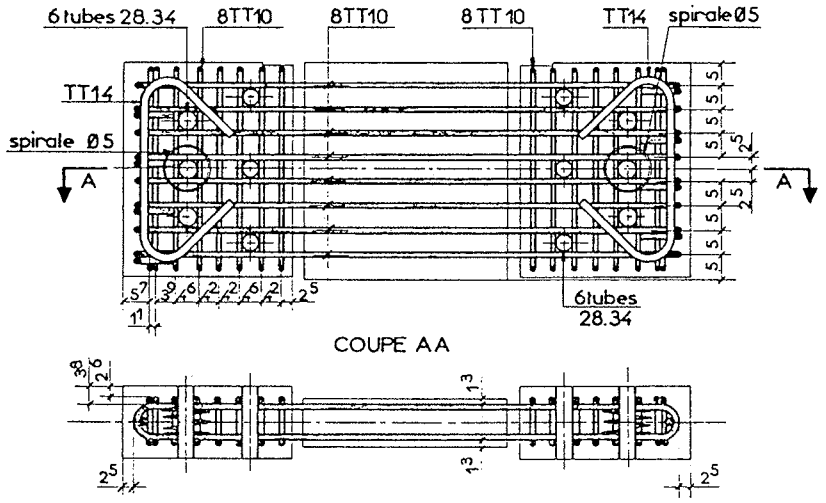

Fig.2.1.2 Reinforcement lay-out of the specimens [69,1]

Table 2.1.1 Test results from [69,1]

test	ρ		f_c(kg/cm^2)		CYA		CYB		CYC	
No.	(%)	ϕ(mm)	10 min.	3 hs.	σ	σ/f_c	σ	σ/f_c	σ($f_{c,panel}$)	σ/f_c
CY9	1.56	6	398	378	245	0.65	272	0.72	322	0.85
CY10	1.56	6	196	199	146	0.73	186	0.93	168	0.84
CY11	3.14	10	360	346	230	0.66	314	0.91	311	0.90
CY12	3.14	12	360	346	245	0.71	314	0.91	311	0.90

The test results are listed in Table 2.1.1, where ρ is the reinforcement ratio, ϕ the diameter of the reinforcing bars, and σ the ultimate compressive stress. The compressive cylinder strength of concrete was taken to be the one with 3 hours duration of the test.

The specimens in test group CYC are plain concrete disks subjected to uniaxial compression. The results obtained correspond to what we have termed the compressive panel strength. Compared with the standard uniaxial compressive cylinder strength, a clear reduction in the panel strength can be seen. In this test series the ratio of the panel compressive strength and the standard compressive strength in average is 0.87.

The loading conditions of the specimens in group CYB are the same as in CYC, except that the disks are laterally reinforced. The effect of the lateral reinforcing bars on the ultimate compressive stress is small.

In group CYA disks are subjected to tension-compression. Due to the presence of the lateral tensile stress, the compressive load carrying capacity is substantially reduced. Compared with the standard compressive strength the ratio is in average 0.69, whereas compared with the panel compressive strength the ratio is in average 0.79. The reduction due to the lateral tensile stress is about 21% when panel strength is taken as the basis.

Tests by J.Schlaich & K.Schfer [83,2]

The test series in [83,2] consisted of 10 concrete panels, among which two were plain concrete panels and the rest were reinforced with a net of Bst 500/550 RK. The diameter of the bars was 10mm and the bar spacing was 50mm or 100mm resulting in the reinforcement ratios 3.14% and 1.56%, respectively.

The test specimens were divided into two groups. In one group the panels were subjected to uniaxial compressive stresses, while in another one the panels were subjected to combined tensile and compressive loads. The direction of the reinforcement net was also varied. The reinforcement details are shown in Fig.2.1.3.

Test results are listed in table 2.1.2.

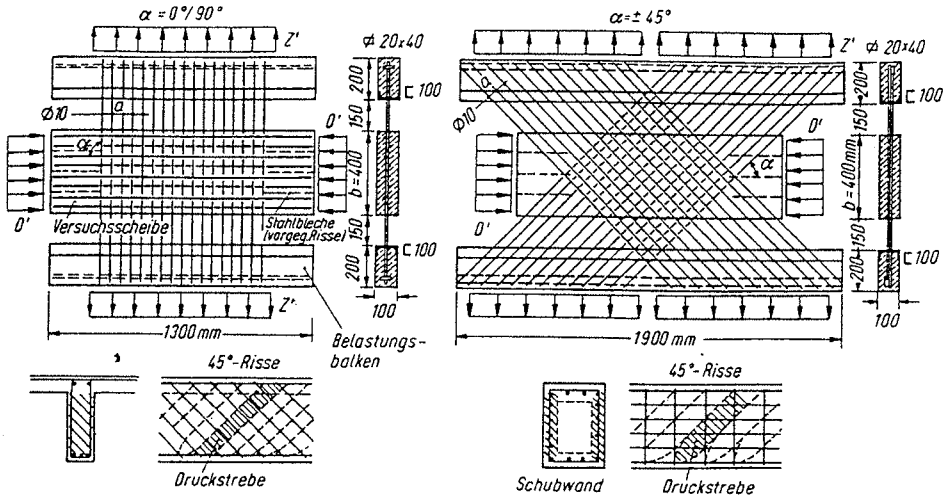

Fig.2.1.3 Reinforcement details and load principle in [83,2]

Table 2.1.2 Test results from [83,2]

specimen No.	f_c (MPa)	α (°)	s (mm)	stress state	f_p/f_c	f_{p45}/f_{p90}
1	23.6	0/90	50	B	1.03	
2	〃	45	〃	B	0.76	0.74
3	〃	0/90	〃	U	1.12	
4	〃	45	〃	U	0.89	0.79
5	21.7	0/90	100	B	1.07	
6	〃	45	〃	B	0.97	0 .91
7	〃	0/90	〃	U	1.18	
8	〃	45	〃	U	0.96	0.81
9	〃	unreinf.	-	U	0.99	
10	23.6	unreinf.	-	U	0.99	

U-uniaxial stress state, B-biaxial stress state, α-reinforcement direction, see Fig.2.1.3, s-reinforcing bar spacing

The results of specimens No.9 and No.10 correspond to what we termed the compressive panel strength. Compared with the standard uniaxial compressive strength, no obvious reduction was observed in $f_{c,panel}$. This is at variance with the results from [69,1][88,1].

With α=0 one set of the reinforcement bars are in the loading directions. In the uniaxial cases, because of the contribution from the reinforcement in the direction of the compressive force, it is natural that the ultimate compressive stress is higher than f_c. Assuming the compressive reinforcement at failure being not yielding for the heavily reinforced specimens and yielding for the lightly reinforced specimens, and taking out the contribution of the reinforcement from the total load carrying capacity, then the compressive stress carried by the concrete in average is $0.85f_c$. This is not in the agreement with the results of test specimens No.9 and No.10 (unreinforced panels), but similar to the results from [69,1][81,1]

With α=45° the stress conditions along the edges become more complicated, and more damage to the surrounding concrete due to the anchorage of the reinforcing bars will be caused. Therefore, the ultimate load carrying capacity of the disks with α=45° is lower than the load carrying capacity of the corresponding disks with α=0. From these tests, it is seen that test results for such specimens might be strongly influenced by the conditions around the steel bars at the edges. Since we are mainly concerned with the dependence of the load carrying capacity on the transverse tensile stresses or strains, we will not investigate the anchorage problems introduced when the steel bars are inclined in detail. Instead, we will concentrate on the specimens where the reinforcing bars are in the direction of the loading.

It is seen that even when lateral tensile stresses are present, the compressive load carrying capacity is not substantially reduced. This is rather controversial to what is commonly believed. The reasons are not clearly understood.

Tests by J.Eibl & U.Neuroth [88,1]

The test series by J.Eibl & U.Neuroth consisted of 14 panels to investigate the compressive strength of reinforced in-plane loaded concrete panels in a tension-compression field. Six panels were subjected to uniaxial compression, while the rest were subjected first to horizontal load until the reinforcing bars in this direction were stressed to yielding, and then a vertical compressive load was applied until compression failure occurred in the concrete.

The sections of the test specimens are shown in Fig.2.1.5. The reinforcing bars were placed into one or two layers, and the diameter and the spacing of the bars were also varied.

The test results are listed in table 2.1.3.

In group I, plain concrete panels were loaded uniaxially. The uniaxial compressive panel strength thus obtained in average was around $0.7f_c$.

The panels subjected to uniaxial compressive stresses in group II were laterally reinforced, and the reinforcement was placed in one layer. The ultimate compressive stress obtained in average was $0.7f_c$. Panel 11 in group V had two layers of reinforcement, the resulting ultimate compressive stress was $0.75f_c$.

As in [69,1], it is seen that the lateral reinforcement has little effect on the uniaxial load carrying capacity.

From the experiments, it was found that the reduction of the compressive load carrying capacity due to the transverse tensile strains was less than 15%.

Table 2.1.3 Test results from [88,1]

Group	test No.	f_c (MPa)	reinf. bars		loading condition	σ_u(MPa)	
			ϕ–s(mm)	ρ(%)		σ_u	σ_u/f_c
I	1	32.3	/	/	C	22.0	0.68
	8	34.3	/	/	C	24.5	0.71
II	2	31.1	ϕ20-130	1.5	C	22.0	0.71
	3	30.5	〃	〃	C	19.0	0.62
	10	35.2	〃	〃	C	26.5	0.75
III	4	33.5	〃	〃	T	**	
	5	31.3	〃	〃	C-T	18.5	0.59
	9	33.7	〃	〃	C-T	22.0	0.65
IV	6	33.4	ϕ10-65	1.5	C-T	20.0	0.60
	7	36.5	〃	〃	C-T	22.5	0.62
V	11	35.5	ϕ10-100	1.6	C	26.5	0.75
VI	12	34.8	〃	〃	C-T	23.5	0.68
	13	34.1	〃	〃	C-T	26.5	0.66
VII	14	32.4	ϕ16-100	1.0	C-T	21.0	0.65
	0	34.8	ϕ16-100	2.5	C-T	20.0	0.57

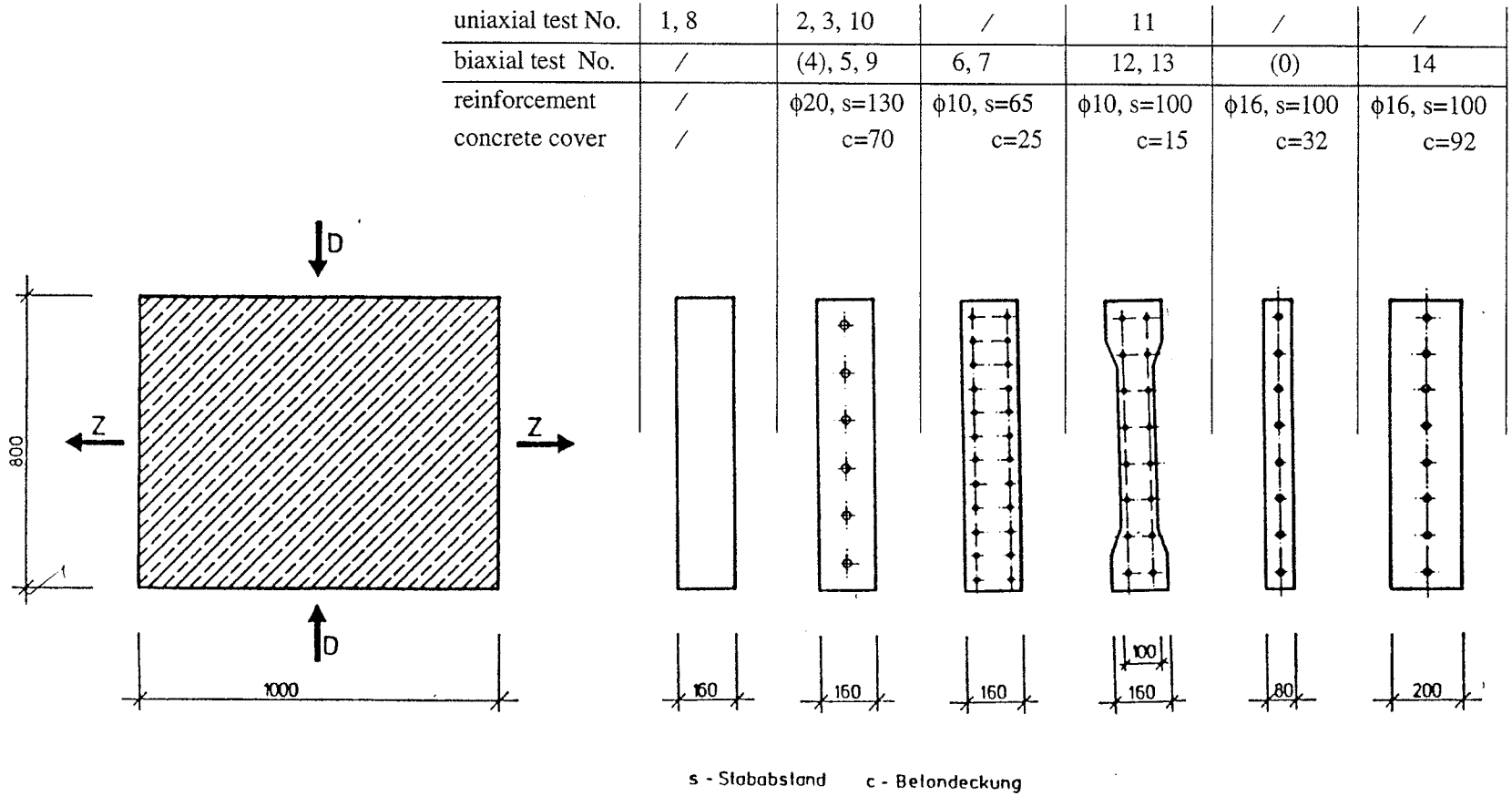

Fig.2.1.4 Lay out of test specimen in [88,1]

Tests by T.Miyahara, T.Kawakami and K.Maekawa [88,2]

The tests were carried out on cylindrical shells of concrete. The height of the cylinder was 480mm, the outer diameter 332mm, and the thickness of the cylinder 37mm. The specimens were lightly reinforced by hoops in the circumferential direction, and the reinforcement ratio was varied with the maximum at 0.9%. Details about the specimens are shown in Fig.2.1.5. To produce cracks in the axial direction, hydrostatic pressure was applied inside the shells. After producing the cracks, the specimens were loaded in the axial direction until failure.

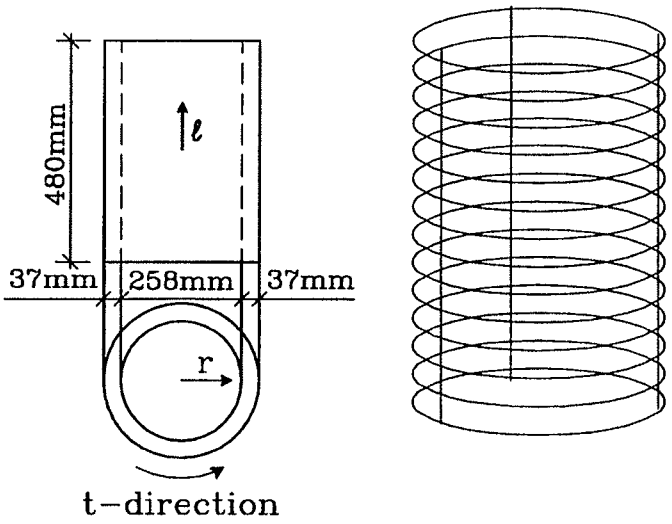

Fig.2.1.5 Skematical illustration of the specimen from [88,1]

The test results are listed in Table 2.1.4.

The ratio λ of the reduced compressive strength of the specimens to the standard compressive strength of concrete versus the initial tensile strain normal to cracks is shown in Fig.2.1.6. In the figure, some empirical formulas for the prediction of the strength reduction are shown as well. The ultimate compressive stress of the specimens is reduced compared to the standard compressive strength of concrete when the tensile strain normal to the crack increased. However, from a certain value of ε_{ti} and further, the ratio λ is almost constant. This tendency is not in agreement with that found by Vecchio and Collins [82,1]. As a matter of fact, when the tensile strain normal to the crack was large, the concrete was damaged, and the two parts at the sides of the crack became almost separate. In this case,

Table 2.1.4 Test results from [88,1]

spec. No.	f_c (MPa)	ρ (%)	$\lambda=\sigma_c'/f_c$	ε_{ti} (μ)	cracks	l_c (mm)	ω (mm)
C0	30.4	0	0.95	0	0	—	—
1	21.4	0.6	0.96	0	0	—	—
2	28.6	0.9	0.90	760	3	384	0.26
3	36.7	〃	0.80	1900	5	209	0.40
4	21.4	0.6	0.74	1910	6	174	0.33
5	28.6	0.3	0.74	2170	2	522	1.13
6	27.3	〃	0.67	3750	4	149	1.05
7	44.2	0.6	0.71	3865	6	174	0.67
8	36.7	〃	0.73	3950	3	348	1.37
9	44.2	〃	0.67	7080	7	149	1.05
10	28.6	0.9	0.65	7600	15	70	0.53
11	27.3	0.3	0.67	8070	5	209	1.68

f_c - the standard compressive strength of concrete
σ_c' - the ultimate compressive stress measured on the specimens
ε_{ti} - initial average tensile strain normal to crack
l_c, ω - the crack spacing and crack width, respectively

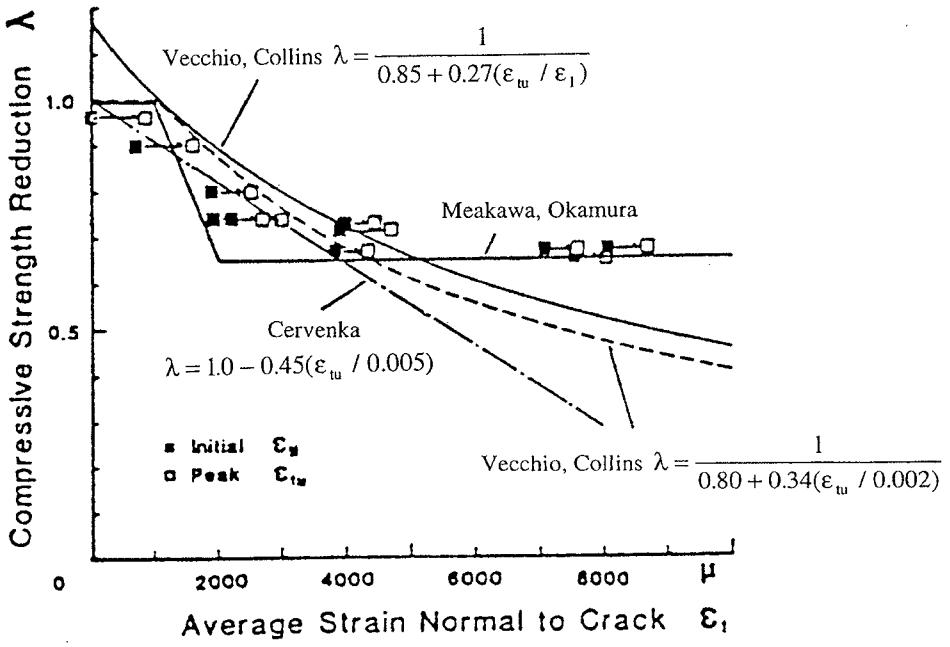

Fig.2.1.6 Strength reduction factor λ versus average tensile strain normal to crack ε_t

increasing further the tensile strain makes little change to the cracking state of the concrete, and each part of the specimen into which it was separated by the major cracks acts as prism loaded by a uniaxial load in the axial direction. The ultimate load thus obtained would not be affected furthermore by the tensile strain normal to the cracks. Here, a stepped approximation for the strength reduction factor λ is suggested where a lower limit of λ is set at about 0.65 which is obtained when the average tensile strain normal to the crack ε_{ti} exceeds 2000μ (2‰).

Tests by S.Hamada and H.Noguchi [88,3]

The specimens in the test program of [88,3] were subjected to tension-compression. The size of the specimens was 100×180×50mm. The details of the specimens are illustrated in Fig.2.1.7.

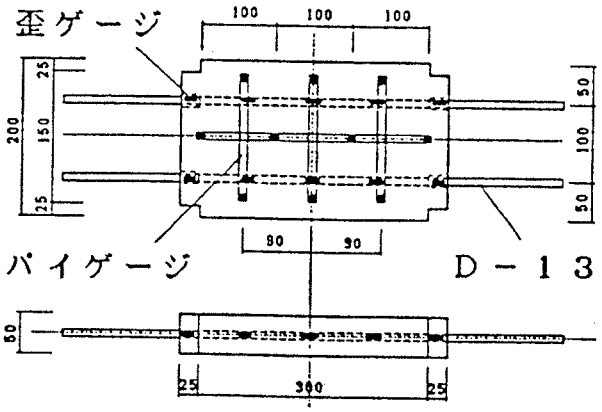

Fig.2.1.7 Details of the specimens [88,3]

The specimen was first loaded by tensile forces until the concrete was cracked. Then the compressive load was applied while the tensile stress was kept constant until failure. The average compressive strength obtained is denoted f_{c2}.

The test results are listed in table 2.1.5.

The specimen PH0-1 was plain concrete subjected to uniaxial compression. The compressive panel strength thus obtained is $f_{c.panel}=0.866f_c$.

In Fig.2.1.8 the curve of the factor f_{c2}/f_c as a function of the average tensile strain across the cracks is drawn, and the corresponding empirical

Table 2.1.5 Test results from [88,3]

Spec. No.	f_c (kg/cm^2)	reinfroce-ment type*	f_Y (kg/cm^2)	ρ (%)	ultimate strain (μ) across crack	ultimate strain (μ) in bars	ratio of f_{c2}/f_c
PH0-1	220	D13	3832	–	2180	–	0.866
PH0-2	234	D13	〃	2.54	4790	–	0.921
PH0-3	227	D13	〃	〃	3090	1060	0.893
PH0-4	213	D13	〃	〃	2660	1860	0.839
PH0-5	222	D13	〃	〃	4160	4160	0.874
PH0-6	219	D13	〃	〃	7200	3330	0.862
PH0-7	171	D13	〃	〃	8040	15900	0.673
PH0-8	184	D13	〃	〃	11940	26710	0.722
PH0-9	163	D13	〃	〃	15340	11220	0.642
PH0-10	236	φ13	3213	2.65	2300	1560	0.929
PH0-11	186	φ13	〃	〃	2930	26750	0.732
PH0-12	204	φ13	〃	〃	4020	17250	0.803

Note: f_c - the uniaxial compressive strength of concrete from φ100×200 cylinders
f_{c2} - the ultimate compressive stress of the specimen
** - D denotes deformed bars, φ plain bars*

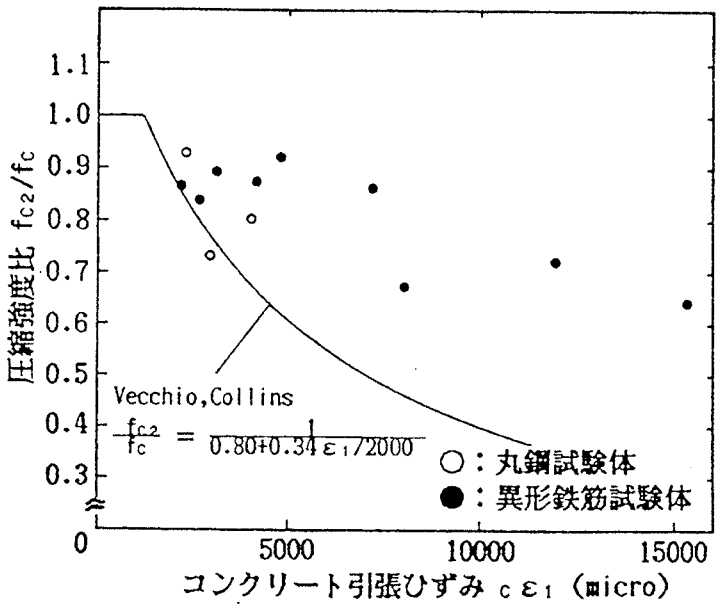

Fig.2.1.8 f_{c2} / f_c as function of average transverse tensile strain

expression for this reduction factor proposed by Vecchio & Collins is shown as well in the figure. It is immediately seen that the strength reduction obtained from this test series at large transverse tensile strain is not as much as that predicted by the Vecchio/Collins' expression.

Tests by T.Dyngeland [89,1]

The test program was divided into two main series, one series consisting of 8 reinforced concrete specimens subjected to uniaxial tensile stresses, and another consisting of 9 reinforced concrete specimens subjected to different biaxial stress states. In the biaxially tested series, the specimens were further divided into two groups. One group consisted of 4 specimens (CS1~ CS4). These specimens were loaded first by a transversal compressive stress σ_t which was kept constant while the longitudinal tensile stress σ_l varied from 0 to 4.76MPa, and then σ_l was kept constant while σ_t increased until failure. Another group consisted of 5 specimens (CS5 ~ CS9). These specimens were first subjected to varying longitudinal tensile stresses σ_l, then the transversal compressive stresses σ_t increased until failure while σ_l was kept constant. The test arrangement and the dimensions of the concrete specimens are shown in Fig.2.1.9. Two splits were made at the edges of the concrete specimens as shown in the figure to

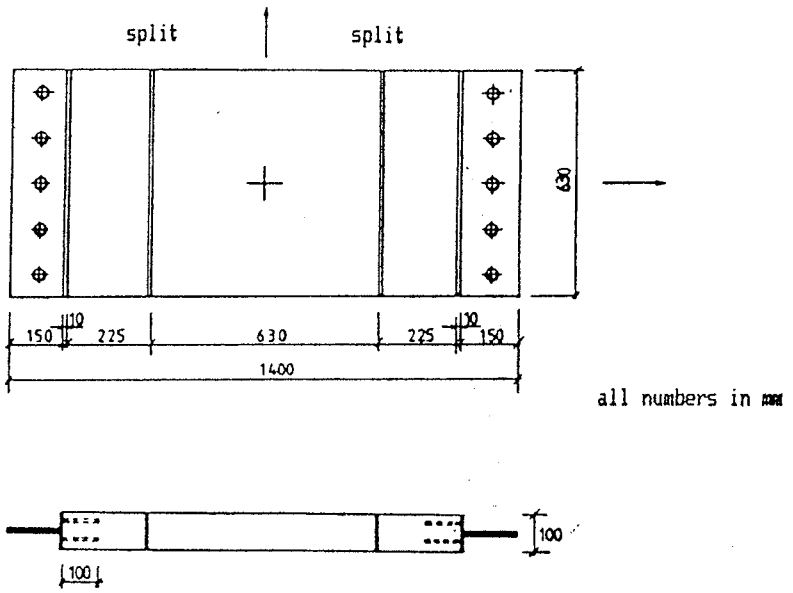

Fig.2.1.9 Test principle and dimensions of the concrete specimens

allow the inner section of the specimen to deform freely in the transverse direction, this being of course true if the dowel action of the reinforcing bars crossing these splits may be disregarded, and thus avoid the influence of the rigid steel end-anchorage on the transversely loaded inner sections of the specimen.

The test specimens were orthogonally reinforced. Fig.2.1.10 illustrates the reinforcement lay out where $\mu=\rho_x/\rho_y$, and α being the angle between the reinforcing bars and the loading directions.

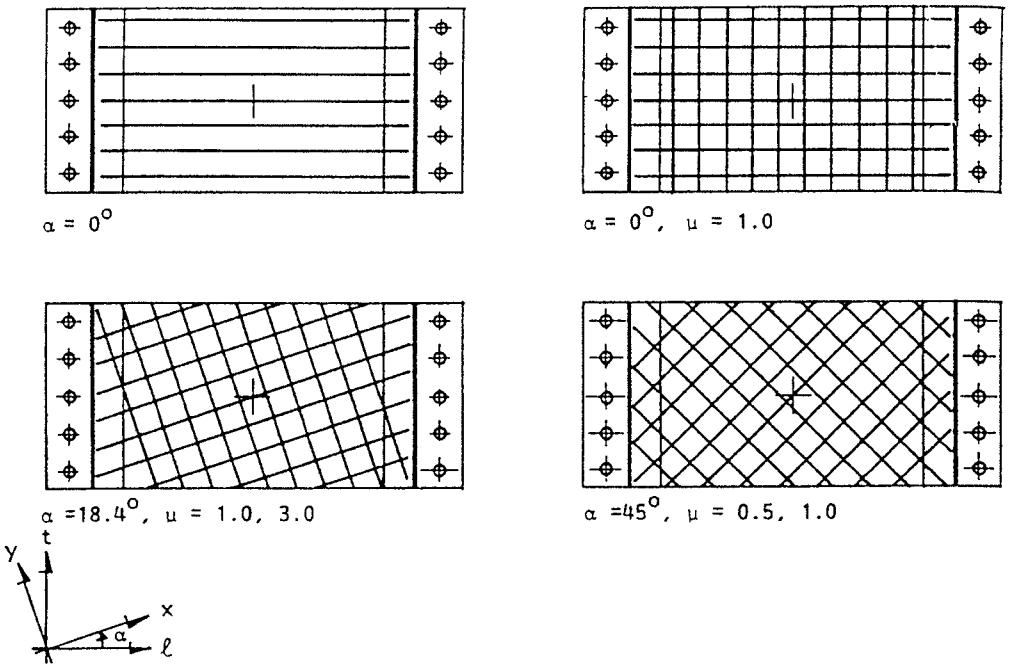

Fig.2.1.10 Lay out of the reinforcing net for different specimens

For the biaxial test specimens, six 100mm control cubes, three ϕ100×285mm cylinders and two ϕ150×300mm cylinders were cast. The cylinders were stored with the concrete specimens and tested the same day the specimens were tested to obtain the stress-strain relationship, Young's modulus and the compressive strength of concrete. The compressive strengths of concrete obtained from ϕ100×285mm cylinders and ϕ150×300mm cylinders are denoted by f_{ccs} and f_{cc}, respectively. The control cubes were stored in water with temperature of 20°C. The strength determined from these cubes at 28 days is denoted by f_c. In [89,1] the concrete cylinder strength of the ϕ100×285mm cylinders f_{ccs} was used in the comparison of the experimental results. For the specimens CS1, CS5 and

Table 2.1.6 Test results from [89,1]

spec.No	f_{cc} (MPa)	α (°)	$\mu=\rho_x/\rho_y$		σ_l (MPa)	σ_t (MPa)	σ_c (MPa)	σ_c/f_{cc}	σ_l/f_{cc}	σ_t/f_{cc}
				compre.stress level σ_t/f_{ccs}						
CS1	19.71	0/90	∞(1.12/0.00)	0.25	- 4.67	20.24	20.24	1.03	- 0.24	1.03
CS2	20.26	0/90	∞(1.12/0.00)	0.50	- 5.61	19.46	19.46	0.96	- 0.28	0.96
CS3	21.24	45	1 (1.12/1.12)	0.25	- 4.67	13.24	17.91	0.84	- 0.22	0.62
CS4	22.99	45	1 (1.12/1.12)	0.50	- 3.74	12.46	16.20	0.70	- 0.16	0.54
				tensile stress level σ_l/f_{cr}						
CS5	21.33	0/90	1 (1.12/1.12)	0.00	0.00	25.69	25.69	1.20	- 0.00	1.20
CS6	22.78	0/90	1 (1.12/1.12)	1.50	- 5.61	25.69	25.69	1.13	- 0.25	1.13
CS7	19.25	45	1 (2.51/2.51)	0.00	- 0.00	17.91	17.91	0.93	- 0.00	0.93
CS8	21.57	45	1 (2.51/2.51)	1.50	- 4.20	14.01	18.21	0.84	- 0.19	0.65
CS9	23.08	45	1 (2.51/2.51)	1.50	- 6.54	12.77	19.31	0.84	- 0.28	0.55

f_{ccs}- compressive strength of concrete from ϕ100×285mm cylinder *α- reinforcement direction, see Fig.2.1.6*

f_{cc}- compressive strength of concrete from ϕ145×300mm cylinder

σ_t/f_{ccs}, σ_l/f_{ccs} - the compressive stress level and the tensile stress level which are the constant transversal compressive or longitudinal tensile stresses applied on the specimen when the load in another direction varies.

σ_c- the internal compressive stress in concrete, for inclined reinforcement with $\alpha=45°$, $\sigma_c=\sigma_t-\sigma_l$.

CS6 f_{ccs} was modified because the cylinder strength f_{ccs} of the corresponding specimens compared with other specimens were far too low. The adjustment was made in such way that the average ratio of f_{ccs}/f_c for all specimens was about 0.90.

In the following, no readjustment on the compressive strength is made, and the results by the ϕ150×300mm cylinders are used as the uniaxial compressive strength of the concrete.

All the specimens were reinforced with K500TS with bar diameter 8mm, except CS7 and CS9 where the K400TS with 12mm were used.

Only the biaxial test results are of interest in this report, and we will not treat the uniaxial tensile tests. The test results of biaxially tested specimens are listed in Table 2.1.6.

As stated previously, the specimens with inclined bars will not be treated here, only those where the reinforcing bars are parallel or perpendicular to the loading directions are studied. The results from those specimens are shaded in Table 2.1.6.

In the test results σ_t is the stress over the whole section, including the contribution from the reinforcement in this section. By assuming yielding of the reinforcing bars at failure, we can approximately calculate the stress carried by the concrete which is denoted by σ_{tc}.

The values of σ_{tc} calculated from the test results are listed in Table 2.1.7.

Table 2.1.7 Ultimate stresses in concrete from test series [89,1]

No.	ρ_x/ρ_y	ε_{ts}(%)	E_s (MPa)	σ_{ts}	f_y(MPa)	σ_t/f_{cc}	σ_{tc}/f_{cc}	σ_l/f_{cc}
CS1	1.12/0.00	0.293	200000	586	500	1.03	1.03	-0.24
CS2	1.12/0.00	-	200000	-	500	0.96	0.96	-0.28
CS5	1.12/1.12	0.272	200000	544	500	1.20	0.94	0
CS6	1.12/1.12	0.311	200000	622	500	1.13	0.88	-0.25

It appears from the table that the higher the transverse tensile stress, the lower the ultimate compressive stresses in the concrete at failure, which is as expected. However, the ultimate compressive stresses are not reduced to any high degree due to the existence of the transversal tensile stress. This result is at variance with the results by other researchers.

Tests by J.Kollegger & G.Mehlhorn [90,3]

In the test program described in [90,3], 47 panels were tested to investigate the effect of the transverse tensile stresses and strains on the compressive strength of concrete.

The size of the specimens was 500×1000×100mm, and the orthogonal reinforcing bars were placed in two layers. The directions of the reinforcement are at $\theta=0$ or at $\theta=45°$ to the loading directions. Dimensions of the specimens and the reinforcement lay out are shown in Fig.2.1.11.

The loading principle is illustrated in Fig.2.1.12.

According to the difference in the reinforcement, the specimens are divided into 5 main series. In table 2.1.8 and 2.1.9 the test results for the panels where the reinforcing bars at $\theta=0$ and $\theta=45°$ to the loading directions are listed.

The results from the series 5 where the panels were nonreinforced correspond to what we termed the compressive panel strength $f_{c.panel}$ which we found to be rather low.

The ultimate principal compressive stresses σ_{b2}/f_{cu} are plotted versus the transverse tensile strain $\varepsilon_{1.max}$ and the principal tensile stress σ_{b1}/f_{cu} in Fig.2.1.13 and Fig.2.1.14, respectively.

From the figures it is seen that the compressive strength of the panels displayed neither a dependency on the transverse tensile strain nor on the transverse stress. In average the compressive strength reduction of the panels compared with the cube crushing compressive strength of concrete is about 0.7, that means around 20% reduction compared with corresponding cylinder strength. If compared with the corresponding panel strength, little reduction of the ultimate compressive stress is observed.

The test results obtained here are at variance with the conclusions by many other research groups.

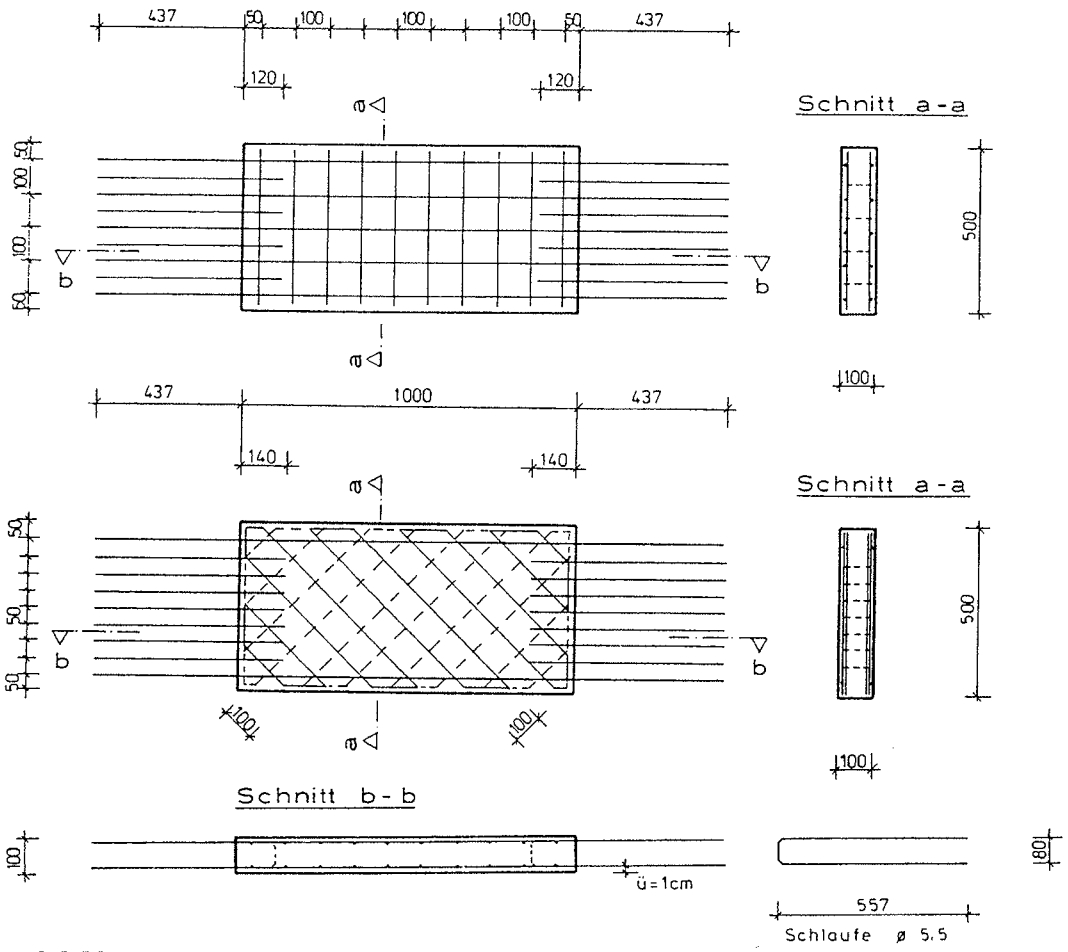

Fig.2.1.11 Dimensions of specimen and reinforcement lay out [90,3]

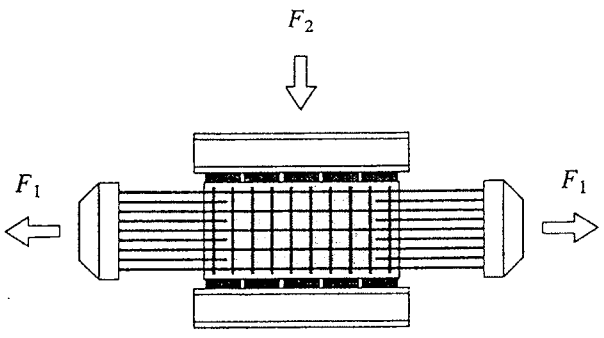

Fig.2.1.12 Loading principle [90,3]

Table 2.1.8 Test results for specimens with reinforcing bar angle θ=0 from [90,3]

Series		No.	f_{cu} MPa	d mm	rebars quality	σ_1 MPa	$\varepsilon_{1.max}$ ‰	σ_{b1}/f_{cu}	σ_{b2}/f_{cu}
		EGE102	22.2			1.9	1.34	0.104	0.66
		103	14.0			1.2	0.72	0.049	0.68
		104	21.3			2.2	1.52	0.113	0.71
		105	17.6			3.5	2.10	0.137	0.69
		106	16.9			6.0	4.07	0.024	0.73
		107	17.9			6.2	—	—	—
		108	20.8		ribbed bar	0.0	1.81	0.043	0.60
1		110	17.4	10.0	420/500 RU	6.3	5.54	0.000	0.64
		111	19.1			6.6	7.73	0.000	0.63
		112	22.3			6.7	7.55	-0.009	0.59
		113	11.9			0.0	0.67	0.176	0.71
		114	16.3			1.2	1.08	0.135	0.75
		115	16.3			2.8	1.43	0.029	0.62
		116	21.9			4.4	1.84	0.050	0.59
		117*	18.3			6.3	6.25	0.000	0.48
2	2A	EGE601	18.1		ribbed bar	2.3	3.27	0.017	0.69
		602	20.8		420/500RU	1.2	1.66	0.043	0.72
		603	16.1	6.5		0.0	1.15	0.093	0.77
	2B	EGE701	17.2		ribbed bar	2.4	2.51	0.058	0.61
		702	21.0		500/550RK	2.4	2.71	0.038	0.62
		703	15.4			0.0	1.18	0.104	0.66
		704	17.7			3.0	2.21	0.204	0.61
3	3A	EGE851	16.1		ribbed bar	2.0	1.52	0.093	0.66
		852	20.1		500/550RK	3.4	2.53	0.085	0.65
		853	21.2			4.8	3.62	0.038	0.56
	3B	MGE851	18.5		ribbed bar	2.0	1.44	0.065	0.71
		852	18.3	8.5	500/550RK	3.4	2.68	0.071	0.67
		853	19.3			4.6	4.62	0.026	0.66
	3C	MGL851	19.4		plain bar	2.0	1.76	0.109	0.64
		852	21.5		500/550GK	3.4	2.26	0.084	0.66
		853	19.2			4.8	3.37	0.083	0.56
5		OHNE01	21.3				1.79	0.042	0.74
		02	25.7	—	—	—	2.23	0.043	0.71
		03	20.8				3.46	0.000	0.53
		04	19.6				3.56	0.000	0.59

*Note: * local failure*

f_{cu} - compressive crushing strength of concrete from cubes 200×200×200mm

σ_1 - applied principal tensile stress *$\varepsilon_{1.max}$ - principal tensile strain at failure*

σ_{b1} - tensile stress in concrete at failure *σ_{b1} - ultimate compressive stress in concrete*

Table 2.1.9 Test results for specimens with reinforcing bars at angle θ=45° from [90,3]

Serie		No.	f_{cu} MPa	d mm	rebars quality	σ_1 MPa	$\varepsilon_{1,max}$ °/oo	σ_{b1}/f_{cu}	σ_{b2}/f_{cu}
4	4A	EGE6F1	19.8		ribbed bar	2.0	4.42	-0.035	0.71
		6F2	20.0		420/500RU	2.5	4.58	-0.005	0.74
		6F3	18.2			2.9	6.66	0.022	0.72
		6F4	21.4			3.2	7.68	0.019	0.64
		6F5	23.6			0.0	2.68	0.013	0.72
		6F6	23.0	6.5		3.0	2.49	0.026	0.75
		6F7	23.5			1.4	3.61	-0.021	0.66
		6F8	16.4			1.8	4.17	-0.019	0.80
	4B	EGE7F1	19.9		ribbed bar	2.4	5.55	0.020	0.75
		7F2	19.1		500/550	2.8	6.89	0.037	0.75
		7F3	21.6			1.4	3.01	0.009	0.75
		7F4	17.7			0.0	1.93	0.028	0.84

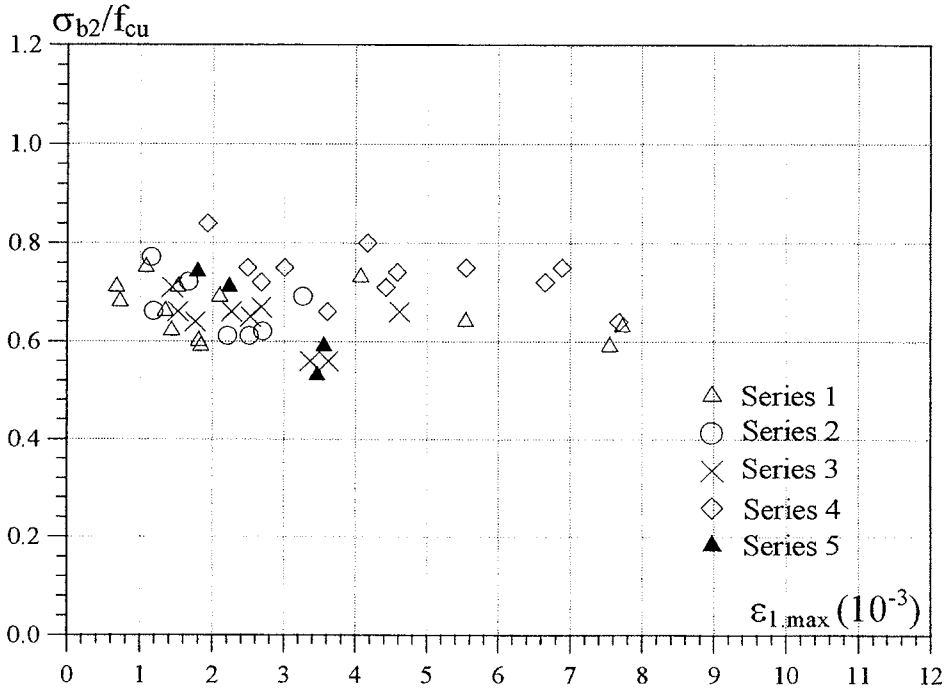

Fig.2.1.13 Compressive strength of concrete versus transverse tensile strain[90,3]

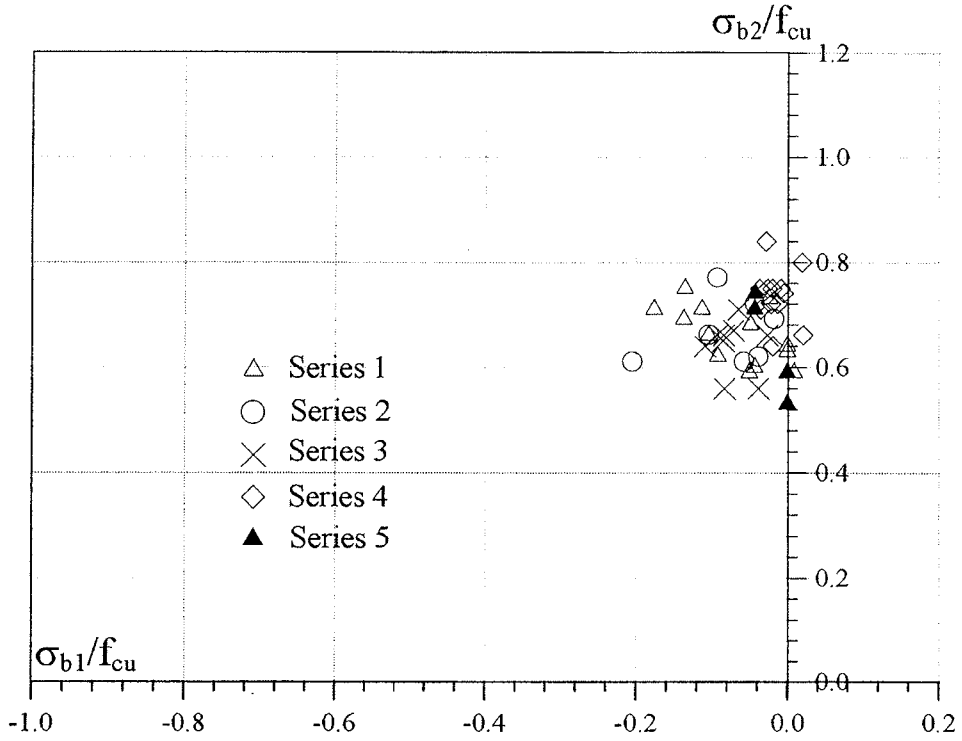

Fig.2.1.14 Compressive strength of concrete versus transverse tensile stress [90,3]

Tests by A.Belarbi & T.T.C. Hsu [95,1]

The test program consists of 22 full-size reinforced concrete panels subjected to tension in one direction and compression in the perpendicular direction. The size of the test panels is 55×55×7in (140×140×18cm). The arrangement of the reinforcement and the loading conditions are illustrated in Fig.2.1.15. The reinforcing bars are placed in two layers adjacent to the faces of the panel. The main reinforcement is arranged in the longitudinal direction along the *l* axis and a minimum reinforcement with ratio of 0.54% is placed orthogonally in the transverse direction along the t axis.

The uniaxial compressive strength of concrete is determined from the standard 6×12in (150×300cm) concrete cylinders at 28 days.

Besides the differences in the lay out of the reinforcement, two loading paths were applied. One is the sequential loading where tensile stress was applied first until a certain strain ε_{ri} in the longitudinal bars was reached and then the compression stress followed in the vertical direction. The

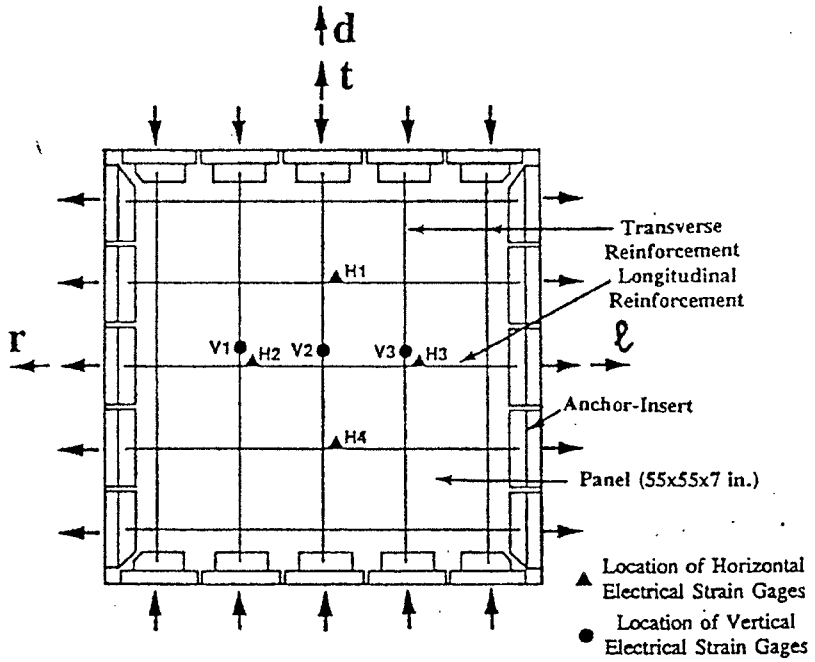

Fig.2.1.15 Lay out of the test specimen [95,1]

other one is proportional loading where the compressive stress and the tensile stress are applied with a fixed ratio. The tests were carried out using a load-controlled procedure.

The specimens were divided into 6 different main groups according to the objective. Panels in **Group I** were mainly subjected to uniaxial compressive stresses. **Group II** panels were sequentially loaded. This group is intended to investigate the influence of the principal tensile strain on the load carrying capacity the reinforcement lay out being fixed. **Group III** was designed to study the effect of the amount of reinforcement. The reinforcement ratio was varied while the other parameters were kept the same as in Group II. **Group IV** was made to investigate the influence of reinforcing bar spacing on the load carrying capacity. **Group V** was similar to Group II except that the loading path differed. Instead of sequential loading, the panels in this group were first tensioned to a certain strain, and then the tensile stress was released. Thereafter, compressive load was applied until failure. The purpose of this group is to check whether the strength reduction is caused by the residual strains or by the presence of the tensile stress. Panels in **Group VI** were subjected to proportional loading.

The details of the specimens and the test results are listed in table 2.1.10.

Table 2.1.10 Test results from [95,1]

No.	f_c (psi)	ρ (%)	Bar size	s (in)	$\varepsilon_{rf}(10^{-3})$	σ_p (psi)	σ_p/f_c	Loading
Group I								
REF	6470	1.20	#6	10.5	0.5260	5058	0.78	U.C.
EO	5410	0.30	#3	"	0.0065	4868	0.90	B.C.
Group II								
E1.5-1	6465	1.20	#6	10.5	2.0245	4111	0.64	S.L.
E2-1	6919	"	"	"	4.3135	3395	0.49	"
E2′-1	5742	"	"	"	4.6355	4335	0.76	"
E2″-1	5982	"	"	"	4.3698	3936	0.66	"
E4-1	5883	"	"	"	9.0160	3014	0.51	"
E10-1	5902	1.27	20M	"	27.6444	1494	0.25	"
Group III								
E4-.5	5687	0.54	#4	10.5	8.6500	5659	1.00	S.L.
E4-1	5883	1.20	#6	"	9.0160	3014	0.51	"
E4-2	5372	2.10	25M	"	9.6970	2747	0.51	"
Group IV								
E2-1	6919	1.20	#6	10.5	4.3135	3395	0.49	S.L.
E2-1A	6506	1.09	#4	5.25	3.1605	4407	0.68	"
E1.5-1B	5656	1.20	#3	2.625	2.8855	4436	0.78	"
E4-1	5883	"	#6	10.5	9.0160	3014	0.51	"
E4-1A	5410	1.09	#4	5.25	8.9500	2973	0.55	"
E2-1B	5558	1.20	#3	2.625	7.3495	3189	0.57	"
E10-1	5902	1.27	20M	10.5	27.6444	1494	0.25	"
E10-1A	5350	1.69	15M	5.25	25.9300	1872	0.35	"
E10-1B	5742	1.69	10M	2.625	37.0750	1815	0.32	"
Group V								
R4-1	6090	1.27	20M	10.5	4.7855	4825	0.79	S.L./R
R10-1	5663	"	"	"	9.6050	3025	0.53	"
R30-1	5905	"	"	"	29.3300	1867	0.32	"
Group VI								
F2	5818	1.27	20M	10.5	27.9800	1719	0.30	P.L.
F3	6181	"	"	"	14.3349	2719	0.44	"
F4	6076	"	"	"	7.2570	3024	0.50	"

Note: 1. Digits after letter E indicates the tensile strain at start of compression phase

2. Digit after Letter F indicates the ratio of the compressive stress to the tensile stress in the proportional loading

3. f_c - Uniaxial compressive cylinder strength of concrete

σ_p - *Peak compressive stress of reinforced concrete panel*

4. *s - Spacing of longitudinal reinforcement*
5. ε_{rf} - *Average principal tensile strain of concrete in principal tensile direction*
6. *U.C. - Uniaxial compression*
   B.C. - Biaxial compression
   S.L. - Sequential loading (tension followed by compression)
   P.L.- Proportional loading
   S.L./R.- Sequential loading (compression after release of tensile forces).

The result of the specimen REF is what we termed the panel strength. It is seen that the ratio of the panel strength to the uniaxial compressive cylinder strength is around 0.78. Panel EO is loaded perpendicular to the direction of the main compressive load to compensate for the Poisson effect. The strength reduction of this panel is only about 10% compared with the uniaxial compressive cylinder strength.

The term "peak stress softening coefficient" is by definition the same as the strength reduction factor or the effectiveness factor as mentioned previously.

The strength reduction factor or the peak stress softening coefficient as a function of the principal tensile strain is plotted in Fig.2.1.16. In the figure, the empirical formulas for the estimation of the strength reduction factor suggested by different research groups are also plotted. The large difference between the different empirical formulas is obvious in the figure.

Little difference in the compressive strength of the panels is found between the cases where proportional loading was applied and the ones where the sequential loading was applied provided the tensile stress was retained. In the sequential loading, where the tensile stress was released when the compressive forces were applied, the load path had some influence on the compressive strength of the panels, but only little. An interesting phenomenon is that the strength reduction factor is independent of the amount of the tensile stress released. The reason is probably that the concrete has been spoiled when the tensile stress was applied, and the manner how the tensile stress is applied has little effect on the extent of the damage. If the strength mainly depends on the internal cracking state, it is natural that the load path has little influence on the load carrying capacity. However, when the tensile stress is released by a small amount, some of the cracks will close. The closure of the cracks is not proportional to the release of the tensile stress, actually it is expected that the closure of cracks stops soon.

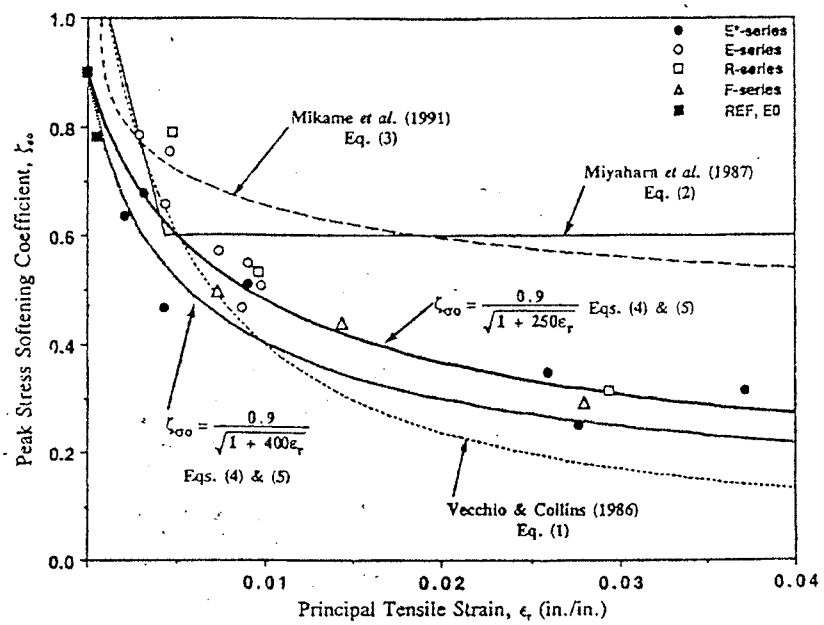

Fig.2.1.16 Strength reduction factor as function of principal tensile strain [95,1]

Therefore, the extent of the releasing of the tensile stress does not make much difference to the load carrying capacity.

The strength reduction factor increases when the reinforcement ratio is increased. However, this effect is not significant as seen from Fig.2.1.17.

The smaller spacing of the reinforcing bars did improve the strength of the panels. Nevertheless, the effect was small as shown in Fig.2.1.18.

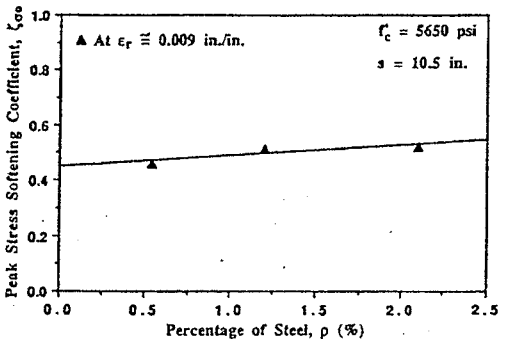

Fig.2.1.17 Effect of ρ

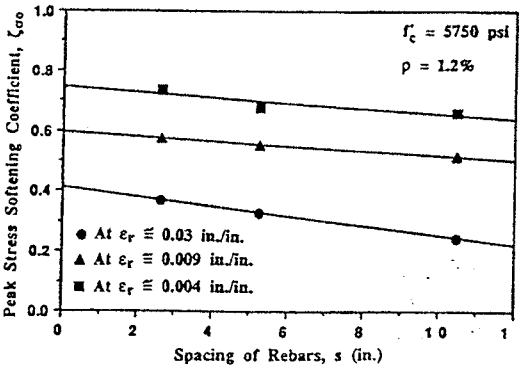

Fig.2.1.18 Effect of rebar spacing

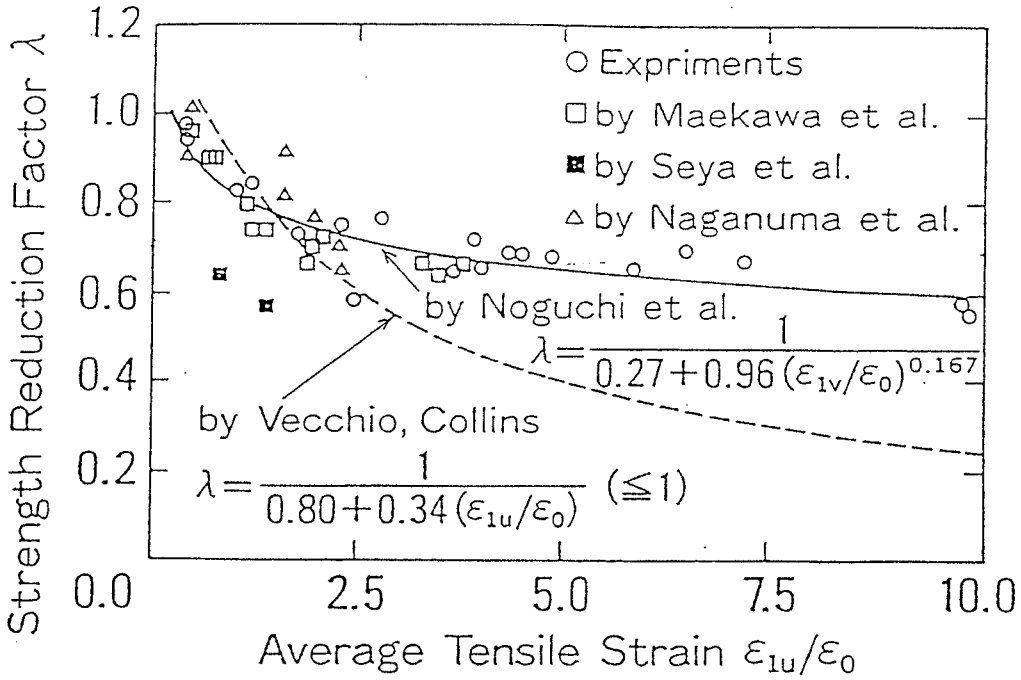

Fig.2.1.19 Strength reduction factor versus transverse tensile strain [88,2]

Concluding Remarks

In the last two decades, numerous experiments have been carried out to investigate the strength reduction of concrete under in-plane stresses states. A general idea about the various research results can be seen in Fig.2.1.6 and Fig.2.1.19, where the two major opinions regarding the compressive strength reduction are illustrated. One opinion, represented by Vecchio/Collins' formulas [82,1], insists that the compressive strength of concrete strongly depends on the transverse tensile strain, and the reduction of the compressive strength may be as high as about 80%. Another opinion, mainly represented by research groups in Japan, suggests that the tensile strain is not dominating factor in the compressive strength reduction, and there exists a lower limit of the compressive strength around $0.65f_c$, where f_c is the standard uniaxial compressive strength. Up to now agreement on the interpretation of the various test results has not been achieved.

2.2 In-plane pure shear tests

Tests by F.Vecchio & M.P.Collins [82,1]

The test program was made to investigate the behaviour of reinforced concrete panels subjected to in-plane stresses. The tests consisted of 30 reinforced concrete panels subjected to different combinations of in-plane normal and shear stresses. Among those, the panels subjected to pure shear are of particular interest to this paper. In the following, we will concentrate on the pure shear tests.

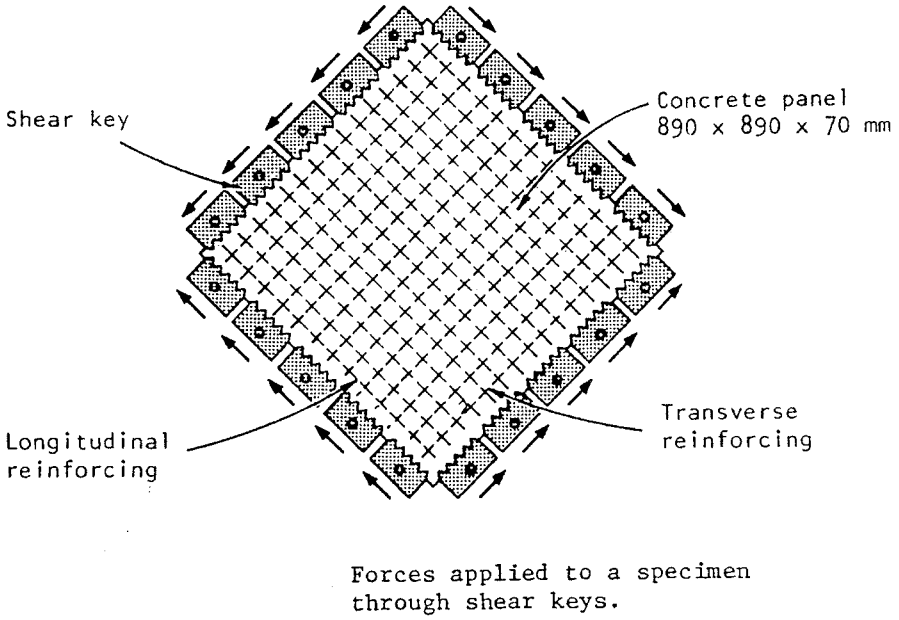

Fig.2.2.1 Schematical illustration of the test set-up in [82,1]

22 panels were tested in pure shear. According to the details of the reinforcement in the two directions, the panels were divided into two groups. In group I, the panels were isotropically reinforced where the ratio of the reinforcement was varied. In group II, the panels were orthotropically reinforced.

Fig.2.2.1 shows schematically the loading principle, and the arrangement of the reinforcement. The load was applied to the panel by means of hydraulic jacks connected to "shear keys" at the perimeter of the panel. Details about the loading arrangement may be found in [82,1].

The size of the concrete panels were 890×890×70mm. The panels were reinforced by two layers of reinforcing nets which were made of smooth bars welded in the crossing points. The thickness of the cover was 6mm. Bar diameter was varied. To avoid local failure in the load transfer regions, a relatively stronger concrete was cast in a 100mm band around the perimeter, while a weaker concrete was used in the center region of the panels. The concrete compressive strength in the center region varied from 15MPa to 30 MPa.

The test results are listed in Table 2.2.1. In the table index L means longitudinal, t transverse. Further v_u is the shear stress at failure, and f_c' the measured compressive stress in the concrete at failure.

In group I tests, the isotropic panels, initial cracks formed at 45° to the reinforcement direction. The number and the width of the cracks increased when the load was increased, but the average crack direction did not change at failure. The ultimate failure occurred either by yielding of reinforcement bars or by a sliding failure of the concrete prior to the yielding of the reinforcing bars. In some of the panels, local failure in the shear keys happened.

In group II tests, the orthotropic panels, the initial cracks also formed at 45° to the reinforcement direction. At failure, new cracks were formed and these cracks became more acute to the longitudinal direction which was the strongest one (regarding the definition of longitudinal and transversal direction, see Fig.2.2.1). The shift of the crack direction was particularly obvious after the yielding of the transverse reinforcement. The failure occurred either by yielding of the reinforcement in both directions or sliding shear failure of concrete prior to the yielding of the reinforcement.

In Fig.2.2.2 typical crack patterns of the orthotropically reinforced specimen are illustrated by showing the pictures of the panel PV12 after failure. Notice the clear shift in the direction of the final cracks compared with the initial cracks in the specimen.

Two panels, PV15 and PV17 were uniaxially loaded by compression. The test results are listed in table 2.2.2. Assuming yielding of the reinforcing bars in the loading direction, the stress carried by the concrete, denoted by f_{cc}', can be determined, which corresponds to what we termed the compressive panel strength. The test of PV15 was terminated before failure occurred. The panel PV17 showed a compressive panel strength which is

Table 2.2.1 Test results from [82,1]

	specimen	ρ_L (%)	f_{yL} (MPa)	ρ_t(%)	f_{yt}(MPa)	f_c (MPa)	v_u (MPa)	f_c' (MPa)	v_u/f_c	f_c'/f_c	mode of failure
Group I isotropic panels	PV 2	0.183	428	0.183	428	23.5	1.16	1.468	0.049	0.062	concrete cracking
	3	0.483	662	0.483	662	26.6	3.07	5.303	0.115	0.199	steel fracture
	16	0.740	255	0.740	255	21.7	2.14	4.070	0.099	0.188	steel yielding
	5	0.742	621	0.742	621	28.3	4.24	7.921	0.156	0.280	pull-out
	4	1.056	242	1.056	242	26.6	2.89	5.598	0.109	0.210	steel yielding
	9	1.785	455	1.785	455	11.6	3.74	7.577	0.322	0.653	concrete shear
	14	1.785	455	1.785	455	20.4	5.24	9.745	0.257	0.478	pull-out
	6	1.785	266	1.785	266	29.8	4.55	8.944	0.153	0.300	steel yielding
	7	1.785	453	1.785	453	31.0	6.81	13.377	0.220	0.432	pull-out
	8	2.616	462	2.616	462	29.8	6.67	13.300	0.224	0.446	pull-out
Group II orthotro-pic panels	PV 13	1.785	248	—	—	18.2	2.01	3.837	0.110	0.211	concrete shear
	18	1.785	431	0.315	412	19.5	3.04	5.769	0.156	0.296	concrete shear
	12	1.785	469	0.446	269	16.0	3.13	5.581	0.196	0.349	concrete shear
	19	1.785	458	0.713	299	19.0	3.95	7.296	0.208	0.384	concrete shear
	20	1.785	460	0.885	297	19.6	4.26	7.815	0.217	0.399	concrete shear
	10	1.785	276	0.999	276	14.5	3.97	7.209	0.274	0.497	concrete shear
	26	1.785	456	1.009	463	21.3	5.41	10.156	0.254	0.477	concrete shear
	21	1.785	458	1.296	302	19.5	5.03	9.532	0.258	0.489	concrete shear
	11	1.785	235	1.306	235	15.6	3.56	7.210	0.228	0.462	steel yielding
	22	1.785	458	1.524	420	19.6	6.07	11.490	0.310	0.586	concrete shear
	PV 1	1.785	483	1.680	483	34.5	8.02	15.748	0.232	0.456	pull-out
	27	1.785	442	1.785	442	20.5	6.35	10.428	0.310	0.509	concrete shear

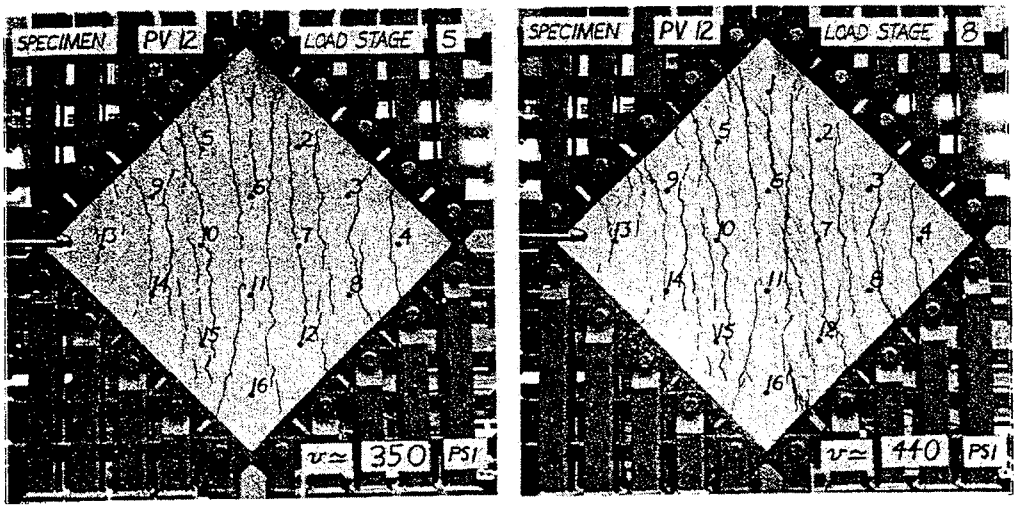

Fig.2.2.2 Crack patterns of orthotropically reinforced panel PV12 [82,1]

Table 2.2.2 Test results from [82,1]-uniaxial compression

No.	ρ_l(%)	f_{yl} (MPa)	ρ_t (%)	f_{yt} (MPa)	f_c (MPa)	f_c'/f_c	f_{cc}'/f_c	note on test
PV15	0.74	255	0.74	255	21.7	0.82	—	not to failure
17	"	255	"	255	18.6	1.04	0.94	ultimate failure

lower than the compressive cylinder strength f_c, but the difference is much smaller than that observed in some of the test previously described. The reason is probably that the panels were cast in horizontal position.

In the experiment, the principal compressive stresses f_c' as well the principal compressive strains were measured. Such a principal compressive stress-strain curve is reproduced in Fig.2.2.3. For comparison also a standard stress-strain curve for concrete is shown. From the figure the concrete is seen to be very ductile but the ultimate strength is substantially reduced compared with the standard uniaxial compressive strength of concrete.

The authors in [82,1] argued that the presence of simultaneous large transverse tensile strains were the cause of this reduction. In Fig.2.2.4 the ratio of the measured peak principal compressive stress of the panels and the uniaxial compressive cylinder strength of the concrete versus the corresponding lateral average tensile strain ratio $\varepsilon_{dt}/\varepsilon_d$ is drawn. Here ε_{dt} and ε_d are the average principle tensile strain and compressive strains observed in the specimens at failure, respectively.

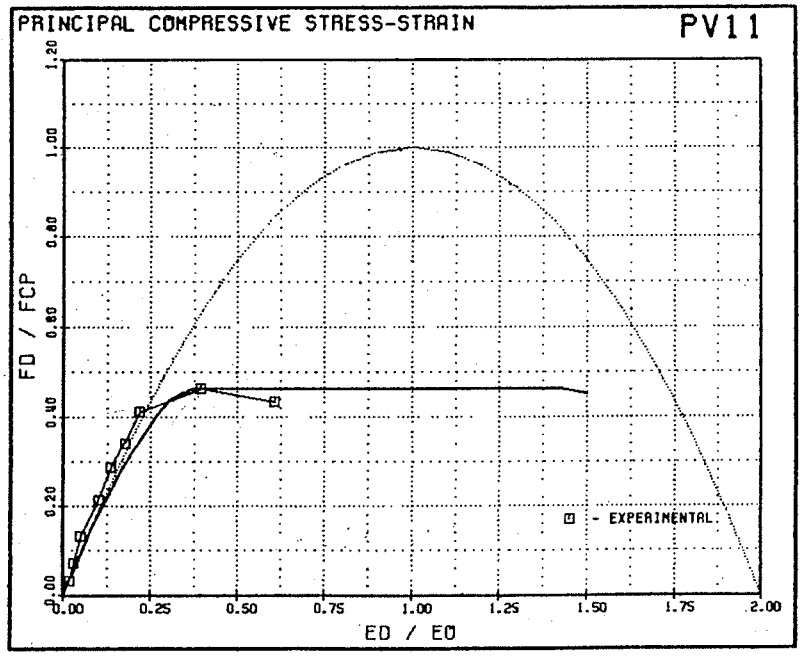

Fig.2.2.3 Principal compressive stress-strain of PV11 [82,1]

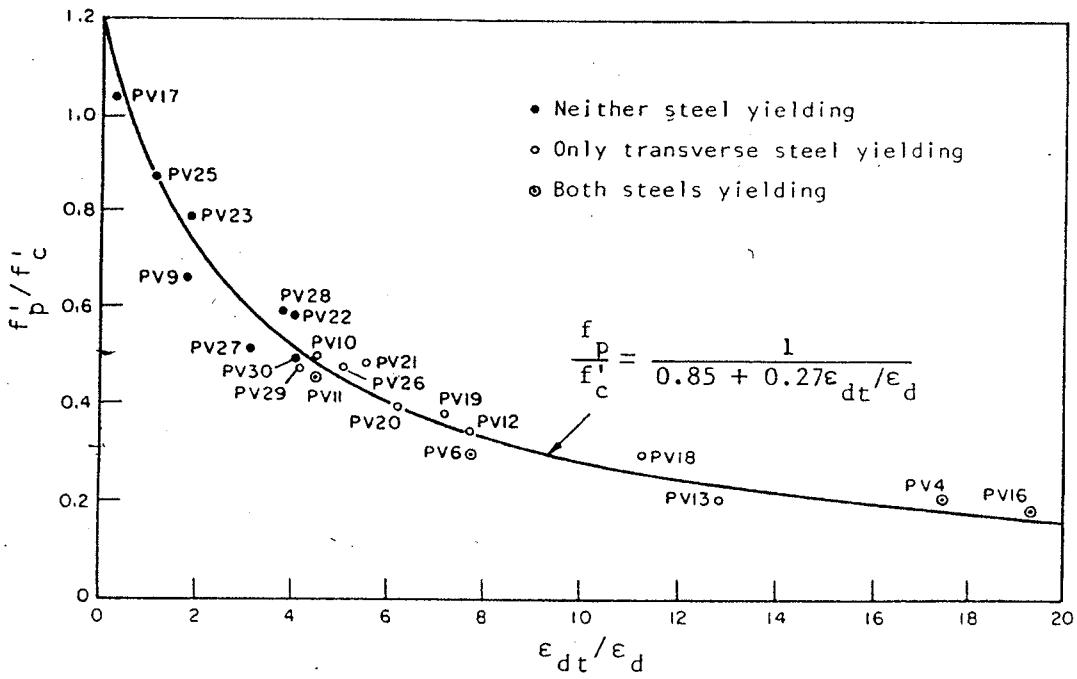

Fig.2.2.4 Peak principal compressive stress reduction as function of ε_{dt} /ε_d [82,2]

An analytical curve proposed by the authors in [82,1] is also depicted in the figure.

By analyzing the test data in details, we can see that four panels, PV4,6,11,16, failed by yielding of both the longitudinal and transverse reinforcing bars, among which one specimen, PV11, was orthotropically reinforced and the rest were isotropically reinforced. Eight of the orthotropically reinforced specimens except PV22 (also one specimen, PV9, of the isotropically reinforced panels), failed by crushing of concrete where the transverse reinforcement had yielded but the longitudinal reinforcing bars did not yield. The rest of the specimens failed by concrete crushing before neither the transverse nor the longitudinal reinforcement had yielded.

When the reinforcement yields prior to the failure, the load carrying capacity is dominated by the strength and the amount of the reinforcement in the panels, instead of the concrete strength. Therefore, it seems improper to include those test results where the reinforcement yielded before the failure in the strength reduction curve of concrete. Excluding the test points with transverse steel yielding and both steel yielding, the peak principal compressive strength compared with the uniaxial compressive strength of concrete does not display the tendency predicted by the analytical formula proposed in [82,1] and shown in Fig.2.2.4. Therefore, the strength reduction of concrete as a function of the transverse tensile strain is rather doubtful.

Besides the pure shear tests, 4 panels subjected to combined shear and normal stresses were tested as well. The test results are listed in Table 2.2.3. In the shear-normal stress test, the specimens were subjected to shear and biaxial compression, except PV28 which was tested in shear and biaxial tension.

From the failure mode of PV28 which was in shear and biaxial tension, it appears that the failure pattern of the panel was almost the same as that of

Table 2.2.3 Test results from [82,1]-combined shear and biaxial stresses

No.	ρ_L (%)	f_{yL} (MPa)	ρ_t (%)	f_{yt} (MPa)	f_c (MPa)	v_u (MPa)	mode of failure
PV23	1.785	518	1.785	518	20.5	8.87	concrete shear
24	〃	492	〃	492	23.8	7.94	〃
25	〃	466	〃	466	19.2	9.12	〃
28	〃	483	〃	483	19.0	5.80	〃

the panels in pure shear. The ultimate shear stress was substantially reduced due to the existence of the tensile stresses.

The failure pattern of the panels subjected to shear and biaxial compression stresses as well as the ultimate shear stress was strongly influenced by the existence of the normal stress. The load carrying capacity was increased considerably due to the compressive stresses.

Tests by K.Sumi, M.Osa & S.Kawamat [90,2]

The test series in [90,2] consists of 39 reinforced panels subjected to in-plane stresses. The objective of the tests was to investigate the post cracking behaviour of panels.

The panels were subjected to pure shear. The shear loading was realized by applying tensile forces to the loading arms in four steel plates around the panel. The loading set up is illustrated in Fig.2.2.5.

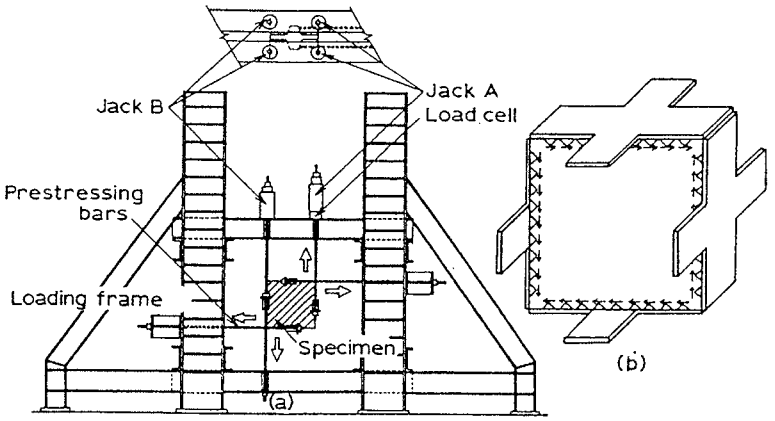

Loading system. (a) Loading apparatus; (b) shear keys.

Fig.2.2.5 Loading system in [90,2]

The specimens were 60×60×8cm, and two layers of reinforcement were used. The diameter of the reinforcing bars was 6mm, and the yield stress f_y=400.5MPa. Shear keys made of pieces of steel angles were welded to the steel plates around the panel. For reducing the restraints to the natural opening of the cracks induced by the steel plates around the specimen, rubber plates were bonded on the surfaces of the shear keys. Details may be found in [90,2].

By the way of reinforcing, the specimens may be subdivided into two groups, isotropically reinforced panels and orthotropically reinforced panels. Within each group, the bond conditions, the aggregate interlock actions as well as the boundary conditions are varied.

Besides the normally cast panels, symbolized by PLA, two other types of specimens were also cast.

To investigate the aggregate interlock action, one type of specimen was provided with a thin steel sheet in the direction of the anticipated cracks, which was at 45° to the edges. This was done to remove the aggregate interlock action artificially. This type of specimen is designated by PLS.

The PLG specimens had grooves of 7mm depth in both surfaces to produce cracks at specified crack-lines. The direction of the grooves was at 45° to the edges.

The arrangement of the PLG and PLS specimens is illustrated in Fig.2.2.6.

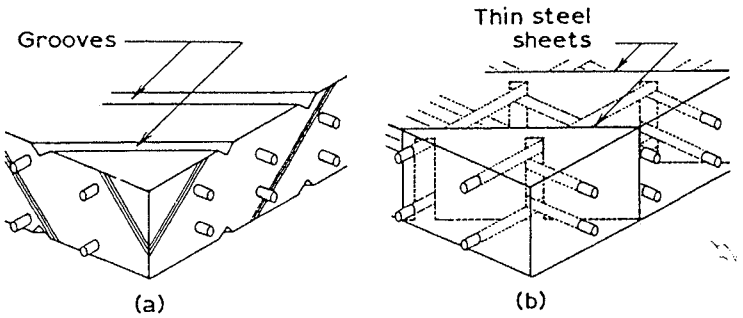

Specified crack-lines. (a) PLG specimen; (b) PLS specimen.

Fig.2.2.6 PLG and PLS specimens

In the tests, the effect of bond between the rebars and the concrete was also investigated. Besides those with normal bond, the rebars in some of the specimens were lapped with cloth tape to exclude bonding to the concrete.

Two ways of fixing the ends of the rebars were used in the tests: one way where the ends of the rebars were lap-welded to screw bolts which were fixed by nuts on the outer surface of the steel plates, and another way where the rebars were welded to square steel bars exterior of the steel plates. The details may be found in [90,2].

The legend for the specimen symbol is the following

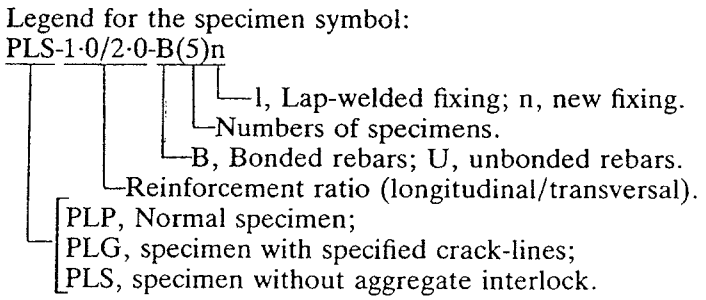

The test results are listed in table 2.2.4.

For series (a) and (b) where the panels were isotropically reinforced, it was observed in the tests that the width of the cracks increased without slipping in the cracks when the load was increased, while for series (c), where the panels were orthotropically reinforced, not only crack opening grows but also slipping of the opposite surfaces occured along the cracks. This observation indicates that sliding failure along the existing cracks takes place at failure.

In series (a) isotropically reinforced panels, normally cast, with grooves and with steel sheets, were tested. The test results τ_{max}/f_c show the tendency that the normally cast panels have higher shear load carrying capacity than the other two types of specimens.

In series (b), isotropically reinforced panels with grooves where the bond condition was varied were tested. The test results did not show a clear effect of the bond on the load carrying capacity. The microcracking state in the concrete will be less severe if the reinforcement is not bonded to the concrete than that if the reinforcement is bonded. From this point of view, the load carrying capacity where the reinforcement was not bonded is expected to be higher or at least equal to that where the reinforcement was bonded. The test results of these two types of specimens did not show this tendency. However, the difference in the load carrying capacity of panels with or without bond is not large, for B-13 (bonded) and B-14 (unbonded) the difference is 14%, and for the rest it is less than 7%.

In series (c), reinforced panels with grooves and with thin steel sheets were tested. The main concern here was to find the effect of the aggregate

Table 2.2.2 Test results from [90,2]

	No.	Symbol	f_c(kg/cm^2)	ρ_y(%)	ρ_x(%)	τ_{max}(kg/cm^2)	τ_{max}/f_c
(a)	A-1	PLP-1.0-B *l*	231	1.06	1.06	46.3	0.200
	A-2	PLP-1.5-B *l*	221	1.47	1.47	58.6	0.265
	A-3	PLP-2.0-B *l*	215	2.00	2.00	72.9	0.339
	A-4	PLG-1.0-B *l*	220	1.06	1.06	49.4	0.225
	A-5	PLG-1.5-B *l*	220	1.47	1.47	55.7	0.253
	A-6	PLG-2.0-B *l*	245	2.00	2.00	56.8	0.232
	A-7	PLS-1.0-B *l*	252	1.06	1.06	47.6	0.189
	A-8	PLS-1.5-B *l*	252	1.47	1.47	58.7	0.233
	A-9	PLS-2.0-B *l*	238	2.00	2.00	71.9	0.302
(b)	B-1	PLG-0.5-B *n*	238	0.53	0.53	26.6	0.112
	B-2	PLG-0.5-U *n*	250	0.53	0.53	26.9	0.108
	B-3	PLG-1.0-B(1) *l*	265	1.06	1.06	42.2	0.159
	B-4	PLG-1.0-U(1) *l*	265	1.06	1.06	42.6	0.161
	B-5	PLG-1.0-B(2) *n*	306	1.06	1.06	46.1	0.151
	B-6	PLG-1.0-U(2) *n*	315	1.06	1.06	46.6	0.148
	B-7	PLG-1.5-B(1) *l*	231	1.47	1.47	56.6	0.245
	B-8	PLG-1.5-U(1) *l*	231	1.47	1.47	60.0	0.260
	B-9	PLG-1.5-B(2) *n*	250	1.47	1.47	63.1	0.252
	B-10	PLG-1.5-U(2) *n*	245	1.47	1.47	61.6	0.251
	B-11	PLG-2.0-B(1) *l*[a]	273	2.00	2.00	52.9	0.194
	B-12	PLG-2.0-U(1) *l*[a]	273	2.00	2.00	52.2	0.191
	B-13	PLG-2.0-B(2) *l*	317	2.00	2.00	64.5	0.203
	B-14	PLG-2.0-U(2) *l*	317	2.00	2.00	56.1	0.178
	B-15	PLG-2.0-B(3) *n*	317	2.00	2.00	69.0	0.218
	B-16	PLG-2.0-U(3) *n*	312	2.00	2.00	63.7	0.204
(c)	C-1	PLG-0.75/1.5-B(1) *l*	320	0.74	1.47	36.3	0.113
	C-2	PLS-0.75/1.5-B(1) *l*	318	0.74	1.47	38.3	0.120
	C-3	PLG-1.5/0.75-B(2) *n*	249	1.47	0.74	45.5	0.183
	C-4	PLS-1.5/0.75-B(2) *n*	249	1.47	0.74	43.9	0.176
	C-5	PLG-2.0/1.0-B(1) *l*	234	2.00	1.06	55.8	0.238
	C-6	PLS-1.0/2.0-B(1) *l*	237	1.06	2.00	60.7	0.256
	C-7	PLG-1.0/2.0-B(2) *l*[a]	312	1.06	2.00	43.2	0.138
	C-8	PLS-2.0/1.0-B(2) *l*[a]	299	2.00	1.06	46.9	0.157
	C-9	PLG-2.0/1.0-B(3) *l*[a]	341	2.00	1.06	40.7	0.119
	C-10	PLS-1.0/2.0-B(3) *l*[a]	341	1.06	2.00	48.7	0.143
	C-11	PLG-2.0/1.0-B(4) *n*	253	2.00	1.06	58.2	0.230
	C-12	PLS-2.0/1.0-B(4) *n*	247	2.00	1.06	58.6	0.237
	C-13	PLG-1.0/2.0-B(5) *n*	268	1.06	2.00	61.8	0.231
	C-14	PLS-1.0/2.0-B(5) *n*	241	1.06	2.00	65.2	0.271

Note: [a]Premature failure τ_{max} *- ultimate shear stress*

f_c *- compressive strength of concrete from* $\phi 100 \times 200$ *cylinders*

interlock action on the load carrying capacity. For panels where the reinforcement yielded prior to the failure, no noticeable influence on the load carrying capacity or deformation capacity was observed. For specimens where the failure was determined by the crushing of the concrete, an increase in the load carrying capacity, and particularly in the deformation capacity, was obtained for the panels where the aggregate interlock action was eliminated. As described in the report [90,2], the direction of the thin steel sheets was determined by reference to the normal cast specimens. Thus, the compressive stress field found in this way may be the most beneficial one. According to plastic theory, see the following, the contribution of the sliding resistance of concrete along the cracks to the load carrying capacity is negligible in this situation. Therefore, change of the aggregate interlock action does not change the picture very much.

Tests by T.Yamaguchi & K.Naganuma [91,1]

The objective of the test program reported in [91,1] was to investigate the mechanical characteristics of reinforced panels under in-plane stresses with emphases on the ultimate strength governed by concrete failure. 32 specimens were tested where the reinforcement ratios and the load combinations were varied.

The loading condition, the reinforcement arrangement and the corresponding designation of the specimens are illustrated in Fig.2.2.7. The test set-up is shown in Fig.2.2.8.

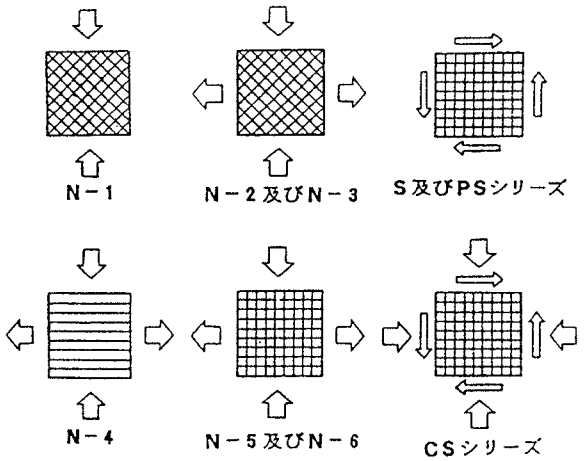

Fig.2.2.7 Reinforcement arrangement and loading principle of the specimens [91,1]

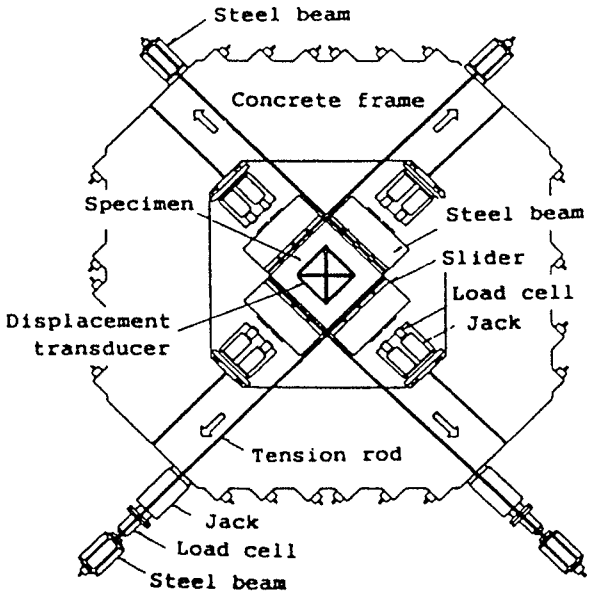

Fig.2.2.8 Test set- up [91,1]

The size of the specimens was 112×112×15cm for N-1,2,3, 120×120×15cm for N-4,5,6 and 120×120×20cm for the rest. For the N series tests, the reinforcing bars were placed in one layer and in the middle of the section, and for other types of test specimens, the reinforcing bars are placed in two layers. The distance between the center of the outer layer of rebars and the concrete surfaces was 37mm.

The specimens were monotonically loaded up to failure. Table 2.2.3 lists the test results of the N series biaxial specimens. Compressive stresses are taken to be positive in the table.

Table 2.2.3 Test results of tension-compression panels [91,1]

No.	f_c(kg/cm^2)	ρ(%)	f_y(kg/cm^2)	σ_1(kg/cm^2)	σ_{cmax}(kg/cm^2)	σ_1/f_c	σ_{cmax}/f_c
N-1	313	2.58	4200	—	274	—	0.88
-2	〃	〃	〃	94	208	0.300	0.66
-3	〃	〃	〃	99	205	0.316	0.65
-4	〃	〃	〃	101	239	0.323	0.76
-5	〃	〃	〃	100	293	0.319	0.94
-6	〃	〃	〃	100	281	0.319	0.90

Note: σ_1 *- tensile stress in panels at failure*
σ_{cmax} *- ultimate compressive stress*

Disregarding the effect of the lateral reinforcing bars on the microcracking conditions in the concrete, the test result of N-4 is what we termed the compressive panel strength, which is about $0.76f_c$.

The test results of panels, both isotropically reinforced and orthotropically reinforced, subjected to pure shear and shear-compression are listed in table 2.2.4 and 2.2.5.

Table 2.2.4 Test results of isotropic panels from [91,1]

Spec. No.	f_c kg/cm^2	Reinforcement type	ρ (%)	f_y (kg/cm^2)	σ_0 kg/cm^2	τ_{max} kg/cm^2	f_c' kg/cm^2	τ_{max}/f_c	f_c'/f_c
S-21	194	D29	4.28	3850	0	67	132	0.345	0.68
-31	308	〃	〃	〃	〃	85	169	0.276	0.55
-32	314	D25	3.38	3880	〃	89	178	0.283	0.57
-33*	320	D22	2.58	4000	〃	83	162	0.259	0.51
-34*	353	D19	1.91	4260	〃	75	148	0.212	0.42
-35**	353	D16	1.33	3770	〃	58	108	0.264	0.31
S-41	395	D29	4.28	4170	〃	121	244	0.306	0.62
-42	〃	〃	〃	〃	〃	130	263	0.329	0.67
-43	418	〃	〃	〃	〃	121	243	0.289	0.58
-44	〃	〃	〃	〃	〃	124	244	0.297	0.58
S-61	619	〃	〃	〃	〃	157	316	0.254	0.51
-62	〃	〃	〃	〃	〃	159	322	0.257	0.52
S-81	812	〃	〃	〃	〃	165	334	0.203	0.41
-82	〃	〃	〃	〃	〃	166	336	0.204	0.41
CS-1	318	D19	1.91	4367	22	107	208	0.336	0.65
-2***	〃	〃	〃	〃	(0) 47	103	205	0.324	0.64
-3	〃	〃	〃	〃	46	121	232	0.381	0.73
-4	〃	〃	〃	〃	66	136	265	0.435	0.83

*Note: * S-33,34: local boundary failure*
*** S-35: reinforcement yielding prior to failure*
**** normal stress in one direction is zero*
f_c': principal compressive stress at failure

Table 2.2.5 Test results of orthotropic panels in pure shear from [91,1]

Spec. No.	f_c kg/cm^2	Reinforcement type	ρ (%)	f_y (kg/cm^2)	τ_{max} kg/cm^2	f_c' kg/cm^2	τ_{max}/f_c	f_c'/f_c
PS-1	318	D19	4.28	4367	86	168	0.270	0.53
PS-2	〃	D22	2.58	4327	107	206	0.336	0.65

PS-3	〃	D19	1.91	4367	98	189	0.308	0.59
		D22	2.58	4327				
PS-4	〃	D19	1.91	4327	108	207	0.340	0.65
		D25	3.38	4309				
PS-5		D19	1.91	4367	114	226	0.358	0.71
		D32	5.29	4006				
PS-6	〃	D13	0.85	3710	58	112	0.182	0.35
		D19	1.91	4367				
PS-7	〃	D13	0.85	3710	68	125	0.214	0.39
		D22	2.58	4327				
PS-8	〃	D13	0.85	3710	68	129	0.214	0.41
		D25	3.38	4309				

Note: f_c': principal compressive stress at failure

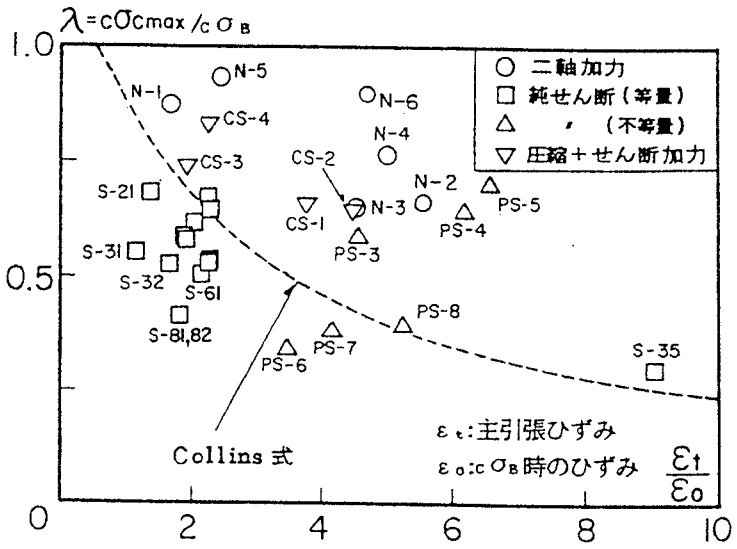

Fig.2.2.9 Compressive strength reduction factor λ versus transverse tensile strain ε_t [91,1]

The compressive strength reduction versus the transverse tensile strain is shown in Fig.2.2.9. The scatter is seen to be rather large. Excluding those panels (S-35) where the reinforcing bars were yielding before the specimens failed and those where local boundary failure occurred , the strong dependency of the compressive strength reduction factor λ on the transverse tensile strain as predicted by Vecchio/Collins formulas [82,1] is not obvious.

A formula for the ultimate shear strength for isotropic reinforced panels versus compressive cylinder strength of concrete proposed by T.Takeda et al. in [91,2] based on the above tests is reproduced in Fig.2.2.10.

In terms of plastic theory, this gives the effectiveness factor in the form of

$$\nu = \frac{1.9}{f_c^{0.34}} \qquad (f_c \text{ in MPa}) \tag{2.2.1}$$

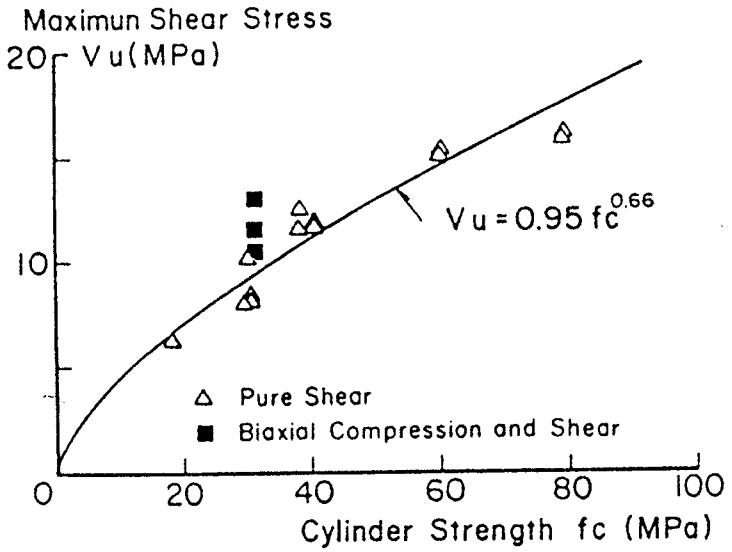

Fig.2.2.10 Ultimate shear stress of isotropic panels versus f_c [91,2]

2.3 Cracked Concrete under Compression

Tests by H.E.Jensen [93,1]

This test program consisted of 225 disks which were subjected to uniaxial compressive loading after a crack was produced in the concrete by splitting. The splitting cracks were made at three different angles: 0°, 30° and 45° to the loading direction. Part of the specimens were plain concrete, and the rest were orthogonally reinforced by reinforcing nets in two layers. The reinforcing bars in half of those reinforced concrete disks were parallel to the edges of the specimens while in the rest the bars were at 45° to the edges. The reinforcement ratio was also varied.

Fig.2.3.1 shows the loading direction and the angle of the induced cracks. The spacing of the cracks is a=60mm.

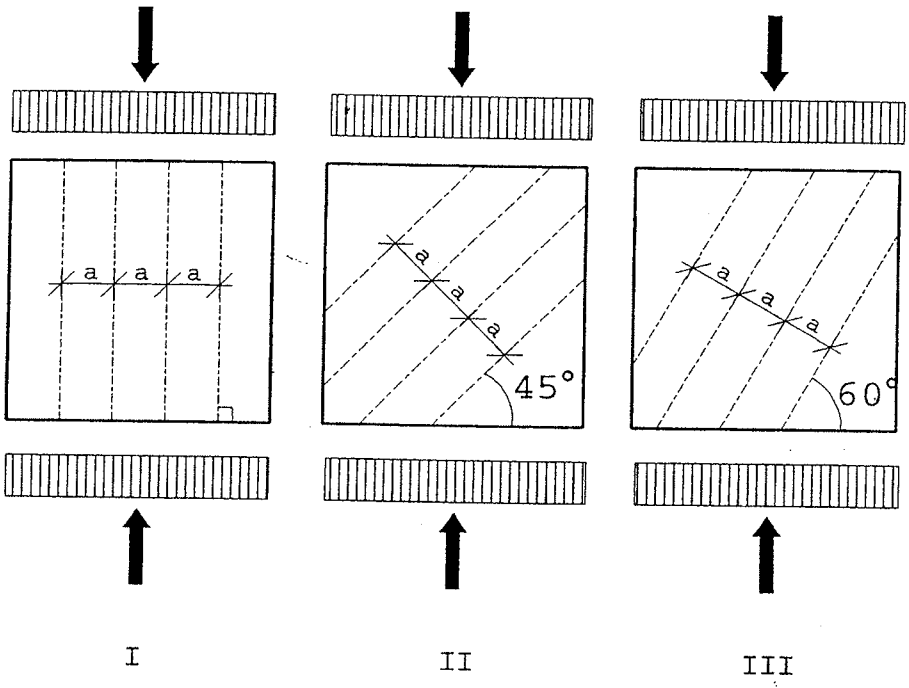

Fig.2.3.1 Loading direction and angle of the induced cracks [93,1]

Specimen type 0 was uncracked plain concrete.

The compressive strength of the concrete was obtained on ϕ100×200mm cylinders. The reinforcing bars were K420 with diameter ϕ8mm and the nominal yield stress f_y=420MPa.

The test results are listed in Table 2.3.1. The symbol of the specimen No. is arranged as: the first number (1,2,3) denotes the strength level of concrete, the second number (1,3,4) the level of the reinforcement ratio, and the last character the arrangement of the reinforcing nets (A-bars perpendicular to the edges, D-bars inclined at 45° to the edges).

By assuming yielding of the reinforcing bars in the compressive at failure, the load carried by the concrete may be calculated, which is denoted by σ_c in the table.

Qualitatively, the test results showed that the cracks at any angle reduced the load carrying capacity, and those at 30° to the loading direction reduced the most. The reinforcement direction also influenced the load carrying capacity. The specimens with reinforcing net parallel/perpendicular to the edges of the disks displayed a higher load carrying capacity than those with inclined reinforcing nets.

The scatter of the test results was rather large. Hence, a reliable quantitative conclusion is difficult to obtain.

Table 2.3.1 Test results from [93,1]

specimen No.	f_c (MPa)	ρ (%)	crack dir. θ (°)	σ (MPa)	σ/f_c	σ_c/f_c
F1.0	48	—	—	44.72	0.93	0.93
F1.1.A	40	1.12	0	37.34	0.93	0.83
F1.1.A	〃	〃	30	27.91	0.70	0.57
F1.1.A	〃	〃	45	31.89	0.80	0.69
F1.1.A	〃	〃	90	36.79	0.92	0.81
F1.1.D	52	〃	0	40.56	0.78	
F1.1.D	〃	〃	30	32.46	0.62	
F1.1.D	〃	〃	45	31.68	0.61	
F1.1.D	〃	〃	90	33.83	0.65	
F1.3.A	48	2.24	0	46.45	0.97	0.79
F1.3.A	〃	〃	30	40.42	0.84	0.66
F1.3.A	〃	〃	45	40.86	0.85	0.67
F1.3.A	〃	〃	90	41.36	0.86	0.68
F1.3.D	46	〃	0	29.22	0.64	
F1.3.D	〃	〃	30	24.39	0.53	
F1.3.D	〃	〃	45	24.61	0.54	
F1.3.D	〃	〃	90	26.83	0.58	

specimen No.	f_c (MPa)	ρ (%)	crack dir. θ (°)	σ (MPa)	σ/f_c	σ_o/f_c
F1.4.A	44	2.79	0	40.44	0.92	0.67
F1.4.A	〃	〃	30	39.00	0.87	0.64
F1.4.A	〃	〃	45	35.33	0.80	0.55
F1.4.A	〃	〃	90	37.44	0.85	0.60
F1.4.D	34	〃	0	28.13	0.83	
F1.4.D	〃	〃	30	30.63	0.90	
F1.4.D	〃	〃	45	25.76	0.76	
F1.4.D	〃	〃	90	27.32	0.80	
F2.0	94	—	—	78.47	0.83	0.83
F2.1.A	85	1.12	0	58.67	0.69	0.64
F2.1.A	〃	〃	30	43.28	0.51	0.46
F2.1.A	〃	〃	45	48.00	0.56	0.52
F2.1.A	〃	〃	90	50.28	0.59	0.54
F2.1.D	86	〃	0	57.67	0.67	
F2.1.D	〃	〃	30	40.22	0.47	
F2.1.D	〃	〃	45	41.22	0.48	
F2.1.D	〃	〃	90	46.94	0.55	
F2.3.A	94	2.24	0	82.92	0.88	0.80
F2.3.A	〃	〃	30	61.09	0.65	0.56
F2.3.A	〃	〃	45	65.39	0.70	0.61
F2.3.A	〃	〃	90	73.27	0.78	0.69
F2.3.D	82	2.24	0	52.72	0.64	
F2.3.D	〃	〃	30	33.72	0.41	
F2.3.D	〃	〃	45	42.78	0.52	
F2.3.D	〃	〃	90	42.44	0.52	
F2.4.A	85	2.79	0	59.83	0.70	0.58
F2.4.A	〃	〃	30	62.41	0.73	0.61
F2.4.A	〃	〃	45	56.79	0.67	0.55
F2.4.A	〃	〃	90	59.71	0.70	0.58
F2.4.D	73	〃	0	50.17	0.69	
F2.4.D	〃	〃	30	47.64	0.65	
F2.4.D	〃	〃	45	42.09	0.58	
F2.4.D	〃	〃	90	51.96	0.71	
F3.0	88	—	—	66.33	0.75	0.75
F3.1.A	74	1.12	0	65.11	0.88	0.83
F3.1.A	〃	〃	30	47.83	0.65	0.59
F3.1.A	〃	〃	45	51.28	0.69	0.64
F3.1.A	〃	〃	90	52.94	0.72	0.66
F3.1.D	88	〃	0	58.78	0.67	

specimen No.	f_c (MPa)	ρ (%)	crack dir. θ (°)	σ (MPa)	σ/f_c	σ_c/f_c
F3.1.D	〃	〃	30	40.67	0.46	
F3.1.D	〃	〃	45	42.44	0.48	
F3.1.D	〃	〃	90	50.33	0.57	
F3.3.A	76	2.24	0	61.61	0.81	0.70
F3.3.A	〃	〃	30	51.33	0.68	0.56
F3.3.A	〃	〃	45	49.78	0.65	0.54
F3.3.A	〃	〃	90	54.56	0.72	0.61
F3.3.D	87	〃	0	58.00	0.67	
F3.3.D	〃	〃	30	46.87	0.54	
F3.3.D	〃	〃	45	52.06	0.60	
F3.3.D	〃	〃	90	55.06	0.63	
F3.4.A*	57	2.79	0	75.35	1.32	1.15
F3.4.A*	〃	〃	30	63.58	1.16	0.94
F3.4.A*	〃	〃	45	49.83	0.87	0.68
F3.4.A*	〃	〃	90	56.29	0.99	0.80
F3.4.D	82	〃	0	54.13	0.66	
F3.4.D	〃	〃	30	45.29	0.55	
F3.4.D	〃	〃	45	48.79	0.60	
F3.4.D	〃	〃	90	47.57	0.58	

Note: The cylinder compressive strength of F4.3.A was extraordinary low compared to what was expected.*

III. Joints and Pull-out Specimens Effectiveness Factors

In this chapter, the failure of joints particularly in the form of cracks, and pull-out specimens will be discussed. Further, the local damage around transverse stressed reinforcement bars will be approximately treated. Based on the results obtained, the possible failure mechanism of specimens in tension-compression stress states and the cause of the strength reduction will be postulated.

3.1 Load carrying capacity of joints

The joint we are considering is a discontinuity in the material, for instance in the form of a crack in the specimen formed prior to the loading.

In [77,1] upper bound solutions according to plastic theory were developed. A summary is given in the following.

In this section concrete is assumed to be a modified Coulomb material with cohesion c and friction angle φ. Along the joints the cohesion and the friction angle are c' and φ', respectively. As stated in Part 1 and Part 2 of the thesis, we have $c'=\nu_s c$ where ν_s is the sliding reduction factor and $\varphi'=\varphi$. For normal gravel concrete it is reasonable to take $\varphi=37°$, and in the following we assume $\nu_s=0.5$ for a crack as in Part 1 and Part 2.

A model of the joint in the form of a crack has already been developed in Part 2 of this thesis. This model was made by assuming the properties of the cement paste to be known, and from these assumptions the model was developed for the composite material, cement paste and aggregate.

3.1.1 Plain concrete joints

Consider a joint in a concrete block forming an angle β with a normal to the loading direction as shown in Fig.3.1.1.1

The thickness of the specimen is set to a unit length. For joints plane strain may normally be assumed.

Since the strength is substantially reduced in the joint, the failure mechanism will preferably choose a yield line along the joint, where the relative displacement u forms an angle α with the yield line.

$\underline{\alpha=\varphi}$

The external work is

$$W_E = \sigma b u \sin(\beta - \varphi) \qquad (3.1.1.1)$$

The internal work is

$$W_I = c' u \cos\varphi' \cdot \frac{b}{\cos\beta} \qquad (3.1.1.2)$$

By the work equation $W_E=W_I$ we get an upper bound solution for the load carrying capacity

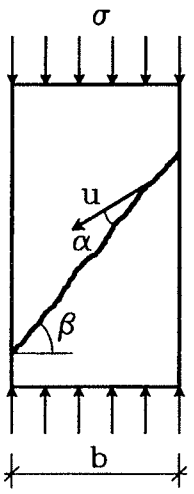

$\alpha \geq \varphi$

Fig.3.1.1.1 Sliding failure in a joint

$$\sigma = \frac{c' \cdot \cos\varphi}{\sin(\beta - \varphi) \cdot \cos\beta} \qquad (3.1.1.3)$$

The minimum is found by optimizing eq.(3.1.1.3) with respect to β

$$\sigma_{min} = \frac{2c' \cdot \cos\varphi}{1 - \sin\varphi} = \nu_s \cdot \frac{2c \cdot \cos\varphi}{1 - \sin\varphi} = \nu_s f_c \quad \text{at} \quad \beta = \frac{\pi}{4} + \frac{\varphi}{2} \qquad (3.1.1.4)$$

Compared with the failure pattern of monolithic concrete, it is seen that the load carrying capacity is the lowest when the joint coincides with the position of the most dangerous yield line in the monolithic case.

When the slope of the joint β differs from the value found in eq.(3.1.1.4), σ will be increased. However, the load carrying capacity can not be higher than that of monolithic concrete. For those values of β which give rise to σ larger than f_c, the failure will simply occur outside the joint and the load carrying capacity is $\sigma=f_c$.

The load carrying capacity as a function of β is depicted in Fig.3.1.1.2.

$\underline{\alpha \geq \varphi}$

In plane strain problem where $\alpha \geq \varphi$, the internal work is found to be

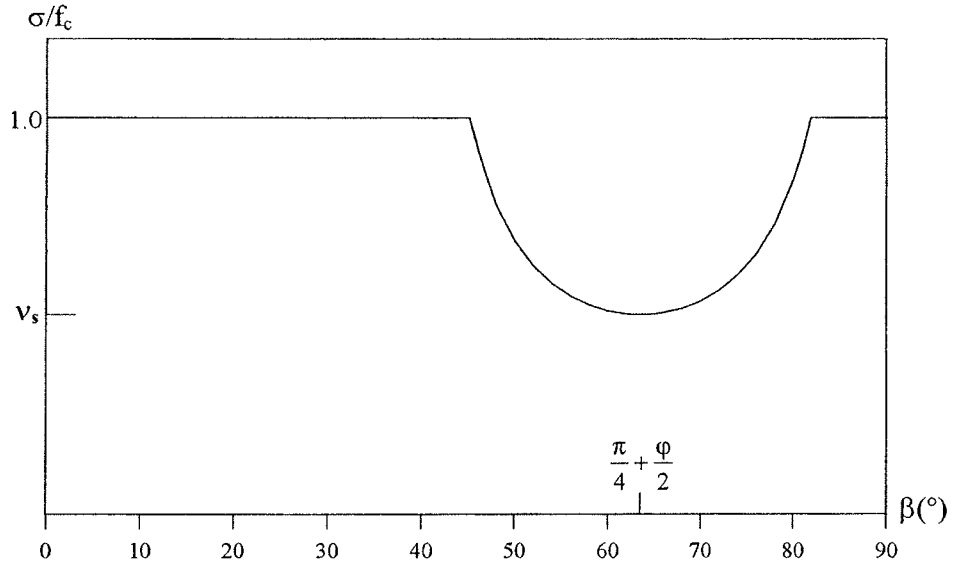

Fig.3.1.1.2 Load carrying capacity as a function of the slope of construction joint

$$W_I = \left(\frac{c' \cdot \cos\varphi \cdot (1-\sin\alpha)}{1-\sin\varphi} + f_t' \frac{\sin\alpha - \sin\varphi}{1-\sin\varphi}\right) \cdot \frac{b}{\cos\beta} \cdot u \qquad (3.1.1.5)$$

where f_t' denotes the tensile strength of concrete perpendicular to the joint, which is smaller than the tensile strength of monolithic concrete. α is a variable.

The external work is

$$W_E = \sigma b u \sin(\beta - \alpha) \qquad (3.1.1.6)$$

By setting $W_E = W_I$, we have

$$\sigma = \frac{c'(1-\sin\alpha)\cdot\cos\varphi + f_t'(\sin\alpha - \sin\varphi)}{\cos\beta \cdot \sin(\beta-\alpha)\cdot(1-\sin\varphi)} \qquad (3.1.1.7)$$

$f_t'=0$

If the tensile strength perpendicular to the joint is ignored, which is rather natural, the load carrying capacity will be

$$\sigma = \frac{c' \cdot \cos\varphi \cdot (1 - \sin\alpha)}{(1 - \sin\varphi) \cdot \cos\beta \cdot \sin(\beta - \alpha)} \qquad (3.1.1.8)$$

Here α is a variable. By optimizing with respect to α, we find the following minimum of σ for arbitrary β

$$\sigma = \frac{2c' \cdot \cos\varphi}{1 - \sin\varphi} = \nu_s \frac{2c \cdot \cos\varphi}{1 - \sin\varphi} = \nu_s f_c \quad \text{at} \quad \alpha = 2\beta - \frac{\pi}{2} \qquad (3.1.1.9)$$

For $\beta \leq \pi/4 + \varphi/2$ where $\alpha = \varphi$, eq.(3.1.1.4) is valid. Thus, the load carrying capacity σ as a function of the inclination of the joint is as shown in Fig.3.1.1.4. When the position of the joint is steeper than the position of the yield line in the monolithic concrete, the load carrying capacity will be a constant. The reduced strength is $f_c' = \nu_s f_c$. However, this value is not valid when $\beta = \pi/2$.

With $\beta = \pi/2$, the construction joint is vertical, see Fig.3.1.1.3. When the specimen is loaded as shown in the figure, the two parts separated by the joint act individually as if uniaxially loaded since no tensile strength is considered perpendicular to the joint. The load carrying capacity in this case obviously is f_c as for monolithic concrete instead of f_c'. Therefore, the point on the curve $\sigma = \nu_s f_c$ at $\beta = \pi/2$ is not valid, which is indicated by a circle in Fig.3.1.1.4. Instead, at $\beta = \pi/2$ we have $\sigma = f_c$, and this is plotted as a solid circle in the figure.

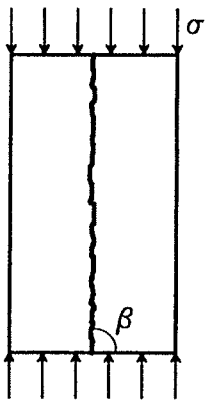

Fig.3.1.1.3 Joint with $\beta = 90°$

The physical significance on the failure mechanism is instructive. When the inclination of the joint $\beta \leq \pi/4 + \varphi/2$, the load carrying capacity is decreased with increasing steepness of the joint until the lowest value $\sigma = \nu_s f_c$ is reached. When the inclination of the joint $\pi/4 + \varphi/2 \leq \beta < \pi/2$, the load carrying capacity is constant at $\nu_s f_c$, meaning that the load carrying capacity is not affected by the slope of the joint. When the joint is strictly vertical, there is no effect of the joint and the load carrying capacity is f_c. When the inclination of the joint is slightly deviated from vertical, the load carrying capacity immediately falls to $\nu_s f_c$. This means that the load carrying

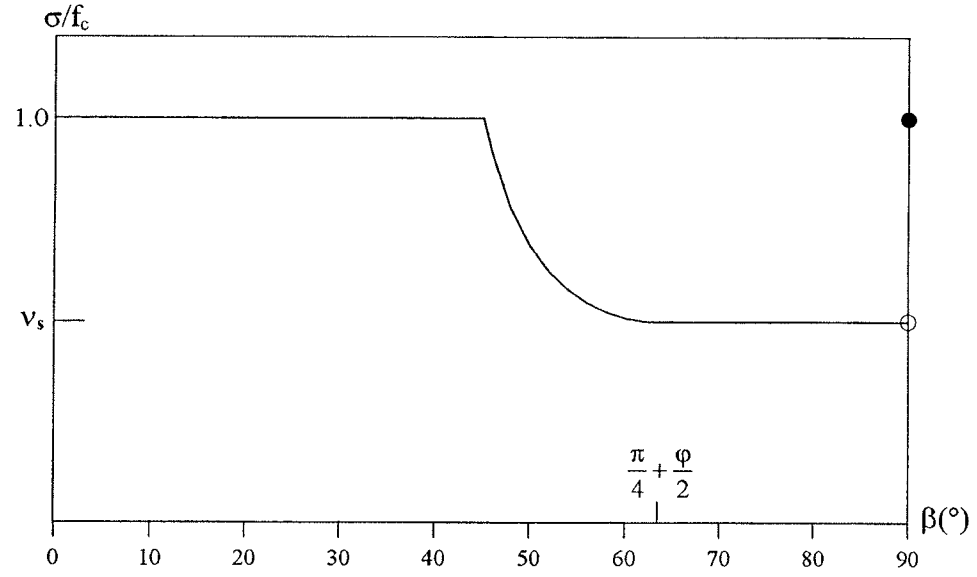

Fig.3.1.1.4 Load carrying capacity for $\alpha \geq \varphi$ and $f_t=0$

capacity is extremely sensitive to the change of the inclination of the crack when the joint is close to the loading direction.

Of course, the result rests heavily on our assumptions regarding both failure condition, flow rule and tensile strength.

If taken seriously, this might explain partly why the test results of tension-compression specimens have a large scatter. When a crack is formed due to a tensile force, the surface of the crack is zigzagged. This means that when the specimen is compressively loaded perpendicular to the tensile force, the existing crack is not exactly in the direction of the compressive force. Those sections of the crack which coincide with the direction of the compressive force give the uniaxial compressive strength, while those parts which deviate even slightly from the direction of the crack have a reduced strength. Therefore, the test results would depend to a large extent on the formation of the cracked surface. Due to the uncertainty of the surface of the crack, the load carrying capacity certainly displays a large scatter in the tests.

However, when assuming the tensile strength to be zero, we at the same time, according to our yield condition, assume that no shear stress may be carried when the normal stress in the joint is zero. In fact this is the reason for the paradoxical results shown in Fig.3.1.1.4. This is probably not realistic. A certain shear stress is likely to be carried even when the normal

stress is zero. For a crack a model was developed in Part 2 of this thesis, and the model was compared with a large number of tests. Both the model and the tests showed that a shear capacity remains even if the normal stress in the joint is zero. We return to this point later.

$f_t' \neq 0$

If the tensile strength perpendicular to the joint is taken into account, the minimum load carrying capacity is obtained by optimizing eq.(3.1.1.7) with respect to α. Denoting

$$f_t' = \lambda f_c' = \lambda \frac{2c'\cos\varphi}{1-\sin\varphi} \tag{3.1.1.10}$$

the minimum is found at

$$\tan(\beta-\alpha) = \frac{(1-\sin\varphi)(1-\sin\alpha)+2\lambda(\sin\alpha-\sin\varphi)}{(1-\sin\varphi-2\lambda)\cos\alpha} \tag{3.1.1.11}$$

For $\alpha=\varphi$, eq.(3.1.1.4) is valid, while for $\alpha\geq\varphi$, eq.(3.1.1.7) and eq.(3.1.1.11) are valid. At the limit of the validity of eq.(3.1.1.4), the slope β_1 of the joint is given by

$$\tan(\beta_1-\varphi) = \frac{(1-\sin\varphi)^2}{(1-\sin\varphi-2\lambda)\cos\varphi} \tag{3.1.1.12}$$

This can be rewritten as

$$\tan(\beta_1-\varphi) = \tan(\frac{\pi}{4}-\frac{\varphi}{2})\frac{1-\sin\varphi}{1-\sin\varphi-2\lambda} \tag{3.1.1.13}$$

Since $\lambda>0$, it is seen that

$$\tan(\beta_1-\varphi) > \tan(\frac{\pi}{4}-\frac{\varphi}{2}) \tag{3.1.1.14}$$

Thus

$$\beta_1 > \frac{\pi}{4}+\frac{\varphi}{2} \tag{3.1.1.15}$$

The domain of validity of eq.(3.1.1.4) is increased when the tensile strength of the construction joint is increased. Fig.3.1.1.5 shows the dependency of the load carrying capacity of the tensile strength when f_t' varies from 0 to $0.05f_c'$.

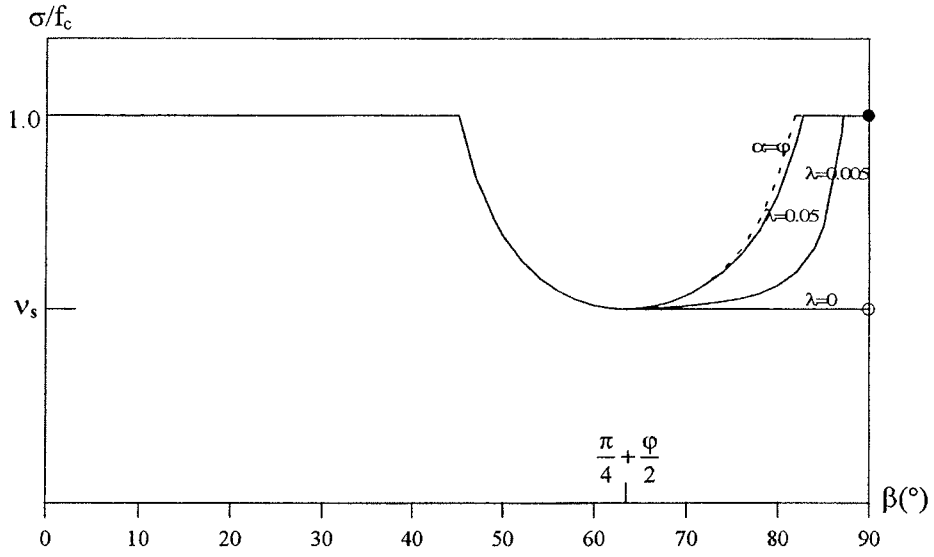

Fig. 3.1.1.5 Load carrying capacity for $\alpha \geq \varphi$ and $f_t' \neq 0$

It is seen that even a small increase of the tensile strength from 0 to $f_c'/200$ will change the picture significantly. The tensile strength of monolithic concrete f_t may be roughly taken to be about $f_c/10$. For plain concrete joints, the tensile strength as a fraction of the reduced compressive strength f_c' must be less, i.e. $\lambda << 0.1$. In the calculation, the two curves determined by eq.(3.1.1.4) and eq.(3.1.1.7) almost overlap for $\lambda > 0.05$. Thus, a larger tensile strength of the joint forces the failure to occur as a pure sliding failure with $\alpha = \varphi$.

The reason why we in a pure compression state get an enhancement of the load carrying capacity when f_t' is assumed larger than zero is that in this case a shear stress may be carried even if the normal stress in the joint is zero.

In [77,1] the theoretical solutions were compared with tests on casting joints performed by Johansen [30,1]. In the experiment, f_c=30MPa which resulted in c=7.5MPa if φ=37°. In the comparison, the cohesion of the joint was chosen to be c'=3MPa. Thus ν_s=c'/c=0.4. A good agreement between the calculation and the experimental results was found in the

whole β-interval. Thus the test results did not reflect the results shown in Fig.3.1.1.4.

Assuming a certain small tensile strength in the joint is one way of repairing the erroneous property of our yield condition for $f_t'=0$, namely that no shear stress at all may be carried when the normal stress in the joint is zero.

3.1.2. Reinforced concrete joints

Consider a joint only laterally reinforced as shown in Fig.3.1.2.1, where the reinforcement ratio is ρ_x and the corresponding reinforcement degree is Φ_x. We may imagine that the reinforcing bars are anchored by an anchor plate on the surfaces of the specimen. Thus it is seen that when the specimen is compressively loaded in the axial direction, the reinforcing bars provide lateral confinement.

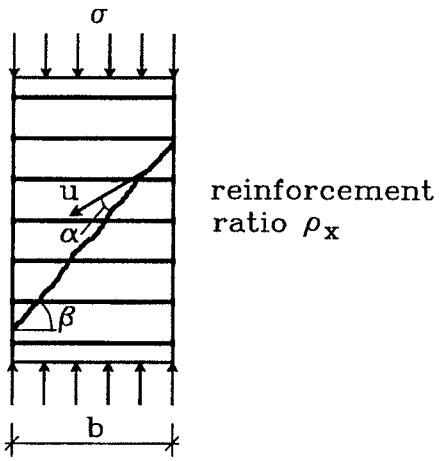

Fig.3.1.2.1 Reinforced concrete joint

In this case it is natural to disregard the tensile strength normal to the construction joint. As above, we assume the yield line coinciding with the joint and the relative displacement u is at an angle α to the yield line. The thickness of the specimen is set to a unit of length.

α=φ

For sliding failure with α=φ, assuming the reinforcement yields at failure, the internal work is

$$W_I = \frac{1}{2} f_c' (1-\sin\varphi)\frac{b}{\cos\beta}\cdot u + \rho_x f_y \tan\beta\cos(\beta-\varphi) b\cdot u \qquad (3.1.2.1)$$

The external work

$$W_E = \sigma\cdot b\cdot u\sin(\beta-\varphi) \qquad (3.1.2.2)$$

Putting $W_I=W_E$, we get

$$\frac{\sigma}{f_c}=\frac{1}{2}\nu_s\frac{1-\sin\varphi}{\cos\beta\cdot\sin(\beta-\varphi)}+\Phi_x\frac{\tan\beta}{\tan(\beta-\varphi)} \qquad (3.1.2.3)$$

The minimum of σ is found to be

$$\frac{\sigma}{f_c}=\nu_s+k\Phi_x \quad \text{at} \quad \beta=\frac{\pi}{4}+\frac{\varphi}{2} \qquad (3.1.2.4)$$

where $k=(1+\sin\varphi)/(1-\sin\varphi)$.

Thus in this case the reinforcement contributes to the load carrying capacity in exactly the same way as a lateral confining pressure.

As for a plain concrete joint, the most dangerous slope of the joint is when it coincides with the yield line in a monolithic concrete specimen. When the angle of the joint β is smaller or larger than the value determined by eq.(3.1.2.4), the load carrying capacity is increased. When there is no joint the load carrying capacity will be given by eq.(3.1.2.4) with $\nu_s=1$, i.e. $\sigma/f_c=1+k\Phi_x$. For small reinforcement degrees, $\sigma/f_c\approx 1$. Using this approximation the load carrying capacity of laterally reinforced joint as function of the angle of the joint β is drawn in Fig.3.1.2.3 for different reinforcement degrees Φ_x.

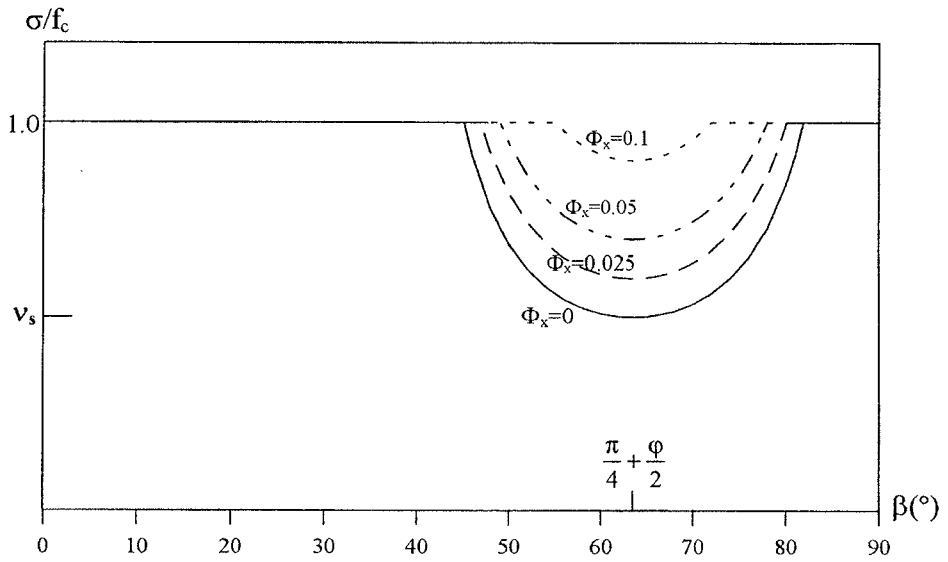

Fig.3.1.2.3 Load carrying capacity of reinforced joint for $\alpha=\varphi$

It appears that the amount of the lateral reinforcement has a strong influence on the load carrying capacity. The larger the amount of the reinforcement, i.e. the larger the constraints, the flatter the curve. When the reinforcement degree reaches a certain value (for ν_s=0.5, Φ_x=0.125), the minimum σ found by eq.(3.1.2.4) equals f_c. This means that when the joint is sufficiently reinforced, the specimen is as strong as unreinforced uncracked concrete.

When the reinforcement is utilized to carry an external transverse tensile stress which is able to produce yielding in the reinforcement, the load carrying capacity is the same as for an unreinforced specimen. For an arbitrary transverse tensile stress σ_x eq.(3.1.2.3) may be used to find the load carrying capacity replacing Φ_x by Φ_x- σ_x/f_c.

This calculation partly explains why the compressive strength of a reinforced concrete block varies, sometimes it is low and sometimes it is relatively high. Normally the block is in a cracked state due to different reasons. When the block is lightly reinforced, then the strength is affected by the presence of the existing cracks, and a lower strength will be found. Increasing the amount of reinforcement, the load carrying capacity gets closer to the uniaxial compressive strength of corresponding uncracked concrete. When the block is heavily reinforced, then the load carrying capacity will not feel the existence of the cracks, and a strength close to the uncracked state will be obtained. Hence, it is seen that by reinforcing sufficiently, the effect of the cracks on the load carrying capacity may be eliminated.

<u>$\alpha \geq \varphi$</u>

In this case, the internal work becomes

$$W_I = \frac{1}{2} f_c' (1 - \sin\alpha) \frac{b}{\cos\beta} \cdot u + \rho_x f_y \tan\beta \cos(\beta - \alpha) b \cdot u \qquad (3.1.2.5)$$

The external work is the same as in eq.(3.1.1.6)

The work equation W_I=W_E gives

$$\frac{\sigma}{f_c} = \frac{1}{2} \nu_s \frac{1 - \sin\alpha}{\cos\beta \cdot \sin(\beta - \alpha)} + \Phi_x \frac{\tan\beta}{\tan(\beta - \alpha)} \qquad (3.1.2.6)$$

Here α is a variable. By optimizing the result of eq.(3.1.2.6) with respect to α, the minimum of σ is found at

$$\cos(\beta-\alpha)=(1-\frac{\Phi_x}{\frac{1}{2}\nu_s})\sin\beta \qquad (3.1.2.7)$$

For $\alpha>\varphi$, eq.(3.1.2.6) and (3.1.2.7) are valid. For $\alpha=\varphi$, eq.(3.1.2.3) is valid. At the limit of the validity of eq.(3.1.2.3) the slope of the joint β_1 is defined by

$$\cos(\beta_1-\varphi)=(1-\frac{\Phi_x}{\frac{1}{2}\nu_s})\sin\beta_1$$

Rewriting the formula, we have

$$\tan\beta_1=\tan(\frac{\pi}{4}+\frac{\varphi}{2})\frac{1-\sin\varphi}{1-\sin\varphi-\frac{\Phi_x}{\frac{1}{2}\nu_s}} \qquad (3.1.2.8)$$

Since Φ_x and ν_s are positive, it is seen that the slope of the joint at the transition from eq.(3.1.2.3) to eq.(3.1.2.6) is given by

$$\beta_1>\frac{\pi}{4}+\frac{\varphi}{2}$$

Similar to the influence of f_t' for a plain concrete joint, an increase of the lateral reinforcement degree will increase the domain of the validity of eq.(3.1.2.3). The load carrying capacity for different reinforcement degrees as a function of the slope of the joint is drawn in Fig.3.1.2.4, where the dashed lines are those valid for $\alpha=\varphi$ with the same reinforcement degree. In the figure we have again used the approximation $\sigma/f_c=1$ for a specimen without a joint.

The influence of the lateral reinforcement on the load carrying capacity is similar to that where the tensile strength perpendicular to the joint is increased.

When the specimen is subjected to tension-compression, the effect of a

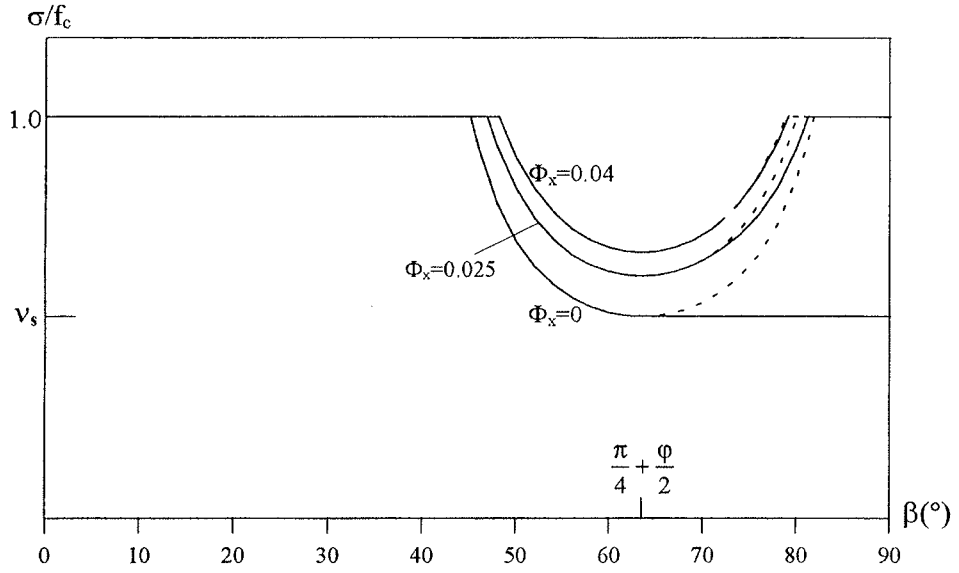

Fig.3.1.2.4 Load carrying capacity for $\alpha \geq \varphi$

transverse tensile stress σ_x can be taken into account in eq.(3.1.2.6) by replacing Φ_x with $\Phi_x - \sigma_x/f_c$.

3.2 Failure of pull-out specimens

When the reinforced concrete specimens are subjected to tension-compression, the concrete around the reinforcement is spoiled to different extent. The damage is in the form of local failures and in what follows we will assume the local damage to be the main cause for the compressive strength reduction. By investigating the failure of pull-out specimens, part of a more rational explanation of the effectiveness factors in plastic theory may be obtained.

3.2.1 Previous work

In investigating crack spacing and crack widths, a pull-out type specimen is often used. Normally, a tensile force is applied to the reinforcing bar placed in the middle of the section or bars placed arbitrarily but with the center of gravity coinciding with that of the concrete section. When the tensile force reaches a certain level, a crack, named the primary crack, will be created. When increasing the load, other primary cracks may be created. Between the primary cracks, some secondary cracks may be formed. Close to the primary cracks, a number of conical failure surfaces are ob-

served in experiments. Fig.3.2.1.1 shows a cut of a pull-out test specimen after failure from [94,1]. The conical failure surfaces can be clearly seen.

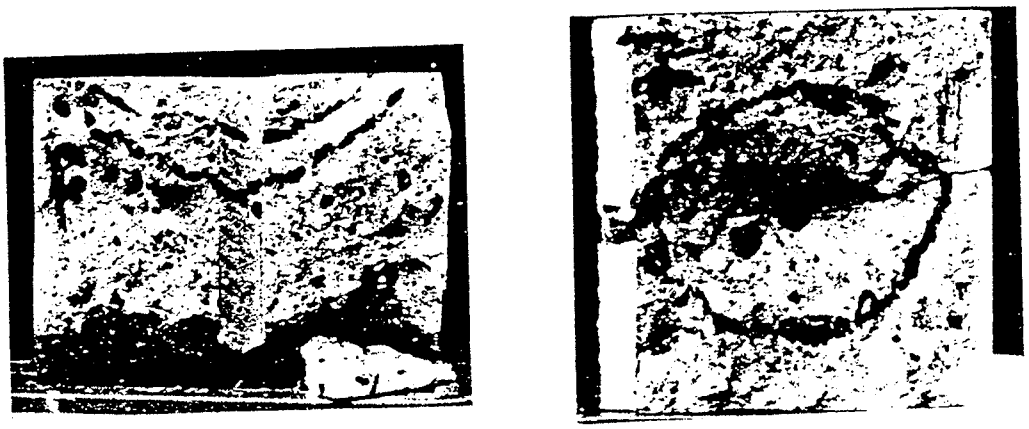

Fig.3.2.1.1 Conical failure surfaces around the primary crack [94,1]

In [90,1] a brief review of the previous research in establishing a relationship between the depth of the conical failure surfaces and the tensile stress in the reinforcing bars was presented. A new expression for l_0 as a function of the tensile stress σ_s in the reinforcing bar, where $l_0/2$ is the depth of the punching cone, was proposed by modeling the failure as a punching failure in concrete according to plastic theory. The expression appears as

$$\frac{l_0}{d} = 1 + \frac{\sigma_s}{100} \qquad (\sigma_s \text{ in MPa}) \qquad (3.2.1.1)$$

where σ_s is the tensile stress in the reinforcing bar, and d the diameter of the bar.

In this model the total tensile force in the reinforcing bar was assumed to be transferred to the concrete by a single rib, which does not seem reasonable because a tensile force will remain in the reinforcement beyond the failure cone.

In the following an alternative derivation will be given.

3.2.2 Analysis of pull-out according to plastic theory

Consider a simple case where a steel bar is placed in the middle of the section. The edge of the specimen simulates the first primary crack. Stresses in reinforcing bars are transferred to the concrete by means of

bond in the interface between these two materials. A certain distance is needed for the transfer of stresses. This distance is referred to as transfer length in the following. At the end of the transfer length the steel bar and the concrete can be assumed again to work together in the usual way, and the strain in the section may be regarded uniform. According to Saint Venant's principle, the transfer length for uncracked elastic material will be of the order of magnitude D, D being the depth of the section.

The real distribution of the bond is affected by many factors. To simplify the problem, we assume a uniformly distributed bond stress τ along the transfer length, which gives

$$\tau = \frac{\sigma_s A_s}{\pi d \cdot D} = \frac{1}{4}\sigma_s \frac{d}{D} \qquad (3.2.2.1)$$

where the small stress in the steel bar at the end of the transfer length is neglected. Here σ_s is the tensile stress in the steel bar, d the diameter and $A_s=\pi d^2/4$ the area of the bar.

For the surrounding concrete, the effect of the bond stress is like a uniform loading acting along a cylindrical surface with the length D in the middle of the section, see Fig.3.2.2.1. The bond stresses may produce a failure similar to a punching failure. What happens may be described as follows. When the primary crack is created, a small part of the concrete close to the crack is normally pulled out, the depth of which is denoted x_0. At this time the rest of the concrete may be regarded to be still uncracked. Thus, the

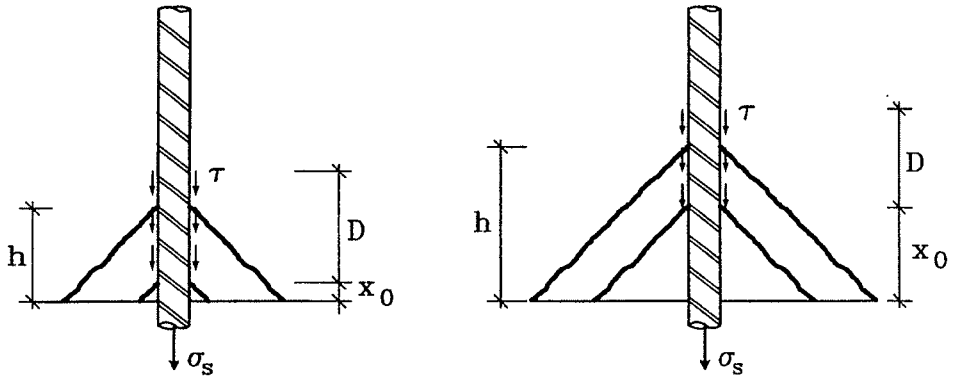

a). Loading stage 1 *b). Loading stage 2*

Fig.3.2.2.1 Loading and failure pattern in concrete in pull-out specimen

bond stress may be assumed as distributed evenly over a transfer length D, shown in Fig.3.2.2.1(a). When the load is increased to such a value that

the punching resistance of concrete along a surface with a depth h is exceeded, then a punching failure in concrete occurs. After the punching failure, the bond needs to be redistributed, i.e. the concrete beyond this punching point may be still assumed to be uncracked, and the shear stress is distributed evenly along a new transfer length D as shown in Fig.3.2.2.1(b), and a new failure as described above takes place. In this way, a succession of punching failure surfaces are formed with increasing tensile stress σ_s. Here we assume the depth of the section to be sufficiently large so that the punching failure surfaces do not reach the faces of the specimen.

By applying the simplified method for punching analysis according to plastic theory, i.e. the average shear stress in a control surface equals the tensile strength at failure, a relationship between the depth of the punching cone h and the tensile stress in the steel bar can be established.

Assuming the control surface to be at a distance of half of the depth of the punching cone, we have

$$f_t \cdot \pi(d+h) \cdot h = \tau \cdot \pi d \cdot (h - x_0) \tag{3.2.2.2}$$

Inserting eq.(3.2.2.1) in (3.2.2.2) we arrive at

$$\frac{h}{d} = \frac{1}{2}\left(\frac{1}{4}\frac{\sigma_s}{f_t}\frac{d}{D} - 1 \pm \sqrt{\left(\frac{1}{4}\frac{\sigma_s}{f_t}\frac{d}{D} - 1\right)^2 - \frac{\sigma_s}{f_t}\frac{d}{D}\frac{x_0}{d}}\right) \tag{3.2.2.3}$$

As can be seen from the failure process, as soon as a punching failure occurs, the stress distribution is changed, and the conditions for the calculation are not valid any more. Thus only the very first failure surface, which may be found by eq.(3.2.2.3), is of interest. Therefore, the value of h from eq.(3.2.2.3) should be the minimum. It is seen that the expression under square root in (3.2.2.3) must not be negative in order to get a meaningful solution. The lowest σ_s that renders h a minimum is found by

$$\left(\frac{1}{4}\frac{\sigma_s}{f_t}\frac{d}{D} - 1\right)^2 - \frac{\sigma_s}{f_t}\frac{d}{D}\frac{x_0}{d} = 0 \tag{3.2.2.4}$$

which has the solution

$$\frac{\sigma_s}{f_t}\frac{d}{D} = 4(1 + 2\frac{x_0}{d} + 2\sqrt{\frac{x_0}{d}(1 + \frac{x_0}{d})}) \qquad (3.2.2.5)$$

Hence

$$h = x_0 + \sqrt{x_0(d + x_0)} \qquad (3.2.2.6)$$

Rearranging eq.(3.2.2.5) we arrive at the simple expression

$$\frac{h}{d} = \frac{1}{2}(\frac{1}{4}\frac{\sigma_s}{f_t}\frac{d}{D} - 1) \qquad (3.2.2.7)$$

Expressing D with the thickness of the cover c, we have D=d+2c.

For the next loading step, we just replace x_0 by h, and a new value of h is determined.

In this way it is seen that if the tensile stress σ_s is less than the value found by eq.(3.2.2.5), no punching cone can be created. Thus, the curve of h as a function of σ_s is not smooth but stepped. However, (3.2.2.7) represents the straight line connecting the upper corners of the steps.

The initial depth of the punching cone before loading x_0 is chosen arbitrarily small.

Fig.3.2.2.2 shows the curves with $x_0/d=0.1$ for different values of the cover c.

By increasing the ratio D/d, where D=2c+d, i.e. by reducing the reinforcement ratio, a smaller depth of the punching cones is found.

In Fig.3.2.2.3 the influence of the initial depth of the punching cone x_0 is studied. It appears that the effect of x_0 can only be felt at the beginning of the loading. When σ_s is increased, all the points at the upper corners of the steps are lying on the line determined by eq.(3.2.2.7). The initial depth of the punching cone closest to the primary cracks is unknown, but at the later stages of loading, the depth of the punching cone may be found by the relationship between h/d and σ_s/f_t satisfying eq.(3.2.2.7).

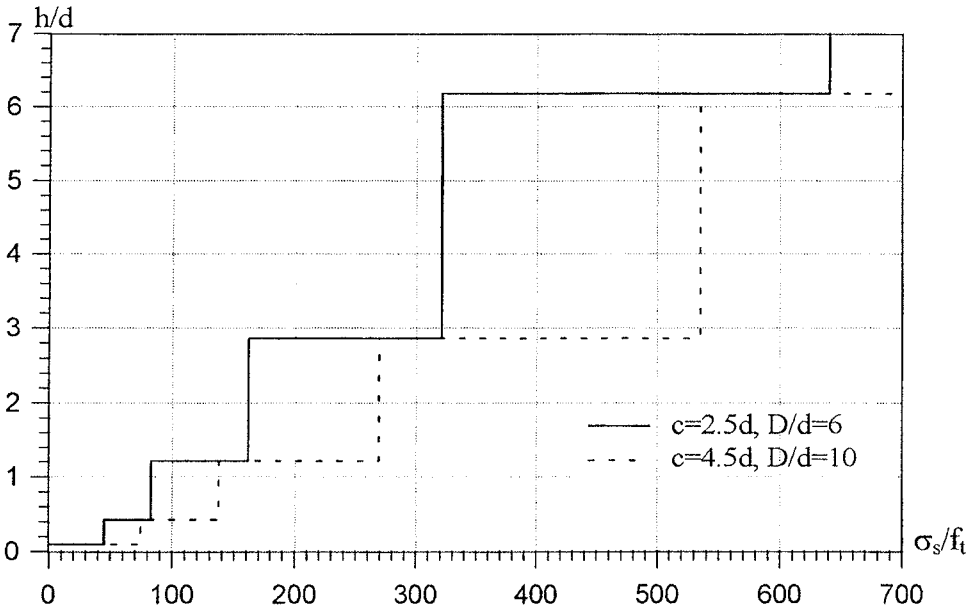

Fig.3.2.2.2 Ratio of h/d as function of σ_s/f_t for different covers c

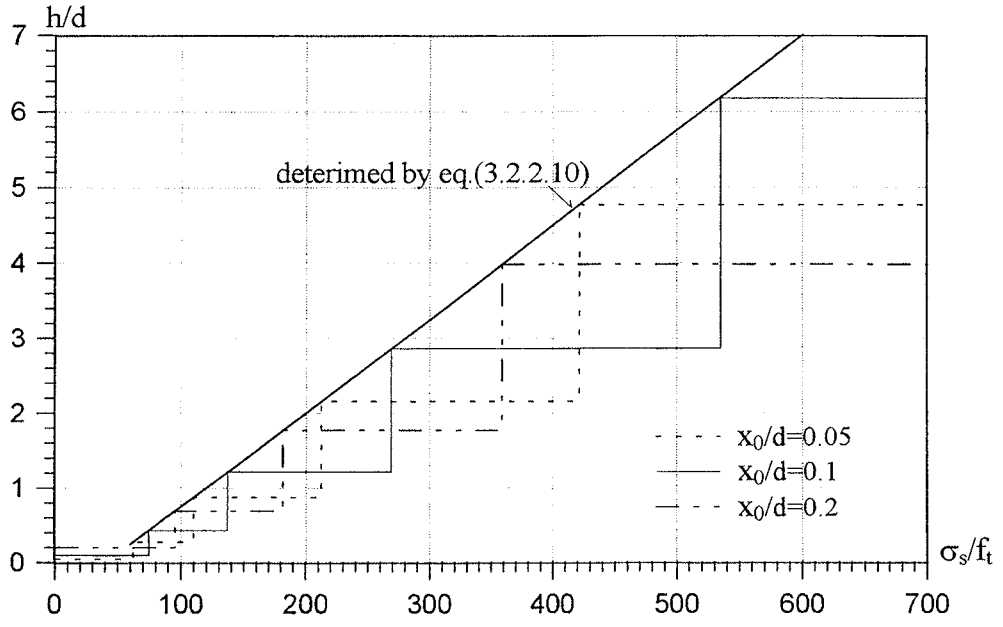

Fig.3.2.2.3 Ratio of h/d versus σ_s/f_t for different initial value of x_0/d

It appears from the above that the depth of the punching cone is decreasing if the tensile strength of the concrete increases. This is rather natural. This means that the secondary cracks in the surrounding concrete are more

closely spaced if the tensile strength is increased.

In Fig.3.2.2.4 the expression from [90,1], eq.(3.2.1.1), is compared with the result of the present analysis identifying h with $l_0/2$. Here, the tensile strength of concrete is assumed to be f_t=2MPa, and the cover c=4.5d which results in D/d=10. If the section is circular, this value of D/d leads to a reinforcement ratio ρ=1%. Thus the parameters assumed are rather typical. The two curves appear reasonably close.

Larger deviations will of course be observed with other values of the cover, which does not enter in eq.(3.2.1.1)

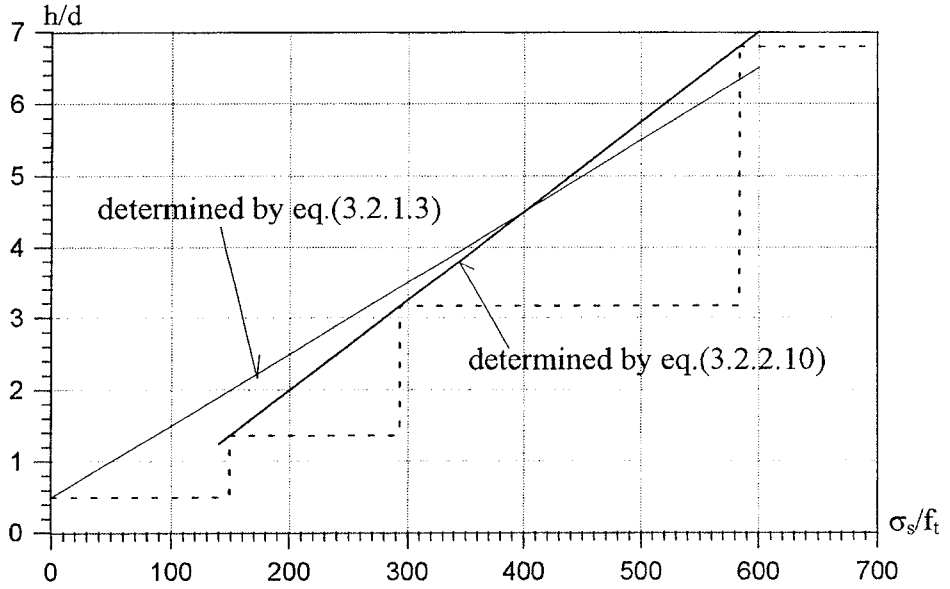

Fig.3.2.2.4 Comparison with eq.(3.2.1.1), x_0/d=0.5, c=4.5d and f_t=2MPa

3.3. Postulation of mechanism of strength reduction

As reviewed in chapter 2, the test results concerning the effect of transverse tensile strain or stress on the compressive strength reduction from various research groups are controversial. What is the rational explanation for the phenomenon? As already mentioned we will explain the strength reduction as a consequence of the local damage around the reinforcement bars.

Effect of pull-out

When subjecting a panel to transverse tensile forces, primary cracks occur

at certain loading stages. At the primary cracks, the tensile forces are taken over by the reinforcing bars. Thus, between the primary cracks, the situation is similar to that of the pull-out specimens. Consequently, punching cones will be formed around the reinforcing bars close to the primary cracks. Due to the punching cones the compressive strength of the concrete will be reduced. We may obtain a rough estimation of the strength reduction due to pull-out in the following way.

The concrete between two cracks may be divided into two zones as shown in Fig.3.3.1(a), where L_{cr} is the crack distance. Zone I is an intact area while zone II is at the end in the area where the punching-out of the concrete occurs. The load carrying capacity may be considered as the sum of these zones.

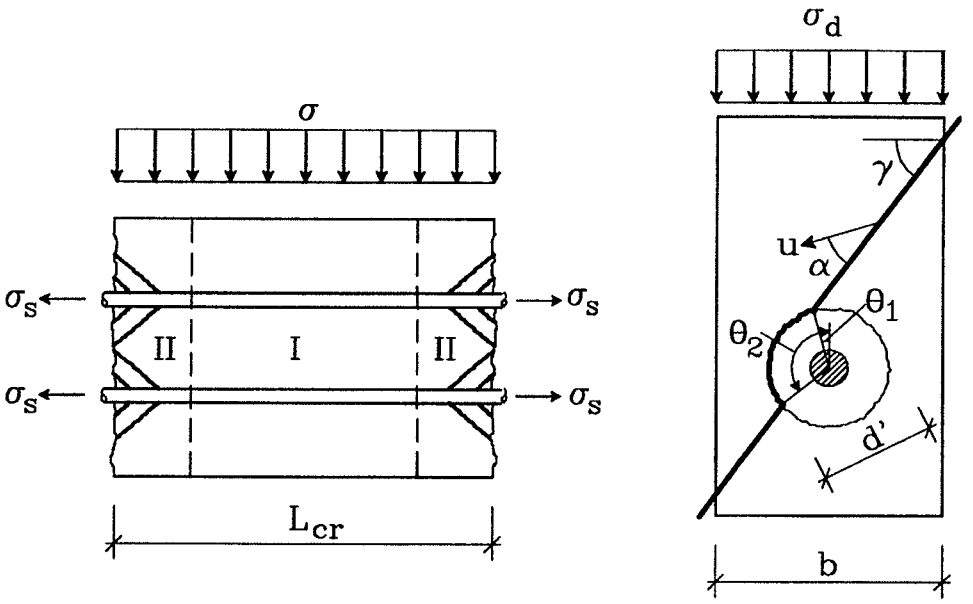

(a) *(b)*

Fig.3.3.1 Effect of punching out of concrete

For zone I, the ultimate compressive stress is f_c.

In zone II, when the sliding resistance is significantly reduced along the cracks, a failure pattern as shown in Fig.3.3.1(b) may take place which gives an ultimate stress $\sigma_d<f_c$. Instead of going through uncracked concrete, the yield line may preferably choose to follow the existing cracks wholly or partly. We consider only the simplest case where the reinforcing bars are placed in one layer. For further simplification, we will use an equivalent cylinder to represent the conical cracks. The diameter of the

equivalent cylinder may be taken as the average of the diameters of the punching cones which is d′=d+h, where h is the depth of the punching cones determined by (3.2.2.7). We assume that the angle of the yield line $\gamma=\pi/4+\varphi/2$ does not change after passing by the cracks.

In plane strain with $\alpha=\varphi$ and the cohesion along the crack being $c'=\nu_s c$, a work equation can be set up to find the upper bound value of the ultimate stress σ_d. The result is

$$\frac{\sigma_d}{f_c} = 1 - B\frac{d'}{b} \tag{3.3.1}$$

where

$$B = \frac{1}{4}\frac{1-\sin\varphi}{\sin(\gamma-\varphi)}\left[\frac{\left|\sin\theta_1 - \sin\theta_2\right|}{\cos\gamma} + \nu_s(\theta_2 - \theta_1 + \cos(\theta_2+\varphi-\gamma) - \cos(\theta_1+\varphi-\gamma)\right]$$

Here b is the width of the section with the reinforcing bar in the center, i.e. b=2c+d. By optimizing with respect to the angles θ_1 and θ_2 indicated in the figure, the minimum is found. For $\nu_s=0.5$, $B\approx 0.2$.

The maximum of the diameter d′ is reached when the punching cone touches the surfaces. This is also the limit of the domain of the validity of the failure mechanism. The strength reduction from this mechanism is not large, the most is around 10%.

Thus pull-out near primary cracks is not likely to be the explanation of the compressive strength reduction. We must look for other mechanism.

Effect of the bursting stresses

When reinforcing bars are stressed, inclined secondary cracks around the bars are created. This kind of cracks originates at the ribs. After the formation of the inclined cracks the shear stresses around the reinforcing bars are carried by skew compressive forces. The surrounding concrete feels these forces as if it is acted upon by a radial pressure. These skew compressive forces are termed bursting forces. When the bursting forces reach a certain level, the concrete cover will be spalled off partly or entirely. Depending on the geometry, the spalling off of the cover might be as shown in Fig.3.3.2.

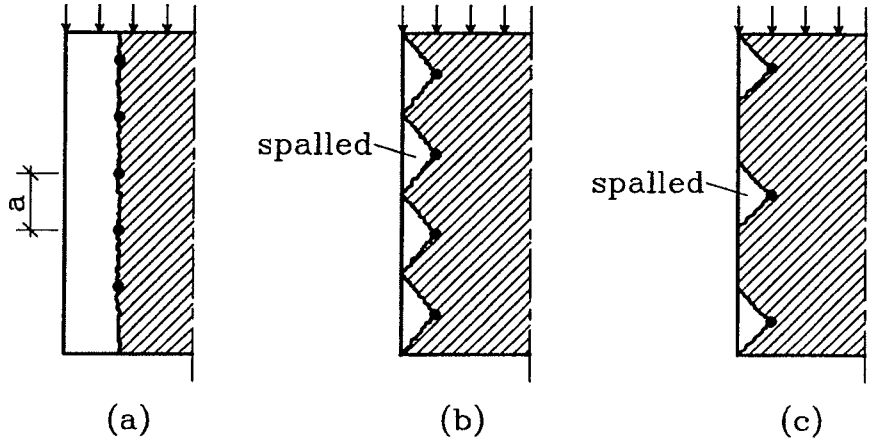

Fig.3.3.2 Spalling of the concrete cover

The worst and the simplest case is (a) where the entire cover is spalled off. Thus the effective thickness of the section is reduced. Since the ultimate stress of the intact part is still approximately f_c, the compression load carrying capacity is simply proportional to the effective thickness of the section. Terming the reduced compressive strength νf_c, where ν is the effectiveness factor, we have in this case

$$\nu = 1 - \frac{2c + d}{b} \tag{3.3.3}$$

Here b is the original thickness of the section.

The tensile stress in the reinforcement necessary to produce a failure by spalling off is dependent on the dimensions.

In [94,1] the ultimate bond stress between a reinforcing bar and the concrete when spalling off of the cover occurs is found to be

$$\frac{\tau_u}{\sqrt{f_c}} = 0.30 + 0.36\sqrt{\frac{l_{tr}}{d}}\frac{a}{d} \qquad (f_c \text{ in MPa}) \tag{3.3.4}$$

In this equation l_{tr} is the transfer length, and a the bar center spacing as shown in Fig.3.3.2.

A simple relation between the tensile stresses in the reinforcing bars and the bond stress τ_u may be found by the following reasoning.

We consider a concrete region with the bar in the center, see Fig.3.3.3. The cover is c. We apply again Saint Venant's principle when determining the transfer length l_{tr}, and thus

$$l_{tr}=2c+d \tag{3.3.5}$$

Over this length the bond stress is assumed as evenly distributed. Hence

$$\tau_0 = \frac{(\sigma_s - \sigma_s') \cdot A_s}{\pi d \cdot l_{tr}} = \frac{1}{4}(\sigma_s - \sigma_s')\frac{d}{l_{tr}} \tag{3.3.6}$$

where σ_s' is the tensile stress in the reinforcing bar at the end of the transfer length, and $A_s=\pi d^2/4$ is the area of the bar. As the concrete is cracked, σ_s' may not be neglected as we did before. The order of the magnitude of σ_s' may be found as follows.

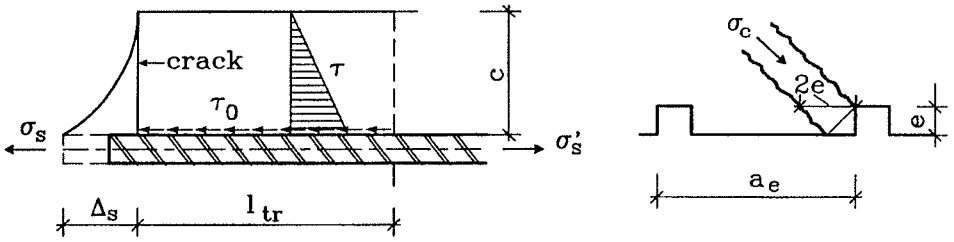

Fig.3.3.3

Due to the existence of the bond, the reinforcing bars and the concrete deform together, meaning that at the interface between the bar and the concrete, the deformation in the reinforcing bar must equal the displacement in the concrete.

For a rough estimate the deformation in the concrete may be assumed to be a pure shear deformation, which is of course not correct since also elongation in the bar direction takes place.

The elongation of the bar over the distance l_{tr} is

$$\Delta_s = \frac{1}{2}\frac{\sigma_s + \sigma_s'}{E_s} l_{tr} \tag{3.3.7}$$

Assuming that the shear stress in the concrete is distributed linearly over the cover with zero shear stress at the surface as shown in Fig.3.3.3 and

assuming that the shear modulus of the cracked concrete is G_c', the displacement at the crack becomes

$$\Delta_c = \frac{1}{2}\frac{\tau_0}{G_c'}c \tag{3.3.8}$$

The displacement due to shear strain in the cover is a parabola, which in a primitive way models the opening of a crack. Putting $\Delta_c = \Delta_s$ and inserting (3.3.6), we get

$$\frac{\sigma_s + \sigma_s'}{\sigma_s - \sigma_s'} = \frac{1}{4}\frac{E_s}{G_c'}\frac{d \cdot c}{l_{tr}^2}$$

Denoting

$$K = \frac{1}{4}\frac{E_s}{G_c'}\frac{d \cdot c}{l_{tr}^2} \tag{3.3.9}$$

we arrive at

$$\begin{aligned} \sigma_s' &= \frac{K-1}{K+1}\sigma_s \\ \tau_0 &= \frac{1}{2(K+1)}\sigma_s \frac{d}{l_{tr}} \end{aligned} \tag{3.3.10}$$

Thus a relation between the bond stress and the tensile stress in the reinforcing bar is obtained.

Now we have to find an estimate of the shear modulus for cracked concrete. Disregarding the Poisson ratio of concrete, the shear modulus for uncracked concrete is $G_{c0}=E_c/2$, where E_c is the Young's modulus of concrete. For cracked concrete, it is reasonable to estimate the shear modulus to be $G_c \approx \frac{1}{2}G_{c0} = \frac{1}{4}E_c$, because the shear stresses are carried by skew compressive stresses. For concrete around a ribbed bar, the shear modulus will be even lower because the shear stresses are carried by compression struts in the concrete in front of the ribs. As shown in Fig.3.3.3(b), the effective area will only be 2e if we take the struts to be at 45° to the bar, e being the depth of the ribs. Thus the shear modulus in the concrete is of the order magnitude

$$G_c' = G_c \frac{2e}{a_e}$$

where a_e is the rib spacing as shown in the figure. For normal deformed bars, we may estimate that $e/a_e \approx 1/10$. Hence

$$G_c' \approx \frac{2}{10} G_c \approx \frac{E_c}{20}$$

Then we have, putting $n=E_s/E_c$

$$K \approx 5 \frac{E_s}{E_c} \frac{d \cdot c}{l_{tr}^2} = 5n \frac{d \cdot c}{l_{tr}^2}$$

For normal concrete and reinforcement we may assume that $n \approx 10$.

When the cover spalls off we have $\tau=\tau_u$ by (3.3.4), and the corresponding tensile stress in the reinforcing bars becomes

$$\frac{\sigma_s}{\sqrt{f_c}} = 2(K+2) \frac{l_{tr}}{d} \frac{\tau_u}{\sqrt{f_c}} \qquad (3.3.12)$$

Now we are able to determine the effectiveness factor ν according to formula (3.3.3) as a function of the reinforcement stress σ_s in the transverse reinforcement. Instead of σ_s we may use the parameter $\rho\sigma_s / \sqrt{f_c}$ (f_c in MPa).

In Fig.3.3.4 curves for ν with a=4d and 10d while c=d and c=2d, respectively, are shown as a function of $\rho\sigma_s / \sqrt{f_c}$. In the figure, the test results from [82,1][88,1] [89,1][90,2] [90,3][91,1] are also shown.

As stated previously, the value of the effectiveness factor found in this way is the lower limit, which is also demonstrated by the test results. It seems likely that the strength reduction due to stressed transverse reinforcement may be explained by local damage around the reinforcement bars. More accurate calculations should of course be carried out considering also the other damage cases shown in Fig.3.3.2.

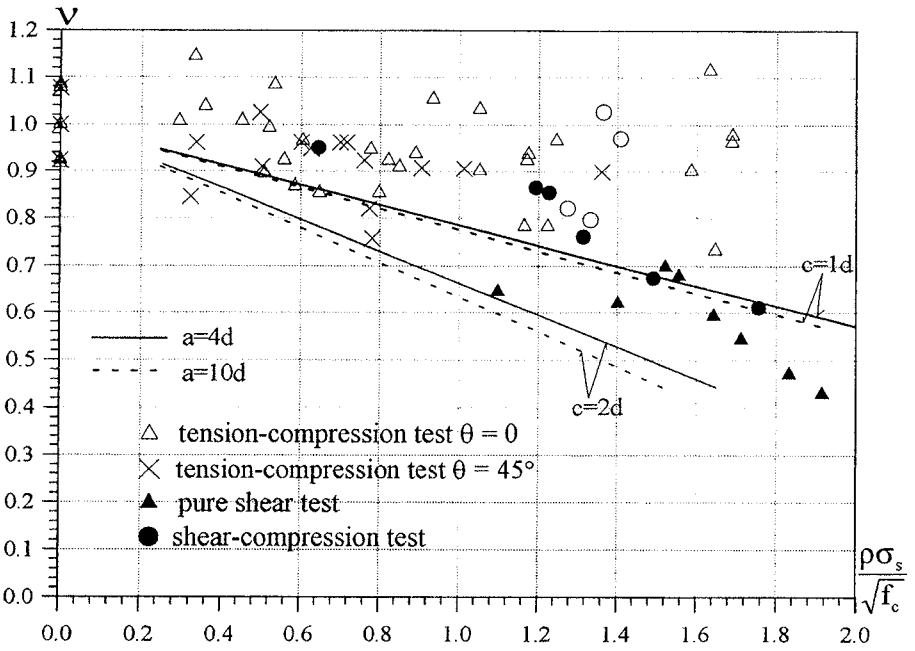

Fig.3.3.4 Effectiveness factor ν *versus* $\rho\sigma_s / \sqrt{f_c}$

Until more is learned about the effect of local damage, the strength reduction may be calculated in an approximate way as follows.

From Fig.3.3.4 it is seen that when the tensile stress in the transverse reinforcement is low, the effectiveness factor is close to 1. At a certain level of the tensile stress, the effectiveness factor decreases with increasing $\rho\sigma_s / \sqrt{f_c}$. It appears that the test data might be approximated by

$$\nu = 1 \qquad \frac{\rho\sigma_s}{\sqrt{f_c}} \le 0.9 \tag{3.3.13}$$

$$\nu = 1.52 - 0.58\frac{\rho\sigma_s}{\sqrt{f_c}} \qquad \frac{\rho\sigma_s}{\sqrt{f_c}} > 0.9 \tag{3.3.14}$$

The comparison of this approximation with the same tests as in Fig.3.3.4 is shown in Fig.3.3.5.

Hence, a formula for the effectiveness factor as a function of the transverse tensile stress is established.

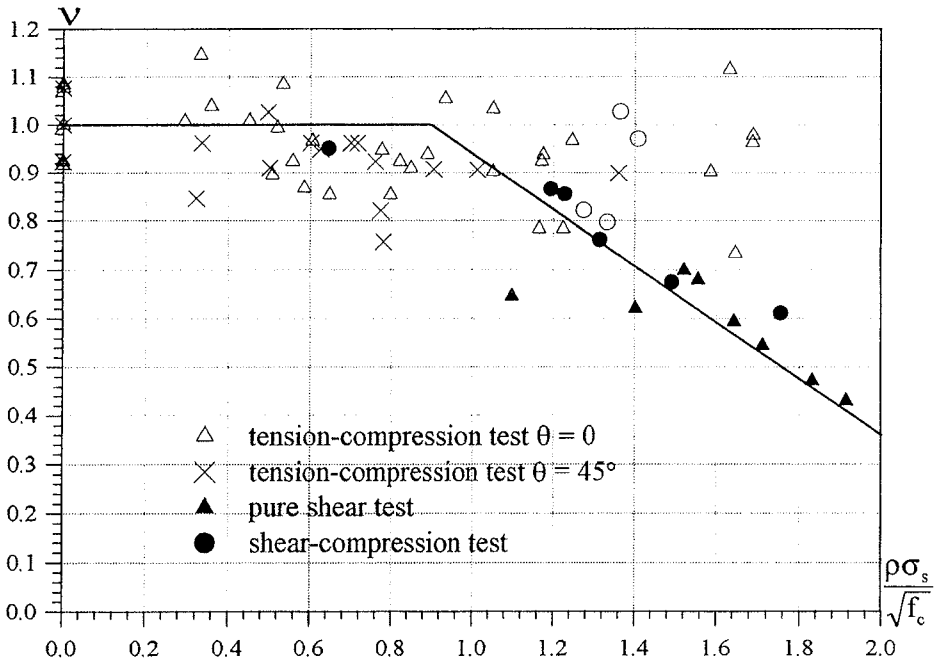

Fig.3.3.5 Approximation of ν *as function of transverse tensile stress*

The formulas (3.3.13) and (3.3.14) approximately cover the formula (2.2.1) valid for pure shear. This may be shown by realizing that in pure shear we have $\rho\sigma_s=\tau$ (isotropic reinforcement parallel to the sides with pure shear stress τ). Inserting this into eq.(3.3.14) and utilizing that at failure by crushing in the concrete $\tau=\frac{1}{2}\nu f_c$, we arrive at an equation which may be solved for τ. Utilizing once again $\tau=\frac{1}{2}\nu f_c$, ν is determined. The result is very close to eq.(2.2.1).

3.4 Conclusions

From the forgoing sections, the following conclusions might be drawn:

1. The compressive ultimate stress is sensitive to the inclination of cracks created by the transverse tensile loads or other effects. This may be one of the reasons for the large scatter in the experimental results of tension-compression tests. By reinforcing the joints, the sensitivity of the compressive strength reduction to the crack inclination may be reduced or eliminated.

2. The compressive strength reduction due to stressed transverse reinforcement might be explained by the spoiling and spalling of the con-

crete. The reduction may be taken as a function of the transverse tensile stress. An approximate formula for the compressive strength reduction factor or the effectiveness factor is given by eq.(3.3.13) and (3.3.14).

IV. Shear load carrying capacity of panels

As summarized in Chapter 2, a large number of specimens subjected to in-plane stresses has been tested, see [82,1][91,1]. In this chapter the panels subjected to pure shear stress are investigated.

4.1 Exact solution in plastic theory

Consider a panel, reinforced in x and y direction and subjected to pure shear as illustrated in Fig.4.1.1. In [84,1], assuming the concrete as a modified Coulomb material with a zero tension cut off, the exact solution of the shear load carrying capacity is found to be

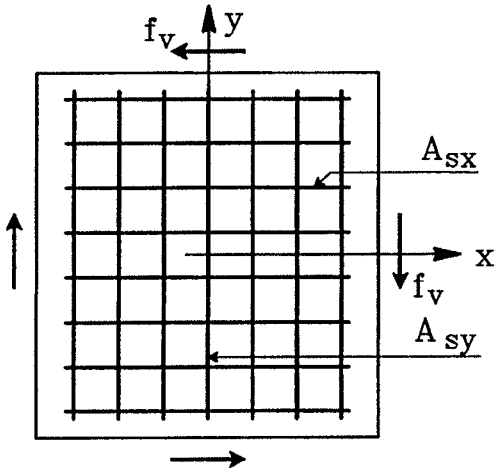

Fig.4.1.1 Panel subjected to pure shear

$$
\begin{aligned}
f_v &= \sqrt{\Phi_x \Phi_y} f_c && \Phi_x + \Phi_y \le \nu \text{ and } \max.(\Phi_x, \Phi_y) \le \frac{1}{2}\nu \\
f_v &= \sqrt{\Phi_i (\nu - \Phi_i)} f_c && \Phi_x + \Phi_y > \nu \text{ and } \Phi_i = \min.(\Phi_x, \Phi_y) < \frac{1}{2}\nu \\
f_v &= \frac{1}{2}\nu f_c && \Phi_x + \Phi_y > \nu \text{ and } \Phi_i = \min.(\Phi_x, \Phi_y) \ge \frac{1}{2}\nu
\end{aligned}
\qquad (4.1.1)
$$

Here Φ_x and Φ_y, defined as before, are the reinforcement degrees in x and y directions, respectively.

The solution has been compared with the test results from [82,1] [90,2]

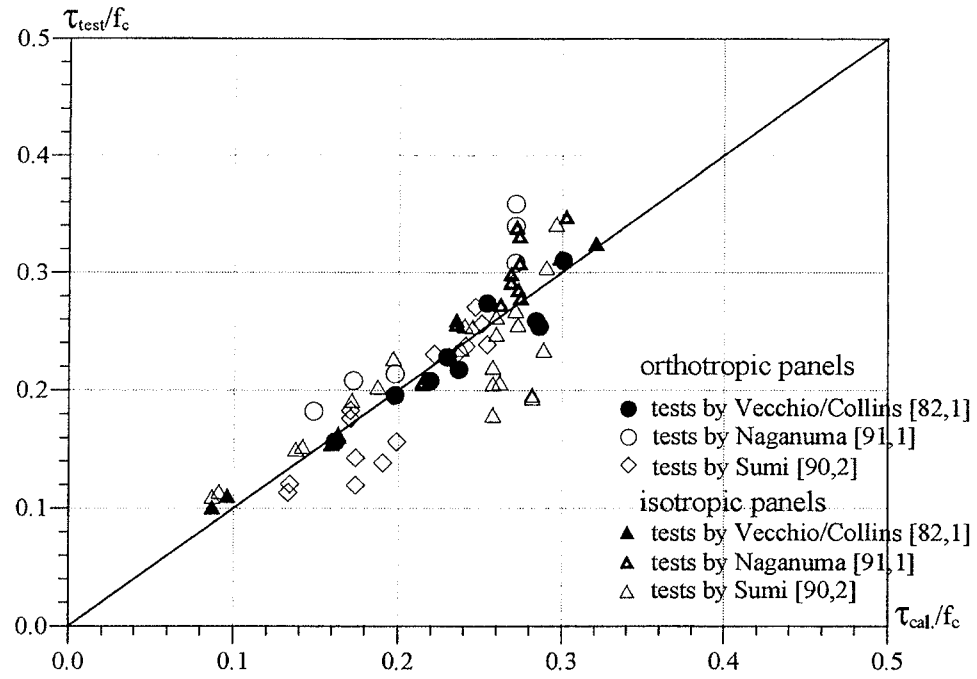

Fig.4.1.2 Comparison of the exact plastic solution with tests from [82,1][90,2] [91,1]

and [91,1] in Fig.4.1.2. As for shear in beams, we set the effectiveness factor

$$\nu = 0.7 - \frac{f_c}{200} \quad (f_c \text{ in MPa}) \tag{4.1.2}$$

The agreement between theory and tests seems to be quite good. However, as noticed before, the measurements of the principal compressive stress at failure performed by Vecchio/Collins show that the compressive stress at failure is much lower than given by eq.(4.1.2). The reason why this is not felt when comparing theory and tests is that the load carrying capacity in most tests is governed by reinforcement yielding, which means that the concrete strength has very little influence on the result.

In what follows we will demonstrate that the low values of the principal compressive stress may be explained as an effect of sliding in initial cracks.

In the experiments with orthotropic panels, an obvious shift of crack system at failure was reported. At first, the cracks, what we term the initial cracks, were created approximately perpendicular to the direction of the principal tensile stress in the uncracked concrete. Since the sliding

resistance is reduced significantly along a crack, a sliding failure along the existing initial cracks might have occurred in the ultimate state. Based on this presumption, the following upper bound and lower bound plastic solutions are proposed.

4.2 Upper Bound Solution Based on Sliding in Initial Cracks

Consider a panel in pure shear. With the purpose of establishing an upper bound solution, we choose a failure mechanism where the yield line follows the initial crack and sliding occurs along the crack as shown in Fig.4.2.1. The relative displacement is at an angle α to the yield line. The panel is reinforced in x and y directions with the reinforcement ratios of ρ_{sx} and ρ_{sy}, respectively.

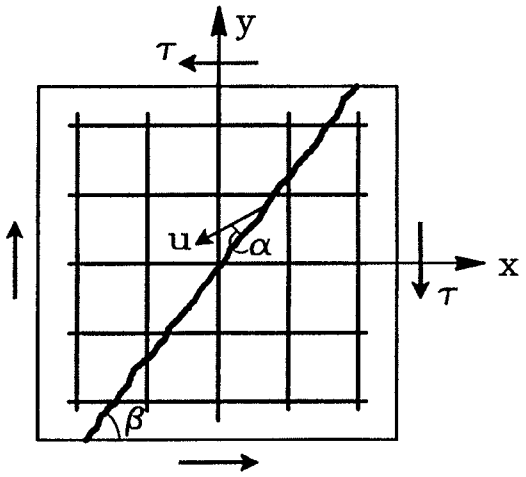

Fig.4.2.1 Yield line along an initial crack

To render the formulas more general, we indicate the angle of the initial crack by β.

As in previous parts, the cohesion of concrete along the crack is reduced to $c'=\nu_s c$, and the friction angle remains the same as for uncracked concrete.

However, the concrete strength is also reduced because the cracks are crossed by stressed transverse reinforcement. Without sliding in initial cracks, the effect of transverse reinforcement is to reduce the concrete strength to $\nu_0 f_c$, where $\nu=\nu_0$ may be determined by (3.3.13) and (3.3.14). We may also use formula (4.1.2) or formula (2.2.1) for high strength concrete to determine the effectiveness factor $\nu=\nu_0$. The internal cracking

leading to the reduction of the concrete strength from f_c to $\nu_0 f_c$ will of course also affect the sliding strength. For instance, if the internal cracking causes the cover to spall off, the sliding resistance will be determined by the reduced panel thickness.

The effective compressive strength along the crack becomes $f_c'=\nu_s\nu_0 f_c$.

Hence, the dissipation along the yield line is,

$$W_I=\frac{1}{2}f_c'(1-\sin\alpha)\frac{b}{\cos\beta}u+\rho_{sx}f_y b\tan\beta\cdot|u\cos(\beta-\alpha)|+\rho_{sy}f_y b\cdot|u\sin(\beta-\alpha)| \tag{4.2.1}$$

putting the thickness of the panel to a unit of length. The tensile strength of concrete along the crack is disregarded. The problem we are dealing with is considered to be a plane strain problem. Thus, we have $\alpha\geq\varphi$.

The external work is

$$W_E=\tau b\cdot u\cos(\beta-\alpha)-\tau b\tan\alpha\cdot u\sin(\beta-\alpha) \tag{4.2.2}$$

The work equation $W_E=W_I$ renders

$$\frac{\tau}{f_c}=\frac{1}{2}\nu_s\nu_0\frac{1-\sin\alpha}{\cos(2\beta-\alpha)}+\Phi_x\left|\frac{\sin\beta\cos(\beta-\alpha)}{\cos(2\beta-\alpha)}\right|+\Phi_y\left|\frac{\cos\beta\sin(\beta-\alpha)}{\cos(2\beta-\alpha)}\right| \tag{4.2.3}$$

If the angle of the initial cracks is known, the minimum of the shear load carrying capacity is found by optimizing eq.(4.2.3) with respect to α.

For panels in pure shear, the direction of the principal tensile stress for uncracked concrete is at 45° to the loaded edges. Thus, the angle of the initial cracks is β=45°.

Of course, the load carrying capacity of cracked concrete can not exceed the maximum shear carrying capacity of uncracked concrete. Thus, we have $\tau/f_c\leq 0.5\nu_0$.

Fig.4.2.2 depicts the comparison of the calculation with the test results from [82,1][90,2] [91,1].

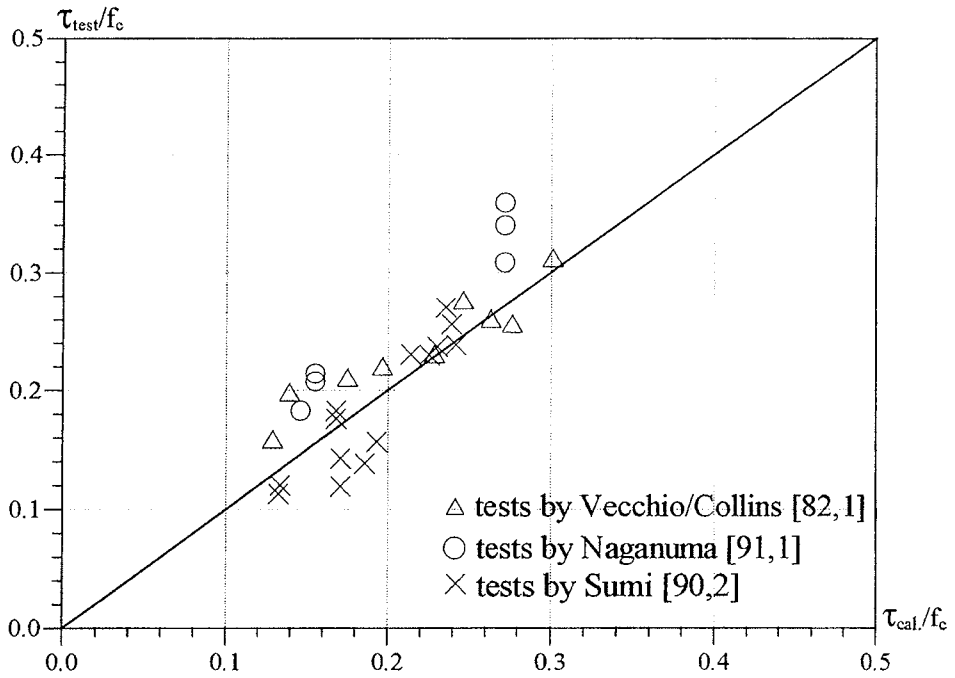

Fig.4.2.2 Comparison of calculation with test results from [82,1][90,2] [91,1]

The expression for ν_0 by (4.1.2) is mainly used for normal strength concrete, say $f_c \leq 60$MPa. It is not reliable to extrapolate this formula to higher values of concrete strength. The effectiveness factor of concrete for the test series in [91,1], where the uniaxial compressive strength of concrete was varied from 19MPa to 80MPa, was found in [92,1] to be, cf. formula (2.2.1),

$$\nu_0 = \frac{1.9}{f_c^{\,0.34}} \qquad (f_c \text{ in MPa}) \tag{4.2.4}$$

Therefore, in the calculation we have used (4.1.2) for $f_c \leq 60$MPa and (4.2.4) for $f_c > 60$MPa to determine ν_0.

As previously, the sliding reduction factor is set to $\nu_s = 0.5$

Fairly good agreement between the calculation and the experimental results can be seen in Fig.4.2.2.

If the panel is heavily reinforced in one direction, the corresponding steel

bars may not yield at failure. This situation is automatically taken into account in the upper bound solution where the relative displacement then will be perpendicular to the reinforcement considered.

4.3 Lower Bound Solution Based on Sliding in Initial Cracks

In the experiments with orthotropic panels in pure shear, the direction of the principal compression stress in concrete is changed. This situation is illustrated in Fig.4.3.1. The compressive stress σ_c in the direction determined by the angle θ is at an angle to the initial cracks, the inclination of which are determined by the angle β. Thus, we may imagine that sliding along the existing initial cracks takes place.

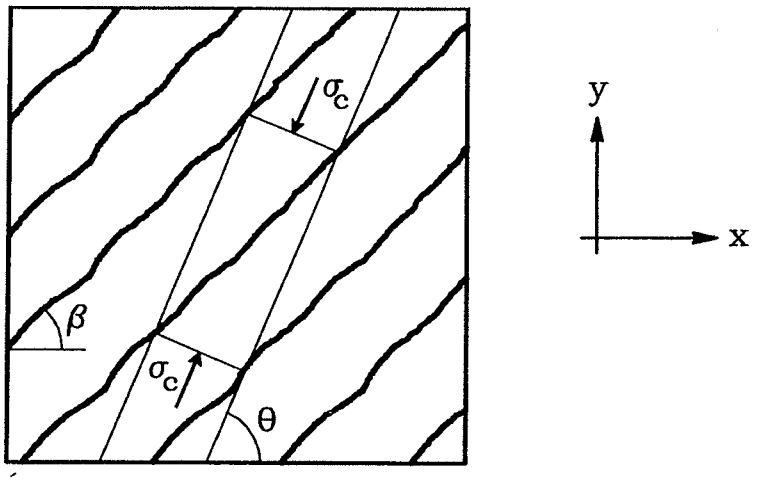

Fig.4.3.1 Sliding along the initial cracks in the lower bound solution

By stress transformation, we get:

$$\sigma_x = -\sigma_c \cos^2\theta \qquad \sigma_y = -\sigma_c \sin^2\theta \qquad |\tau_{xy}| = \sigma_c \sin\theta\cos\theta \qquad (4.3.1)$$

Assuming that the reinforcement in both directions is yielding at failure we have

$$\Phi_x f_c = \sigma_c \cos^2\theta \qquad \Phi_y f_c = \sigma_c \sin^2\theta \qquad (4.3.2)$$

which gives

$$\tan\theta = \sqrt{\frac{\Phi_y}{\Phi_x}} \qquad (4.3.3)$$

In the orthotropically reinforced panels where $\Phi_x \neq \Phi_y$, $\theta \neq 45°$. Thus the direction of the principal compressive stress in concrete at failure is not the same as for uncracked concrete.

The shear and normal stresses in the concrete along the existing initial cracks are

$$|\tau| = \sigma_c |\sin(\theta-\beta)\cos(\theta-\beta)| \qquad \sigma = \sigma_c \sin^2(\theta-\beta) \tag{4.3.4}$$

If applying the modified Coulomb sliding failure criterion along the crack with a reduced cohesion, i.e. $c' = \nu_s c$ and $\varphi' = \varphi$, then at sliding failure along the crack, τ and σ from eq.(4.3.4) must satisfy the condition:

$$|\tau| = c' + \mu' \sigma \qquad \text{where } \mu' = \tan\varphi' = \tan\varphi \tag{4.3.5}$$

For normal strength concrete, we set $\varphi = 37°$, and thus $\mu' = 0.75$.

Inserting (4.3.4) into (4.3.5) we obtain

$$\frac{\sigma_c}{f_c} = \frac{\frac{1}{4}\nu_s \nu_0}{|\sin(\theta-\beta)\cos(\theta-\beta)| - 0.75\sin^2(\theta-\beta)} \tag{4.3.6}$$

For panels in pure shear the initial cracks are approximately following the principal stress trajectories for uncracked concrete, i.e. $\beta = 45°$.

The maximum of σ_c is $\nu_0 f_c$ which is the effective uniaxial compressive strength of uncracked concrete, i.e. $\sigma_c \leq \nu_0 f_c$.

As before, ν_0 may be determined by (4.1.2) for normal strength concrete and ν_s may be set to 0.5.

In Fig.4.3.2 the calculated and the measured values of the principal compressive stress have been compared, and in Fig.4.3.3 the measured principal compressive stress has been drawn as a function of the angle θ. The test results are from [82,1].

The test results of prime interest in Fig.4.3.3 are those where the reinforcement, according to experiments, did only yield in one direction or did not yield at all. When both reinforcement directions are yielding, this

will by itself limit the concrete stress, and the test result might not represent a sliding in initial cracks failure.

The angle θ in the tests has been determined by eq.(4.3.3).

The agreement between the calculation and the experimental results is fairly good. It must be remembered here that when determining θ, reinforcing bars in x and y directions are assumed yielding. This condition was not always fulfilled in the experiments. For the heavily reinforced panels, the reinforcement was not yielding at failure in one or both directions. Since the stresses in the reinforcement prior to yielding can not be found by plastic theory, the angle θ is undetermined in such cases. For this reason, the scatter is acceptable

.

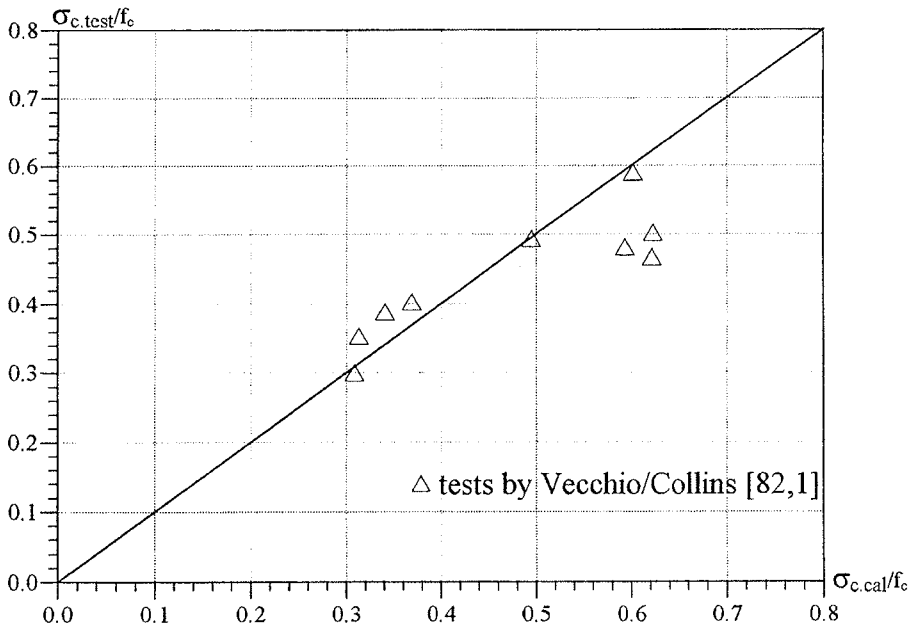

Fig.4.3.2 Comparison between the calculated and measured principal compressive stresses in concrete [82,1]

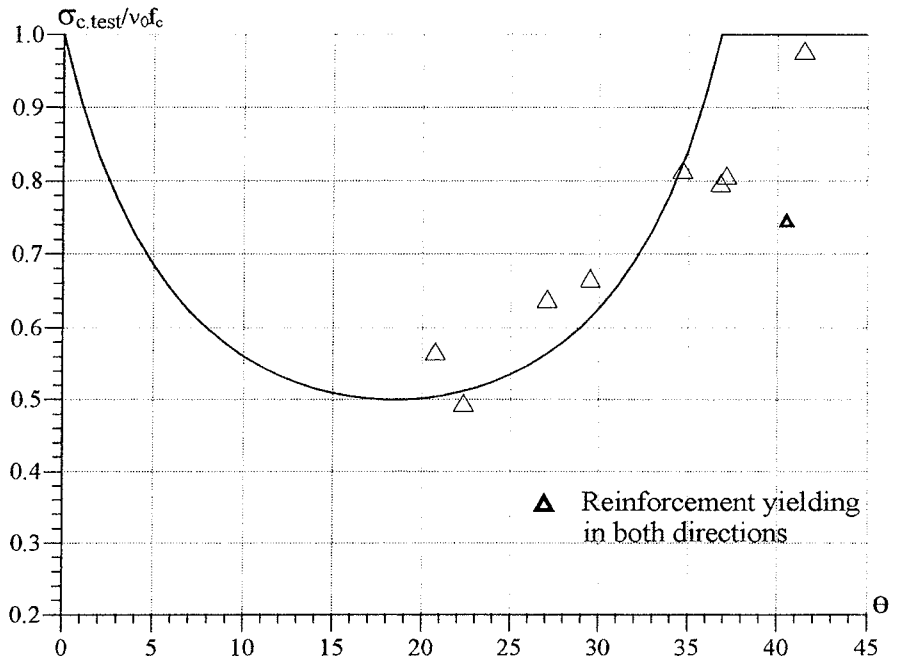

Fig.4.3.3 Comparison of shear capacity with test results [82,1]

4.4 Discussion on the failure criteria applied in the plastic solutions

Due to the reasons stated above, it is natural not to expect the lower bound solution and the upper bound solution to yield the same load carrying capacity. Furthermore, the yield criterion applied in the lower bound solution differs from that in the upper bound solution.

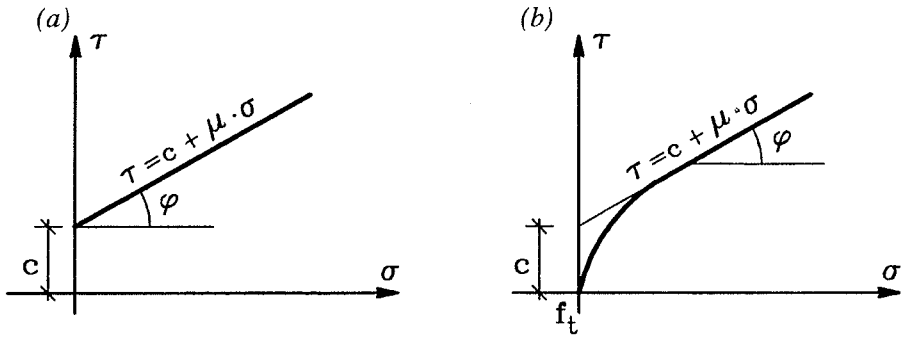

Fig.4.4.1 Sliding failure criteria in(a) lower bound and (b) upper bound solutions

In Fig.4.4.1 the sliding failure criteria used in the lower bound and the upper bound solution are shown assuming the tensile strength to be zero. The sliding failure criterion in the lower bound solution is a straight line

determined by $|\tau| = c + \mu\sigma$ for all the compression stress states. However, the sliding failure criterion in the upper bound solution is composed by two parts: a straight line, and a circle. The circle appears as a result of the transformation of the modified Coulomb failure condition in τ, σ-space to principal stress space and back. If the tensile strength f_t is not zero, the circle will be tangent to the line representing the Coulomb failure condition and the vertical line representing the tensile failure condition. The range of the validity of the straight Coulomb line depends on the tensile strength. The larger the tensile strength, the longer the range of validity. In the extreme, we have a straight line when $\sigma \geq 0$, i.e. for all compression stress state. If we use the straight line shown in Fig.4.4.1 (a) as the failure criterion in the upper bound solution, then the dissipation per unit length of the yield line becomes

$$W_i = c \cos\alpha \cdot u \tag{4.4.1}$$

where $\alpha \geq \varphi$ is the angle of the relative displacement to the yield line.

Compared with the usual dissipation formula with tensile strength equal to zero, cf. eq.(3.1.1.5), eq.(4.4.1) gives higher dissipation.

It will be interesting to illustrate the difference in results by using the two different dissipation formulas.

Consider a joint as shown in Fig.3.1.1.1. In the plane strain case we have $\alpha \geq \varphi$. Using the dissipation formula (3.1.1.5) with the tensile strength $f_t=0$, the load carrying capacity as a function of β is shown in Fig.3.1.1.4.

If we apply the dissipation formula (4.4.1), the compressive strength will be

$$\sigma = c \frac{\cos\alpha}{\cos\beta \sin(\beta - \alpha)} \tag{4.4.2}$$

For a friction angle $\varphi=37°$ the effective cohesion of uncracked concrete is $\nu_0 f_c/4$. Thus the effective cohesion of cracked concrete is $c' = \nu_s \nu_0 f_c/4$. Replacing in eq.(4.4.2) c by c′ we find

$$\frac{\sigma}{f_c} = \frac{1}{4} \nu_s \nu_0 \frac{\cos\alpha}{\cos\beta \sin(\beta - \alpha)} \tag{4.4.3}$$

The minimum of σ is found by optimizing (4.4.3) with respect to α.

It turns out that minimum of (4.4.3) is obtained for $\alpha=\varphi$.

In Fig.4.4.2 the results obtained by the two different dissipation formulas eq.(3.1.1.5) with $f_t'=0$ and eq.(4.4.1) are drawn.

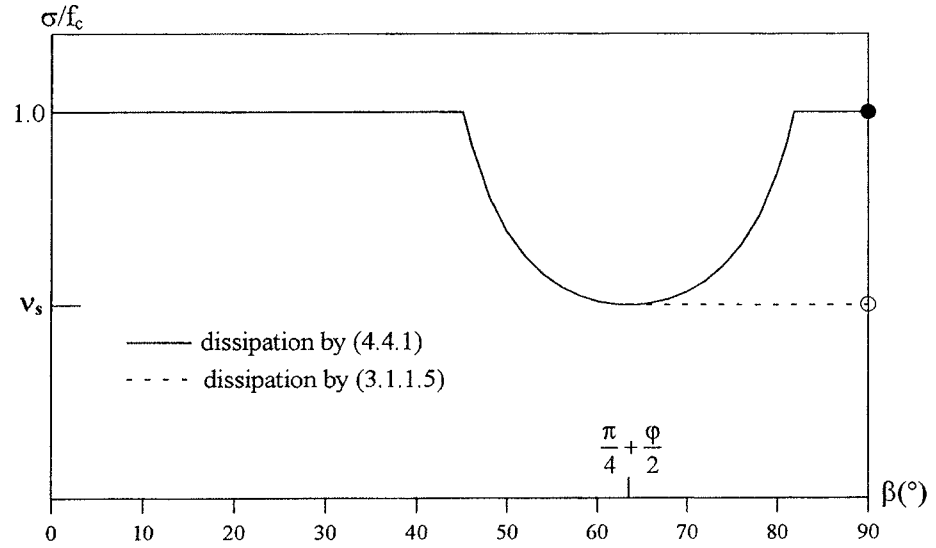

Fig.4.4.2 Compressive strength of a specimen with a joint obtained by two different dissipation formulas (3.1.1.5) and (4.4.1)

The results are rather instructive. Using the dissipation formula (3.1.15) with $f_t=0$, the load carrying capacity is found to be a constant and the angle $\alpha\geq\varphi$ when $\beta>\pi/4+\varphi/2$. However, with the dissipation formula (4.4.1), the angle $\alpha=\varphi$ and instead having a constant, reduced strength for $\beta>\pi/4+\varphi/2$, the strength is growing to $\sigma=f_c$ for increasing β. This means that the curve of the load carrying capacity by using eq.(4.4.1) is the same as that if we use the usual dissipation formulas for $\alpha=\varphi$ or equivalently if we assume a sufficiently large tensile strength f_t..

As appear from section 3.1.1, the calculation with the dissipation formula (4.4.1) shows a good agreement with tests on casting joints reported in [30,1].

For panels in shear, if we use the dissipation formula (4.4.1), the shear load carrying capacity becomes

$$\frac{\tau}{f_c} = \frac{1}{4}\nu_s\nu_0\frac{\cos\alpha}{\cos(2\beta-\alpha)} + \Phi_x\left|\frac{\sin\beta\cos(\beta-\alpha)}{\cos(2\beta-\alpha)}\right| + \Phi_y\left|\frac{\cos\beta\sin(\beta-\alpha)}{\cos(2\beta-\alpha)}\right| \tag{4.4.4}$$

The minimum is found by optimizing eq.(4.4.4) with respect to α. The results obtained in this way are plotted in Fig.4.4.3 together with the test results from [82,1][91,1]. By comparing with Fig.4.2.2 it appears that the load carrying capacity is not altered much. In the calculation, the minimum is found either at the angle α=90° to the yield line, i.e. the relative displacement is perpendicular to the yield line, or with the relative displacement parallel to the minor reinforced direction, meaning that the steel bars in the direction of the larger reinforcement are not yielding. This result is similar to that obtained in the usual exact solution.

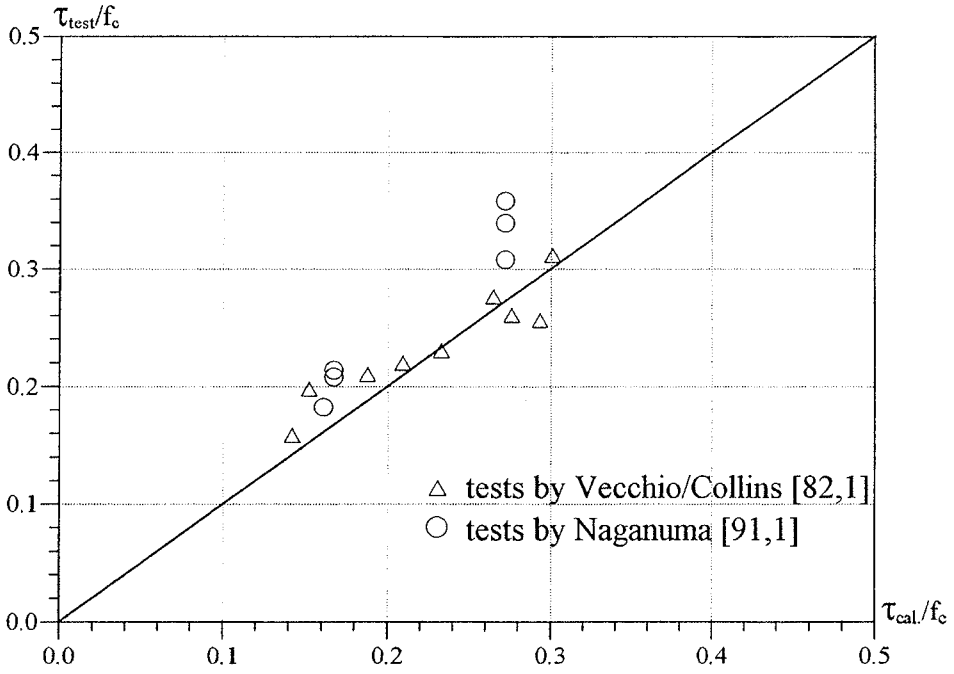

Fig.4.4.3 Comparison of the results by eq.(4.2.4) with test results from [82,1][91,1]

Thus we may conclude that the usual dissipation formula of plastic theory, eq.(3.1.1.5), does not give realistic results when the tensile strength f_t is put to zero and when the angle between the displacement and the yield line is large. The reason is, as mentioned earlier, that when f_t=0 the shear capacity is zero when the normal stress is zero, which is at variance with reality. The discrepancy may be avoided by assuming a small tensile strength. Alternatively, the dissipation formula (4.4.1) may be used. This

formula gives realistic results for casting joints. For panels with sliding in initial cracks, the difference between the results obtained by the two dissipation formulas is not significant.

More accurate models may be developed in the same spirit as it was done for a crack in Part 2 of this thesis.

V. Conclusions

In this report a review on the experiments of concrete specimens subjected to in-plane stresses is carried out. The effect of the position of cracks and joints on the load carrying capacity is analyzed by means of plastic theory, and a mechanism of strength reduction is proposed based on the analysis of the damage caused by stressed transverse reinforcement.

By assuming sliding failure along existing initial cracks, an upper bound solution and a lower bound solution for the load carrying capacity of panels subjected to in-plane shear are proposed.

By the comparison with the test results, the following conclusions may be drawn:

1. The load carrying capacity of plain concrete panels is sensitive to the direction of cracks. This may explain partly why the scatter of the experimental results of panels subjected to tension-compression stresses is very large. By placing reinforcement, the sensitivity of the load carrying capacity to the direction of the cracks may be reduced or eliminated.

2. The effectiveness factor or the strength reduction factor may be expressed as a function of the transverse tensile stress. By comparing with tests, the following approximate formulas for the effectiveness factor may be suggested:

$$\nu = 1 \qquad \frac{\rho\sigma_s}{\sqrt{f_c}} \le 0.9 \quad (f_c \text{ in MPa})$$

$$\nu = 1.52 - 0.58\frac{\rho\sigma_s}{\sqrt{f_c}} \qquad \frac{\rho\sigma_s}{\sqrt{f_c}} > 0.9 \quad (f_c \text{ in MPa})$$

3. By assuming the sliding reduction factor due to cracking ν_s=0.5, the load carrying capacity of orthotropic panels subjected to in-plane shear may be determined.

4. The exact plastic solution can also be applied to determine the load carrying capacity of panels subjected to in-plane shear stresses both in the case of isotropic panels and in the case of orthotropic panels when the load carrying is mainly governed by yielding of the reinforcement.

REFERENCES

[69,1] J.M.Demorieux: Essai de traction-compression sur modèles d'ame de poutre en bèton armè.
Annales de l'Institut Technique du Bâtiment et des Travaux Publics, No.258m Juin, 1969, pp.980-982.

[77,1] B.C.Jensen: Some applications of plastic analysis to plain and reinforced concrete.
Institute of Building Design, Technical University of Denmark, 1977.

[77,2] J.R.Robinson & J.-M.Demorieux: Essais de modèles d'ame de poutres en double tè.
Annales de l'Institut Technique du Bâtiment et des Travaux Publics, No.354, Oct. 1977, pp.79-84.

[82,1] F.Vecchio & M.P.Collins: The response of reinforced concrete to in-plane and normal stresses.
The Department of Civil Engineering, University of Toronto, Canada, Mar. 1982.

[86,1] J.Jokela: Dimensioning of strain or deformation-controlled reinforced concrete beams.
Concrete and Silicate Laboratory, Technical Research Center of Finland, Publication 33, 1986

[88,1] J.Eibl & U.Neuroth: Untersuchungen zur Druckfestigkeit von bewehrten beton bei gleichzeitig wirkenden querzug.
Universität Karlsruhe, Institut für Massivbau und Baustofftechnologie Abteilung Massivbau, 1988.

[88,2] T.Miyahara, T.Kawakami & K.Maekawa: Nonlinear behavior of cracked reinforced concrete plate element under uniaxial compression.
Concrete Library of JSCE, No.11, June 1988, pp.131-144.

[88,3] S.Hamada & H.Naguchi: Basic experiments on the degradation of cracked concrete under biaxial compression and tension.
The Annual Report of the Architectural Institute of Japan, Structures II, Oct. 1988, pp.397-388.

[89,1] T.Dyngeland: Behaviour of reinforced concrete panels - An experimental study of reinforced concrete panels subjected to uniaxial tensile stresses and to combined tensile and compressive stresses.
Institutt for Betongkonstruksjoner, Trondheim, 1989.

[90,1] D.H.Olsen & M.P.Nielsen: Ny teori til bestemmelse af revneafstande og revnevidder i betonkonstruktioner.

Department of Structural Engineering, Technical University of Denmark, Report R No.254, 1990.

[90,2] K.Sumi, M.Osa & S.Kawamata: The governing factors of post cracking behaviour of reinforced concrete wall in in-plane shear.
The International Journal of Structural Mechanics and Materials Science, Elsevier Applied Science, Vol.29, No.3, 1990, pp.221-247.

[90,3] J.Kollegger & G.Mehlhorn: Experimentelle untersuchungen zur bestimmung der druckfestigkeit des gerissenen stahlbetons bei einer querzugbeanspruchung (Experimental investigation into the compressive strength of reinforced concrete subjected to transverse tension).
Deutscher Ausschuss fr Stahlbeton, Heft 413, 1990.

[91,1] T.Yamagochi & K.Naganuma: Experimental study on mechanical characteristics of reinforced concrete panels subjected to in-plane shear force.
Journal of Struct. Constr. Engng, AIJ, No.419, Jan. 1991.

[91,2] T.Takeda, T.Yamaguchi & K.Naganuma: Report on tests of nuclear prestressed containment vessels.
Transactions of the International Workshop on Concrete Shear in Earthquake University of Houston, Texas, USA, Jan. 1991.

[92,1] H.E.Jensen: State-of-the -art rapport for revnet betons styrke.
Department of Structural Engineering, Technical University of Denmark, Report R No.295, 1992.

[93,1] H.E.Jensen: Forsøgsrapport for revnede betonskivers styrke (Test report on the strength of cracked disks).
Det Materialeteknologiske Udviklingsprogram, Højkvalitetsbetoner i 90'erne.
Department of Structural Engineering, Technical University of Denmark, Report 7.10, May 1993.

[93,2] P.H.Feenstra & R.de Borst: Aspects of robust computational modelling for plain and reinforced concrete.
Heron, Vol.38, No.4, 1993.

[94,1] N.Snog: Minimumsarmering.
Department of Structural Engineering, Technical University of Denmark, M.Sc. thesis, 1994.

[95,1] A.Belarby & T.T.C. Hsu: Constitutive laws of softened concrete in biaxial tension-compression.
ACI Structural Journal, Vol.92, No.5, Sept.-Oct. 1995, pp.562-573.

AFDELINGEN FOR BÆRENDE KONSTRUKTIONER
DANMARKS TEKNISKE UNIVERSITET

Department of Structural Engineering and Materials
Technical University of Denmark, DK–2800 Lyngby

SERIE R
(Tidligere: Rapporter)

R 317. JAGD, LARS, CHRISTOFFERSEN, JENS, NIELSEN, M.P.: The HOTCH–POTCH Disk Element – Finite Element for Analysis of Reinforced Concrete Disks. 1994.
R 318. JAGD, LARS, CHRISTOFFERSEN, JENS, NIELSEN, M.P.: The HOTCH–POTCH Disk Element – Finite Element for Analysis of Reinforced Concrete Shells. 1994.
R 319. HANSEN, THOMAS CORNELIUS: Triaxial Tests with Concrete and Cement Paste. 1995.
R 320. PETERSEN, R.I., AGERSKOV, H., MARTINEZ, L. LOPEZ, ASKEGAARD, V.: Fatigue Life of High–Strength Steel Plate Elements under Stochastic Loading. 1995.
R 321. Resuméoversigt 1994 – Summaries of Papers 1994.
R 322. IBSØ, JAN BEHRENDT: Fatigue Life Prediction of Welded Joints Based on Fracture Mechanics and Crack Closure. 1995.
R 323. NIELSEN, CLAUS VESTERGAARD: Ultra High–Strength Steel Fibre Reinforced Concrete. Part I. Basic Strength Properties of Compresit Matrix. 1995.
R 324. NIELSEN, CLAUS VESTERGAARD: Ultra High–Strength Steel Fibre Reinforced Concrete. Part II. Structural Applications of Compresit. 1995.
R 1. R.I. PETERSEN, H. AGERSKOV & L. LOPEZ MARTINEZ: Fatigue Life of High–Strength Steel Offshore Tubular Joints, 1996.
R 2. Resuméoversigt, ABK 1995 – Summaries of Papers, ABK 1995.
R 3. SCHAUMANN, JETTE: Lignocellulosematerialers vandbinding. 1996.
R 4. RASMUSSEN, K.J.R.: State of the Art of Numerical Simulation and Computational Models in Coupled Instabilities. 1996.
R 5. JAGD, LARS KRISTIAN: Non–linear Seismic Analysis of RC Shear Wall. 1996.
R 6. NIELSEN, LAUGE FUGLSANG: Lifetime and residual strength of wood, subjected to static and variable load. 1996.
R 7. NIELSEN, LAUGE FUGLSAND: Træthed og reststyrke i beton og andre viskoelastiske materialer med ældning. 1996.
R 8. Ninth Nordic Seminar on Computational Mechanics. Redigeret af LARS DAMKILDE. 1996.
R 9. HANSEN, THOMAS CORNELIUS: Fatigue in High Strength Steel. A new approach to predict crack propagation behaviour. 1996.
R 10. HANSEN, THOMAS CORNELIUS: Fatigue in Welded Connections. A new approach to predict crack propagation behaviour. 1996.
R 11. HANSEN, THOMAS CORNELIUS, AND OLSEN, DAVID HOLKMANN: Fracture and crack growth in concrete. A new approach to predict crack propagation behaviour. 1996.
R 12. HOANG, LINH CAO AND NIELSEN, M.P.: Continuous Reinforced Concrete Beams – Stress and Stiffness Estimates in the Serviceability Limit State. 1996.
R 13. NIELSEN, LAUGE FUGLSANG: Composite Analysis of Concrete. Creep, Relaxation, and Eigenstrain/Stress. 1996.
R 14. PEDERSEN, CARSTEN: New Production Processes, Materials and Calculation Techniques for Fiber Reinforced Concrete Pipes. 1996.
R 15. NIELSEN, J.A., H. AGERSKOV AND T. VEJRUM: Fatigue in Steel Highway Bridges under Random Loading. 1997.
R 16. HOANG, LINH CAO: Shear Strength of Non–Shear Reinforced Concrete Elements. 1997

Abonnement 1.7.1997 – 30.6.1998 kr. 130,–
Subscription rate 1.7.1997 – 30.6.1998 D.Kr. 130.–.